



U.S. Department
of Transportation

**Federal Railroad
Administration**

Application of Cable-In-Conduit Conductor (CICC) to MAGLEV Magnet Systems

National Maglev Initiative
Washington, D.C. 20590

DOT/FRA/NMI-92/05

July 1992
Final Report

This document is available to the
U.S. public through the National
Technical Information Service,
Springfield, Virginia 22161.

PFC/RR-92-12

**Application of Cable-in-Conduit Conductor (CICC)
to MAGLEV Magnet Systems**

31 July 1992

R. J. Thome, D. B. Montgomery, J. V. Minervini,
P. H. Titus, J. Pisera, J. R. Hale, M. Olmstead, R. J. Camille,
R. D. Pillsbury, Jr., W. R. Mann, J. Feng and M. Ferri

Prepared for
Department of Transportation/Federal Railroad Administration
Volpe National Transportation Systems Center
Contract No. DTFR53-91-C-00042

1. Report No. DOT/FRA/NMI-92/05		2. Government Accession No.		3. Recipient's Catalog No.	
4. Title and Subtitle Application of Cable-in-Conduit Conductor (CICC) to MAGLEV Magnet Systems				5. Report Date 31 July 1992	
				6. Performing Organization Code	
7. Author(s) R.J. Thome, D.B. Montgomery, J.V. Minervini, et al.				8. Performing Organization Report No. PFC-RR-92-12	
9. Performing Organization Name and Address Plasma Fusion Center Massachusetts Institute of Technology Cambridge, Massachusetts				10. Work Unit No. (TRAIS)	
				11. Contract or Grant No. DTFR53-91-C-00042	
12. Sponsoring Agency Name and Address Department of Transportation, Federal Railroad Administration, National Maglev Initiative Office 400 7th St., SW., Wash., D.C. 20590				13. Type of Report and Period Covered Final Report	
				14. Sponsoring Agency Code	
15. Supplementary Notes Dr. Norman Knable, U.S. Department of Transportation, Volpe National Transportation Systems Center, Kendall Square, Cambridge, MA 02142					
16. Abstract This report summarizes the evaluation of CICC as an option for MAGLEV levitation coils. Superconducting magnets are cooled by: 1) immersion in a liquid helium bath at near saturation conditions; 2) conduction cooling of an epoxy-impregnated coil; or 3) use of CICC in which single-phase supercritical helium cooling becomes an intrinsic part of the conductor design with helium contained in the conductor sheath. Major problems with options 1) and 2) are mitigated by use of option 3. Many levitation coil geometries were reviewed and the racetrack coil shape selected for the levitation coil system design task. The study showed that lift force per unit weight (coil plus cryostat) is proportional to the product of the conductor current density, j , and maximum magnetic field, B_M , experienced by the winding divided by the weight density. The lift force is also proportional to coil shape, track and speed characteristics, and dewar functions; however, no variables in this dimensionless group is conductor related. The design was to a maximum product of jB_M for the conductor. Analyses using both Nb_3Sn and $NbTi$ at preselected temperatures and energy margins showed that systems optimized at a low field level from 2.0 to 3.7T, that Nb_3Sn systems have higher jB_s than $NbTi$ at the same temperatures and that Nb_3Sn was therefore preferred. Those studies, although not optimized, indicate clearly that distinct advantages lie in using Nb_3Sn CICC at 8 K as opposed to the 4.5 K of conventional systems. Elevated operating temperature may lead to significant reductions in refrigerator weight.					
17. Key Words Maglev, conductor design, levitation magnet design			18. Distribution Statement Document is Available to the Public Through the National Technical Information Service, Springfield, Virginia 22161		
19. Security Classif. (of this report) Unclassified		20. Security Classif. (of this page) Unclassified		21. No. of Pages 85	22. Price

METRIC/ENGLISH CONVERSION FACTORS

ENGLISH TO METRIC

LENGTH (APPROXIMATE)

1 inch (in.) = 2.5 centimeters (cm)
 1 foot (ft) = 30 centimeters (cm)
 1 yard (yd) = 0.9 meter (m)
 1 mile (mi) = 1.6 kilometers (km)

AREA (APPROXIMATE)

1 square inch (sq in, in²) = 6.5 square centimeters (cm²)
 1 square foot (sq ft, ft²) = 0.09 square meter (m²)
 1 square yard (sq yd, yd²) = 0.8 square meter (m²)
 1 square mile (sq mi, mi²) = 2.6 square kilometers (km²)
 1 acre = 0.4 hectares (he) = 4,000 square meters (m²)

MASS - WEIGHT (APPROXIMATE)

1 ounce (oz) = 28 grams (gr)
 1 pound (lb) = .45 kilogram (kg)
 1 short ton = 2,000 pounds (lb) = 0.9 tonne (t)

VOLUME (APPROXIMATE)

1 teaspoon (tsp) = 5 milliliters (ml)
 1 tablespoon (tbsp) = 15 milliliters (ml)
 1 fluid ounce (fl oz) = 30 milliliters (ml)
 1 cup (c) = 0.24 liter (l)
 1 pint (pt) = 0.47 liter (l)
 1 quart (qt) = 0.96 liter (l)
 1 gallon (gal) = 3.8 liters (l)
 1 cubic foot (cu ft, ft³) = 0.03 cubic meter (m³)
 1 cubic yard (cu yd, yd³) = 0.76 cubic meter (m³)

TEMPERATURE (EXACT)

$$[(x - 32) (5/9)]^{\circ}\text{F} = y^{\circ}\text{C}$$

METRIC TO ENGLISH

LENGTH (APPROXIMATE)

1 millimeter (mm) = 0.04 inch (in)
 1 centimeter (cm) = 0.4 inch (in)
 1 meter (m) = 3.3 feet (ft)
 1 meter (m) = 1.1 yards (yd)
 1 kilometer (km) = 0.6 mile (mi)

AREA (APPROXIMATE)

1 square centimeter (cm²) = 0.16 square inch (sq in, in²)
 1 square meter (m²) = 1.2 square yards (sq yd, yd²)
 1 square kilometer (kn²) = 0.4 square mile (sq mi, mi²)
 1 hectare (he) = 10,000 square meters (m²) = 2.5 acres

MASS - WEIGHT (APPROXIMATE)

1 gram (gr) = 0.036 ounce (oz)
 1 kilogram (kg) = 2.2 pounds (lb)
 1 tonne (t) = 1,000 kilograms (kg) = 1.1 short tons

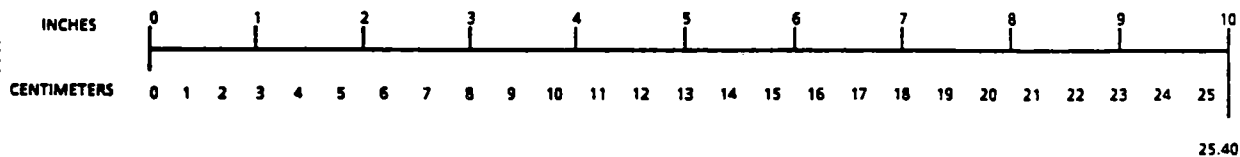
VOLUME (APPROXIMATE)

1 milliliter (ml) = 0.03 fluid ounce (fl oz)
 1 liter (l) = 2.1 pints (pt)
 1 liter (l) = 1.06 quarts (qt)
 1 liter (l) = 0.26 gallon (gal)
 1 cubic meter (m³) = 36 cubic feet (cu ft, ft³)
 1 cubic meter (m³) = 1.3 cubic yards (cu yd, yd³)

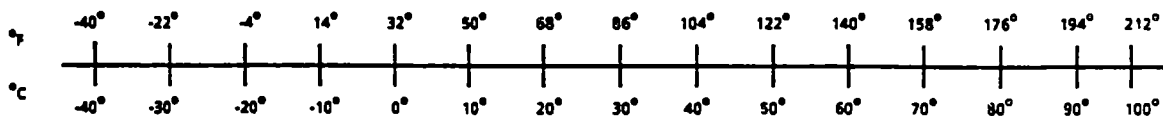
TEMPERATURE (EXACT)

$$[(9/5)y + 32]^{\circ}\text{C} = x^{\circ}\text{F}$$

QUICK INCH-CENTIMETER LENGTH CONVERSION



QUICK FAHRENHEIT-CELSIUS TEMPERATURE CONVERSION



For more exact and or other conversion factors, see NBS Miscellaneous Publication 286, Units of Weights and Measures. Price \$2.50. SD Catalog No. C13 10286.

Foreword

This activity was performed under Contract No. DTFR53-91-C-00042 for the Department of Transportation, Federal Railroad Administration, Volpe National Transportation Systems Center, Cambridge, MA. We would like to acknowledge the guidance provided by and technical discussions with Dr. Norman Knable, who was the Contracting Officers Technical Representative on this program. In addition, we would like to acknowledge the efforts of A. M. Dawson, B. A. Keesler, and D. Marble in preparing and editing this report.

Table of Contents

	Page No.
1.0 Introduction and Summary	1
2.0 Selection of Magnet Geometry	4
3.0 Field Level Trade Study	5
3.1 Parameters for Optimization of Lift per Unit Coil Weight	5
3.2 Comparison of Conductor Options	12
3.3 Selection of Current Density and Field Level	25
3.4 Coil System Parameter Variations	26
3.5 Optimization Including Dewar Weight	29
3.6 Number of Lift Modules per Vehicle	31
4.0 Conceptual Design	32
4.1 Conductor Selection	32
4.2 Selection of an Operating Temperature and Current	38
4.3 Levitation Module Design	42
4.3.1 Component Configuration and Component Functions	42
4.3.2 Structural Design	50
4.3.3 Module Heat Loads and Cryosystem Support	52
4.3.4 Coil System Charge and Discharge	63
4.4 Lift and Drag Characteristics for Coil	65
5.0 Impact of High T _c Superconductors	69
6.0 Information Required and Recommended Research	71
6.1 Conductor Development	71
6.2 Code Development	72
6.3 Joint and Lead Development	72
6.4 Persistent Switch Development	72
Appendix A - Derivation of Equations for Section 3.1	A1

List of Tables

- Table 1.0-1 Operating Points for Selected CICC Conductors and Temperatures to Maximize Lift per Unit Coil Weight for an Energy Margin of 100 mJ/cm³
- Table 3.2-1 Critical Current Densities for CICC Conductors Based on NbTi and Nb₃Sn
- Table 3.3-1 Operating Points for Selected CICC Conductors and Temperatures to Maximize Lift per Unit Coil Weight for an Energy Margin of 100 mJ/cm³
- Table 4.1-1 Preliminary Characteristics of MAGLEV Conductor
- Table 4.2-1 Energy Margin at a Field Level of 2.9 T and a Conductor Current Density of 2.42 x 10⁸ A/m² for Selected Conductors
- Table 4.3-1 Estimated Weights for Racetrack Lift Module Components
- Table 4.3-2 Heat Load Budget Estimate for Multiple Levitation Modules
- Table 4.4-1 Typical Racetrack Lift Coil Characteristics

List of Figures

- Figure 2.0-1 Typical cross section of Miyazaki test facility elevated guideway with MLU-001 test vehicle. (From Canadian Institute of Guided Ground Transport Publ. No. 86-10, Maglev Technology Assessment, Task 5: Development Status of Major Maglev Subsystems and Critical Components.), 1986.
- Figure 2.0-2 Isometric view of single winding superconducting magnet for MLU-001-2 vehicle. (From Canadian Institute of Guided Ground Transport Publ. No. 86-10, Maglev Technology Assessment, Task 5: Development Status of Major Maglev Subsystems and Critical Components.), 1986.
- Figure 2.0-3 Concept development for anticipated Maglev modifications in the JNR program. (From *Railway Gazette International*, July 1990.)
- Figure 2.0-4 Basic features of the baseline Magneplane concept illustrating the saddle-shaped superconducting magnets and retractable wheels in the forward, mid and aft bogies, and the elliptical cross-section guideway with propulsion windings in which the vehicle is free to self-bank. (From Magneplane International Inc., *Master Plan, Part 2: Technical Plan*, Preliminary Draft, May 1990.)
- Figure 3.1-1 Illustration of the dimensions of a racetrack-shaped coil in real and in normalized space.
- Figure 3.1-2 Plot of hyperbolae: $JB_M = \text{constant}$.
- Figure 3.2-1 J_{cond} vs B for selected energy margins for a Nb_3Sn CICC at 4.5 K.
- Figure 3.2-2 J_{cond} vs B for selected energy margins for a Nb_3Sn CICC at 6 K.
- Figure 3.2-3 J_{cond} vs B for selected energy margins for a Nb_3Sn CICC at 8K.
- Figure 3.2-4 J_{cond} vs B for selected energy margins for a Nb_3Sn CICC at 10 K.
- Figure 3.2-5 J_{cond} vs B for selected energy margins for a NbTi CICC at 4.5 K.
- Figure 3.2-6 J_{cond} vs B for selected energy margins for a NbTi CICC at 6 K.
- Figure 3.2-7 J_{cond} vs B for selected energy margins for an epoxy-impregnated Nb_3Sn winding at 4.5 K.
- Figure 3.2-8 J_{cond} vs B for selected energy margins for an epoxy-impregnated NbTi winding at 4.5 K.

- Figure 3.4-1 Dimensionless function F_M for maximum magnetic field experienced by the racetrack with $\nu = 5$ and $\gamma = 0.4$.
- Figure 3.4-2 Contours of dimensionless lift function, F_p for racetrack with $\nu = 5$ and $\gamma = 0.4$.
- Figure 4.1-1 Three CICC conductors used in the Large Coil Task. (Adapted from Figure 3, *Fusion Engineering and Design*, Vol. 7, 1988, p. 6.)
- Figure 4.1-2 Sheathing process for the Westinghouse conductor.
- Figure 4.1-3 Sample cable-in-conduit conductor consisting of 27 strands of multifilamentary copper-stabilized superconductor in a stainless steel sheath (full size $\sim 0.2 \times 0.2$ in.).
- Figure 4.1-4 Critical current density vs flux density at several operating temperatures for the conductor.
- Figure 4.2-1 Weight of commercial cryocoolers vs refrigeration capacity in watts. (From J. L. Smith et al., *Survey of the State-of-the-Art of Miniature Cryocoolers for Superconductive Devices*, NRL Memo Report 5490, December 1984.)
- Figure 4.2-2 Specific power (i.e., power input divided by refrigeration capacity) vs temperature for commercial cryocoolers. (From J. L. Smith et al., *Survey of the State-of-the-Art of Miniature Cryocoolers for Superconductive Devices*, NRL Memo Report 5490, December 1984.)
- Figure 4.3-1 Dipole levitation module.
- Figure 4.3-2 Major components of levitation coil module (cryostat cover removed).
- Figure 4.3-3 Major components of levitation coil module (cryostat cover and thermal radiation shield removed).
- Figure 4.3-4 Cold mass support.
- Figure 4.3-5 Major components of dipole module.
- Figure 4.3-6 Racetrack coil dimensions.
- Figure 4.3-7 Computed loads of EM origin on the racetrack coil.
- Figure 4.3-8 Computed Von Mises stresses in the support shell.
- Figure 4.3-9 Computed vertical displacements of coil and form due to lift and internal EM loads (meters).

Figure 4.3-10 Computed lateral displacement of coil and form due to lift and internal EM loads.

Figure 4.3-11 Computed axial displacement of coil form due to lift and internal EM loads.

Figure 4.3-12 Finite element model using quadrant symmetry for analysis of a cold mass support.

Figure 4.3-13 Stress contours in the cold mass support which is displaced due to loading.

Figure 4.3-14 Displacement contours for the cold mass support under load.

Figure 4.3-15 Schematic of two options for charging a superconducting coil for MAGLEV applications.

Figure 4.4-1 Normalized lift vs speed for several coil heights above a sheet guideway.

Figure 4.4-2 Normalized drag vs speed for several coil heights above a sheet guideway.

Figure 4.4-3 Lift/drag ratio vs speed for several coil heights above a sheet guideway.

Figure A-1 Sheet guideway of thickness, T , and conductivity, σ , moving with velocity, V , relative to a coil carrying a current, I .

1.0 Introduction and Summary

Superconducting coil systems have been utilized in large scale applications in high energy physics, power conversion, magnetic separation, magnetohydrodynamics, fusion and in a myriad of laboratory scale devices. Their commercial application is now well known in medical applications using Magnetic Resonance Imaging (MRI) systems. The ability to create and maintain magnetic fields with superconducting coils is the enabling technology for the feasibility of Maglev because the power required for conventional coil systems would be prohibitive.

The superconducting coils on a Maglev vehicle can be used for two functions: levitation and propulsion. Levitation can be achieved by interacting with the eddy currents induced in an electrically conducting, sheet-like guideway or in passive coils in the guideway. Superconducting propulsion coils on the vehicle also operate in the DC mode and develop the necessary thrust by interacting with the traveling field produced by a conventional winding in the guideway in the form of a linear synchronous motor. In some Maglev concepts, the levitation and propulsion functions are performed independently by different sets of coils on the vehicle and in others, the functions are combined in the same coils.

The three basic options for cooling MAGLEV superconducting coil systems using the so-called low critical temperature materials available today are:

- a) winding immersion in a bath of liquid helium at near saturation conditions;
- b) winding impregnation with epoxy and cooling by conduction to a cold reservoir or refrigeration system; and
- c) use of a CICC (Cable-in-Conduit-Conductor) in which the conductor is a cable of strands of superconductor in a conduit carrying single phase, supercritical helium.

Historically, cooling by immersion in a saturated bath at close to atmospheric pressure (option a) was the approach first studied experimentally and analytically to develop criteria and conditions for stable operation of superconducting coils. This two phase helium approach is complex for a MAGLEV system because of the continuously changing body forces due to acceleration, deceleration, elevation change, and curve execution. The result is a helium cryostat which must be baffled in a complicated fashion and which is subject to high thermal losses because of sloshing of the liquid phase into "warm" sections of the vessel. As a result we have chosen to eliminate this option for MAGLEV systems.

In option b, the approach is based on conduction cooling of an epoxy impregnated winding to either a helium bath, imbedded cooling tube, or the cold end of a refrigeration system. It may present difficulties in a MAGLEV application because of the poor thermal diffusivity of the composite winding. The difficulty involves the limited ability to remove the losses generated throughout the winding as a result of the continuously generated current and field transients which can be expected from coil and track transverse relative motion.

The option c approach to superconducting coil design is to use a conductor consisting of a cable of superconductors in a metal sheath. The sheath serves as a conduit for the helium coolant which flows in the interstices among the cable strands. The operating pressure is chosen to be above 2.2 atm, hence, the helium can only exist in a single phase. As a result, the problems of controlling the liquid-vapor interface which are associated with a two phase system as in option a, are eliminated. The stability and operating characteristics of this type of system have been under study for many years and have been demonstrated in coil systems much larger than those necessary for MAGLEV applications.

We have reviewed several configurations for existing and conceptual levitation coil geometries. The goal was to select a shape for use in a levitation coil system conceptual design task. Toward this end we have decided to use a general, "racetrack" shaped, coil geometry because this is either the baseline in the cases reviewed or topologically very close to the geometries used. The field level trade study task in this program has shown that the lift force per unit (coil+cryostat) weight is proportional to a dimensionless parameter consisting of the product of the conductor current density, j , and maximum field, B_M , experienced by the winding divided by the winding weight density. It also showed that the lift force per unit weight was proportional to a dimensionless function of dimensionless parameters containing coil shape, track, and speed characteristics, and dewar features, but no variables contained in the preceding dimensionless group, which was conductor related. As a result, the conclusion was that we would like to design at the maximum product of jB_M for the conductor, consistent with its stability requirements.

The design of the conductor and coil windings depend on the level of the losses to be removed in the steady state and under the transients associated with current and field changes during operation. The ability of a particular conductor and cooling option to be tolerant or "robust" relative to disturbances or local energy dissipation may be measured by its stability margin.

Estimates have been made for the energy (stability) margin that could be achieved with Nb_3Sn and $NbTi$ conductors in CICC and in impregnated winding configurations. The operational spectrum for the heat load due to transient conditions is not well known at present and will no doubt be the subject of extensive theoretical and experimental analyses in the future. However, if we postulate the need for an energy margin of a given level, say 100 mJ/cm^3 , then the operating point can be found. This is done by first selecting an operating temperature then finding a j and a B_M that gives the highest jB_M product while still satisfying the need for 100 mJ/cm^3 of energy margin. Results are given in Table 1.0-1.

Several conclusions can be drawn from the table:

- all systems optimize at a relatively low field level which ranges from 2.0 to 3.7 T
- the Nb_3Sn systems have substantially higher jB_M products than $NbTi$ at the same temperature; this product is directly proportional to the ratio of lift force to coil plus

Table 1.0-1
Operating Points for Selected CICC Conductors
and Temperatures to Maximize Lift per Unit Coil Weight
for an Energy Margin of 100 mJ/cm³

T [K]	Type	j [kA/cm²]	B_M [T]	jB_M [10⁷N/m³]	Relative F_L/W_c	Relative Power In¹
4.5	Nb ₃ Sn	92	3.7	340	1.0	1.0
4.5	NbTi	38	3.0	114	0.36	1.0
6.0	Nb ₃ Sn	74	3.4	252	0.74	0.75
6.0	NbTi	13	2.0	26	0.08	0.75
8.0	Nb ₃ Sn	46	2.6	120	0.35	0.55
8.0	NbTi	--	---	---	0	0.55
10	Nb ₃ Sn	24	2.0	48	0.14	0.44
10	NbTi	--	---	---	0	0.44

dewar weight for a given coil shape and track/speed characteristic, hence column 6 shows the ratio of F_L/W_c for each case relative to the first to illustrate the relative change [e.g., 1) at 4.5K a NbTi coil will have only 36% of the lift of a Nb₃Sn coil of equivalent weight and 2) Nb₃Sn at 8K has a decrease in lift to 35% of the value for the same weight coil operating at 4.5K]

-NbTi rapidly degrades in performance as temperature increases (e.g., at 8K or 10K it cannot provide the desired 100mJ/cc of energy margin)

-the last column is the ratio of Carnot efficiency for the first case to the Carnot efficiency for the specific line; since the Carnot efficiency is related to the power required by the refrigeration system, this illustrates the advantage of higher temperature operation (e.g., the cryosystem power required for 8K operation would be about 55% of that required for 4.5K operation); higher temperature operation could, therefore, substantially decrease the on-board power requirements for the vehicle

¹Relative Power In = Ratio of Carnot Efficiencies

As a result of this trade study the conceptual design was pursued on the basis of a Nb₃Sn CICC to operate at a temperature in the 8-10K range and with a maximum field level in the 2-4T range.

The module conceptual design is presented in Section 4.0. It is a racetrack in geometry using Nb₃Sn CICC conductor at a maximum temperature of 8 K. The basic size of the dewar envelope is 2.37 m x 0.6 m x 0.17 m and is shown in Figure 4.3-1. The current leads and cryogen vent portion is shown, but not needed on each module if several modules are electrically in series (as is expected).

The lift capability of the module moving relative to an aluminum sheet guideway at a speed of 150 m/s was estimated (section 4.4) and shown to range from 30,000 to 150,000 N depending on the distance from the coil centerline to the surface of the guideway. We believe that a distance of about 0.05 m from the coil center to the surface of the cryostat is practical at the current densities we expect to achieve, hence we assumed an ample clearance of 0.15 m which corresponds to a lift per module of 50,000 N to set the amp turn requirement in the design at 2.4×10^5 A. The total weight per module is then estimated at 2290 N or 234 kg hence the lift capacity is at least 25:1 and could be as high as 75:1 if smaller clearances were found to be feasible. It may also be possible to increase this value through optimization of the lift coil geometry, an activity which was not pursued extensively in this study.

The module chosen was analyzed for use as a lift coil to illustrate the primary features of a magnet system for this function. If it were used as a propulsion coil, it would have similar features, but would probably have different dimensions and a different amp-turn requirement. These would depend on the characteristics of the synchronous winding in the guideway.

The heat loads for the lift modules were estimated in conjunction with assumed series connections among modules for vehicle lift requirements of 3×10^5 N (6 lift modules) and 6×10^5 N (12 lift modules), as examples. For these cases, the heat loads were found to be in the range of capabilities for commercial units and would require cryosystem weights of 1.76×10^4 - 2.55×10^4 N, respectively, and power inputs of 30-55 kW.

The examples given were not optimized for any particular vehicle or system and, as a result, may be expected to be improved in a more comprehensive study. The most significant output from this study is that it shows the feasibility and advantage of using a CICC and, in particular, the advantage of using Nb₃Sn in a CICC at a temperature in excess of usual superconducting magnet design practice, that is, 8 K as opposed to about 4.5 K. The increased operating temperature would be expected to result in a significant decrease in refrigeration system weight and on-board power requirement.

2.0 Selection of Magnet Geometry

We have reviewed several configurations for existing and conceptual levitation coil geometries. The goal was to select a shape for use in the conceptual levitation coil system design task. Toward this end we have decided to use a general, "racetrack" shaped, coil geometry because this

is either the baseline in the cases reviewed or topologically very close to the geometries used.

Figure 2.0-1 shows the cross sectional sketch of the guideway and vehicle at the Miyazaki test facility. It shows the location of the superconducting levitation coils with planes vertical on each side of the lower part of the train. An isometric cutaway of one of the levitation modules is shown in Figure 2.0-2. This indicates the straight side sections and curved ends of the coil form with the winding in a single plane and is typically referred to as a "racetrack" coil geometry. The superconducting coils for the proposed modifications to the Japanese system are illustrated in the inset "Fig 3" of Figure 2.0-3 and are also expected to be racetracks in shape.

Figure 2.0-4 shows the basic features of the Magneplane concept. This system uses superconducting coils which are somewhat curved out-of-plane to conform to the shape of the guideway, but are still very close to being racetrack in shape.

A review of the literature found varying degrees of definition and detail for the levitation coil systems. As a result, we chose a generic racetrack geometry in a single plane for the shape to be used in our field level trade studies. This allowed us to vary design parameters such as current density, field level, coil size, coil cross-sectional shape, and operating temperature to search for an optimum in terms of a selected "cost functional." Initially, the latter was chosen to be coil lift force per unit coil weight, however, the approach is quite general. Later in our program we used a simplified model to show that the same parameter should be optimized if the dewar weight was also included.

3.0 Field Level Trade Study

The previous section showed several magnet geometries of interest for MAGLEV and concluded that a racetrack shape was generic in that it was representative of the most likely fundamental geometry or was similar to more complicated options.

In this section we shall explore the impact of scale and shape of the racetrack on selected optimization parameters. This will allow us to separate the effects of shape from the identification of the desirable properties of the conductor. The latter will be used in Section 3.2 to show the desirability of Nb_3Sn relative to $NbTi$, as well as the advantages of the CICC configuration. Section 3.3 proceeds to combine the results and discuss selection of an operating current and field level; section 3.4 will give some preliminary results from parametric studies on coil shape; section 3.5 will include the weight of the dewar in the optimization process. Section 3.6 will show that the total levitation system weight for a given lift can be reduced by minimizing the number of life modules.

3.1 Parameters for Optimization of Lift per Unit Coil Weight

This section will use a simple form of a "cost functional" for lift optimization to allow separation of the desirable features of a conductor from the desirable features of the coil geometry for MAGLEV. By considering electromagnetic principles alone, it will show that the advantageous

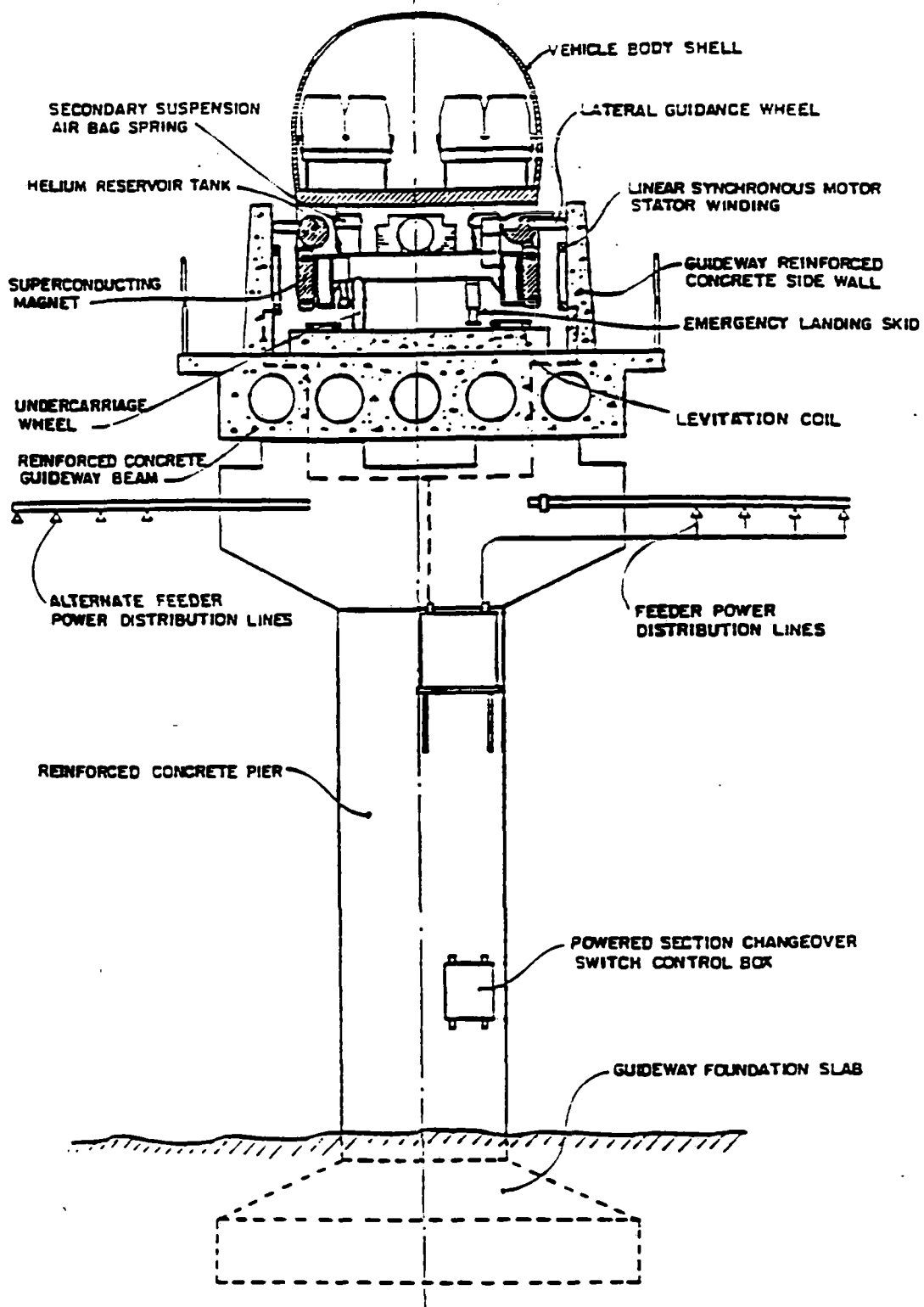


Figure 2.0-1 Typical cross section of Miyazaki test facility elevated guideway with MLU-001 test vehicle. (From Canadian Institute of Guided Ground Transport Publ. No. 86-10, Maglev Technology Assessment, Task 5: Development Status of Major Maglev Subsystems and Critical Components, 1986.)

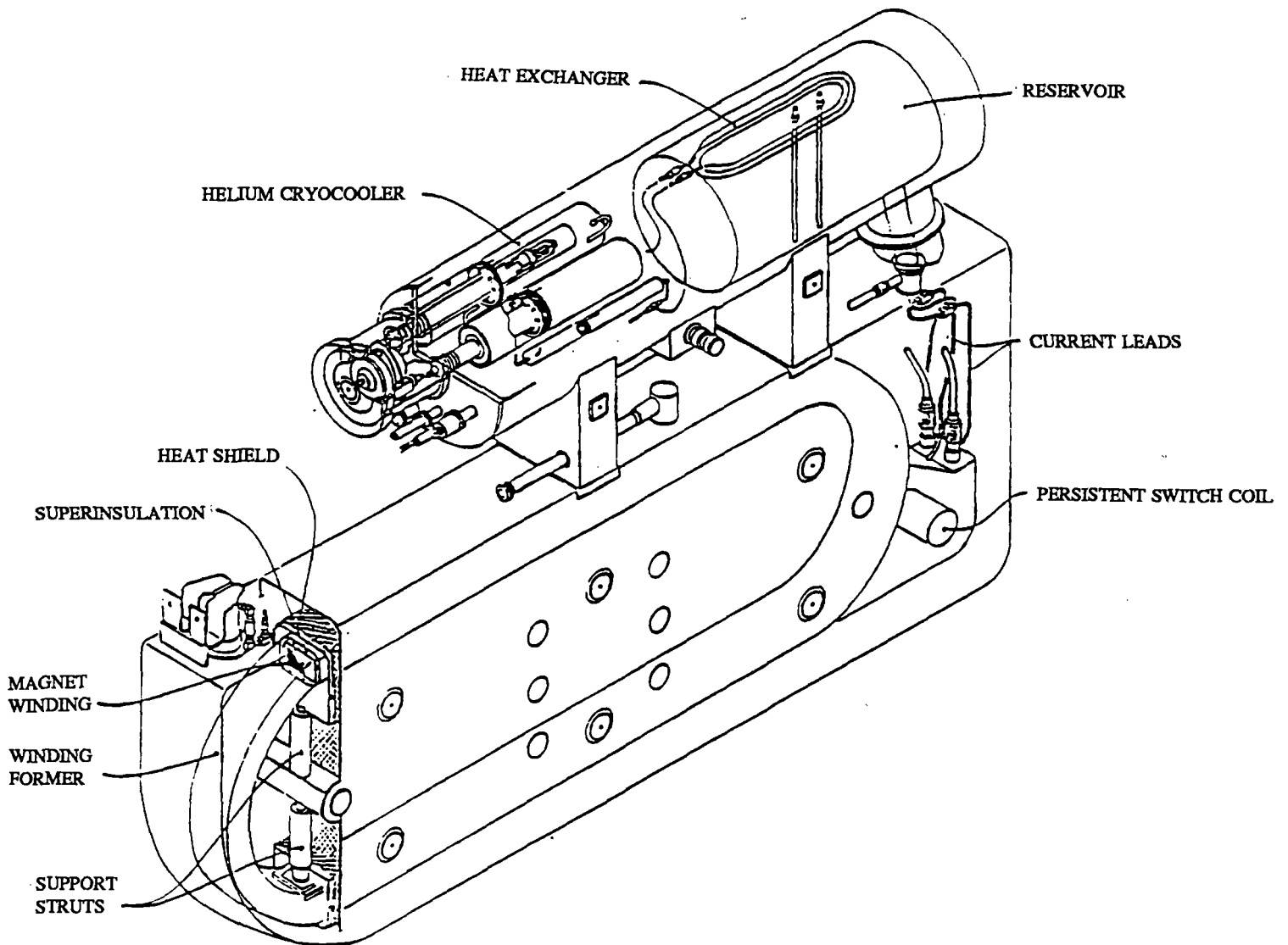


Figure 2.0-2 Isometric view of single winding superconducting magnet for MLU-001-2 vehicle. (From Canadian Institute of Guided Ground Transport Publ. No. 86-10, Maglev Technology Assessment, Task 5: Development Status of Major Maglev Subsystems and Critical Components, 1986.)

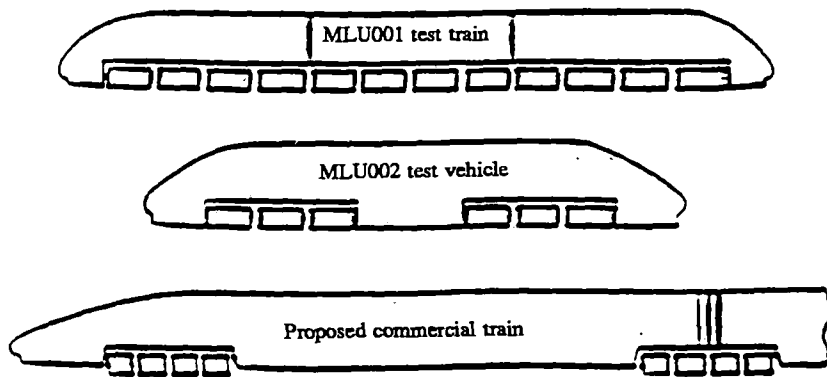


Fig. 1 Whereas the superconducting coils were distributed evenly along the length of the MLU001 test vehicle, they are mounted on articulated bogies on the proposed commercial train.

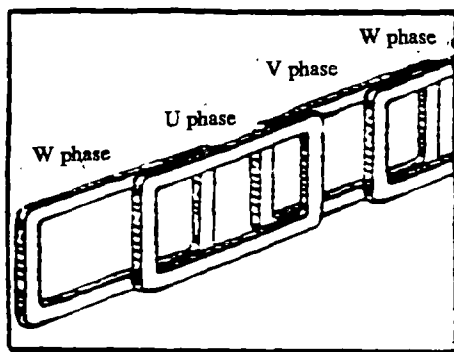


Fig. 2 Propulsion coils on the new maglev test track will be arranged in two overlapping layers on the siderails

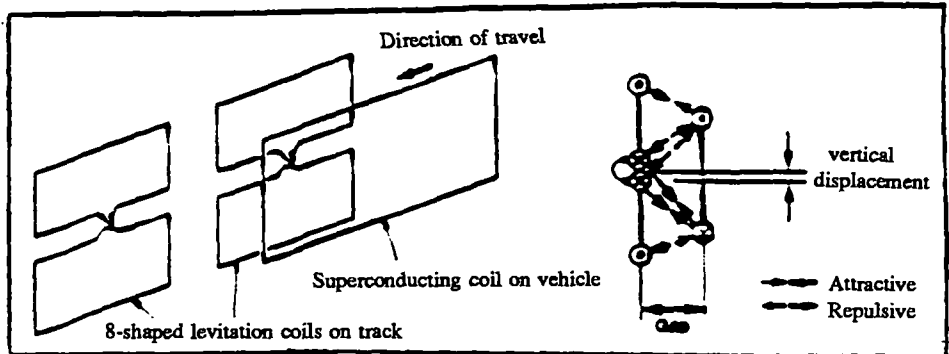


Fig. 3 The siderail levitation system used 8-shaped coils (left) to generate attraction and repulsion forces (right) which support the maglev vehicle

Fig. 4. The overlapping layers of propulsion coils and the 8-shaped coils for levitation and guidance are all mounted on the siderails of the trough guideway

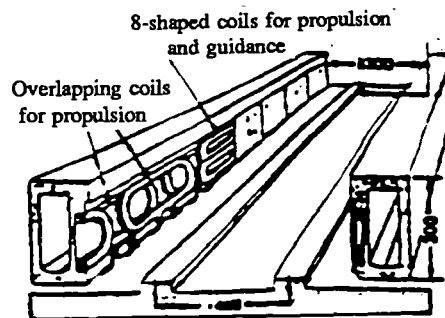


Figure 2.0-3 Concept development for anticipated Maglev modifications in the JNR program. (Adapted from *Railway Gazette International*, July 1990.)

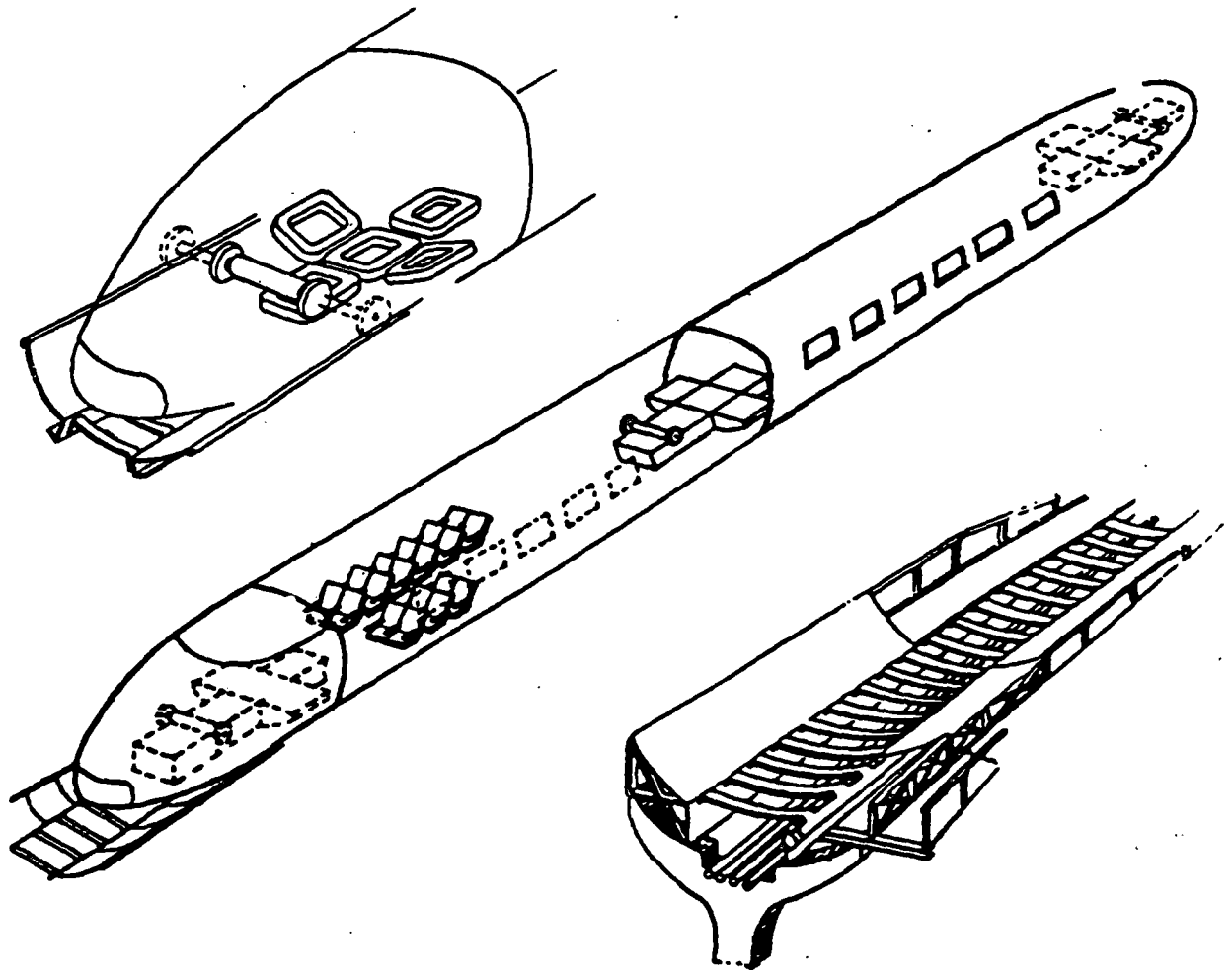


Figure 2.0-4 Basic features of the baseline Magneplane concept illustrating the saddle-shaped superconducting magnets and retractable wheels in the forward, mid and aft bogies, and the elliptical cross-section guideway with propulsion windings in which the vehicle is free to self-bank. (From Magneplane International Inc., *Master Plan, Part 2: Technical Plan*, Preliminary Draft, May 1990.)

conductor is one which allows a maximum value of the product of the winding current density and maximum field experienced by the winding, divided by the density of the winding. In sections 3.2 and 3.3, this requirement will be combined with a stability requirement for superconductor operation and the characteristics of specific conductors, to show that a CICC using Nb₃Sn has a decided advantage over NbTi, and that the Nb₃Sn winding design optimizes at a maximum magnetic field level of 2-4 T.

A reasonable goal for a levitation coil system is to achieve a maximum lift per unit levitation system weight, where the latter includes the coil, cryostat (dewar), cryosystem, etc. This is based on the assumption that it is desirable to reduce the weight (and presumably cost) of components other than "payload". At this stage we shall consider only the weight of the coil and will add the impact of the cryostat and the refrigeration system in a later section. Hence, we now wish to optimize the maximum lift per unit coil weight. To do this we must first consider the form of the equations for coil weight, lift, and the maximum field experienced by the coil.

Figure 3.1-1 shows a generic, racetrack-shaped, lift coil with dimensions defined in real space and in normalized space. The latter dimensions are obtained by normalizing all the real space dimensions to the coil inner dimension, r_i. The weight of the coil may now be shown to be of the form (see Appendix A):

$$W_c = \rho_c \lambda r_i^3 F_w(\alpha, \beta, v) \quad (3-1)$$

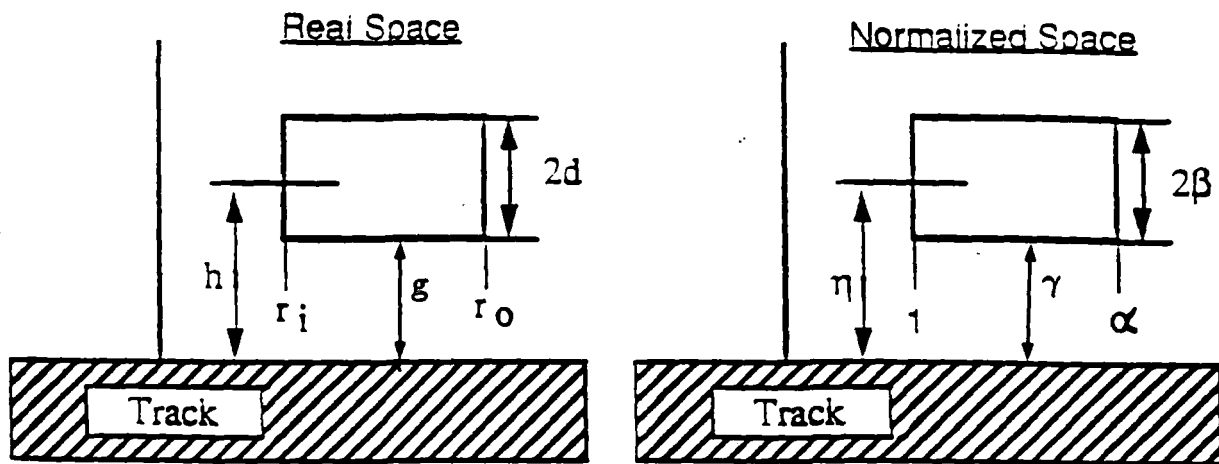
where: ρ_c=weight density for the coil materials
 λ =packing factor for the coil materials in the coil envelope
 F_w=dimensionless function of the dimensionless shape factors α, β, and v

The lift force on the coil may be shown to be of the form (see Appendix A):

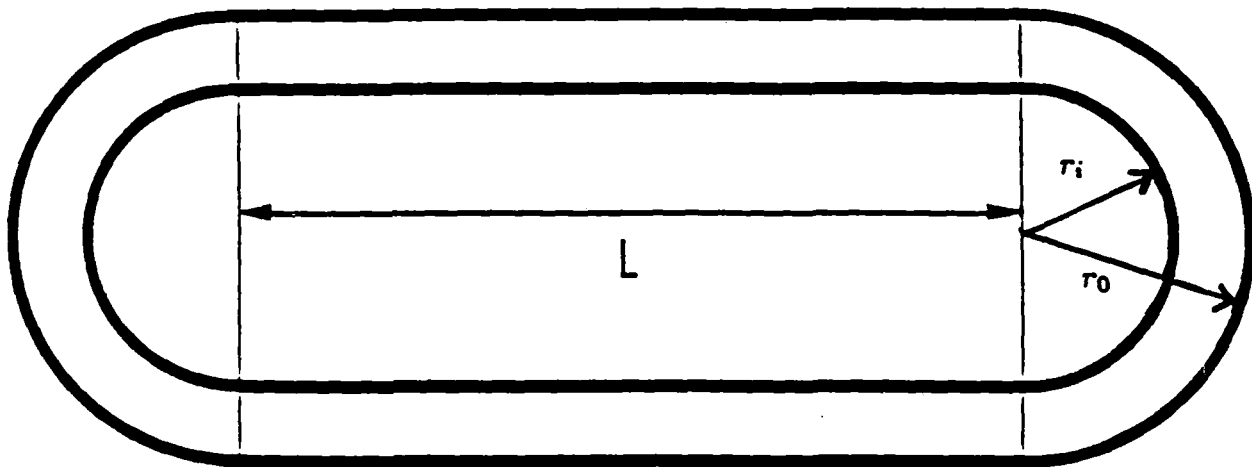
$$F_L = \mu_0 (\lambda j r_i^2)^2 G(R_m, T/g, \gamma, \alpha, \beta, v) \quad (3-2)$$

where: R_m=μ₀σVg=magnetic Reynolds number
 μ₀=permeability of free space
 j =conductor current density
 σ =track conductivity
 V =vehicle velocity
 g =distance from coil lower surface to track (Fig 3.1-1)
 T =track thickness
 γ = g/r_i
 G =dimensionless function of dimensionless parameters

It is important to note here that G is a dimensionless function that is dependent on shape and dimensionless system characteristics, but that it is independent of scale or coil conductor



$$\alpha \equiv \frac{r_o}{r_i}, \quad \beta \equiv \frac{d}{r_i}, \quad \eta \equiv \frac{h}{r_i}, \quad \gamma \equiv \frac{g}{r_i}$$



$$\nu \equiv \frac{L}{r_i}$$

Figure 3.1-1 Illustration of the dimensions of a racetrack-shaped coil in real and in normalized space.

characteristics such as current density.

The maximum field experienced by the coil may be shown to have the form (see Appendix A):

$$B_M = \mu_0 \lambda j r_i F_M(R_m, T/g, \alpha, \beta, \nu, \gamma) \quad (3-3)$$

where F_M is another dimensionless function of the parameters indicated.

Combining the above equations to obtain an expression for the lift force per unit coil weight leads to (see Appendix A):

$$\frac{F_L}{W_c} = \frac{j B_M}{\rho_c} F_p \quad (3-4)$$

where: $F_p = G/(F_w F_M)$

F_p is a dimensionless function which is dependent on shape and dimensionless system characteristics since it is a combination of the previously defined functions G , F_w , and F_M . F_p is also independent of scale and of the lift coil conductor characteristics that comprise the dimensionless group which precedes it. It implies that the geometry and system dimensionless characteristics such as the magnetic Reynolds number can be varied independently of the preceding dimensionless group in searching for an optimum.

The dimensionless group $j B_M / \rho_c$ implies that the lift force per unit coil weight for any coil shape or system can be maximized by finding a conductor that can operate at as high a product of current density and maximum field at the winding as possible while minimizing its weight density. This is an important conclusion that can be reached on the basis of electromagnetic effects alone without consideration of the capabilities of the particular type of conductor. It is also important to note that the conclusion is valid independent of scale.

Figure 3.1-2 is a plot of the hyperbolae represented by $j B_M = \text{constant}$. The previous paragraph implies that we would like to choose an operating point with as high a contour value as possible, but does not tell us where to locate the point on the plot. The operating point depends on the particular conductor and on stability issues, therefore, we will return to this point in section 3.3 after the conductor discussion in section 3.2. Section 3.4 will then give sample contour plots to illustrate the form of the dimensionless function F_p .

3.2 Comparison of Conductor Options

The three basic options for cooling superconducting coil systems using the so-called low critical temperature (T_c) materials available today are:

- a) immersion of the winding in a bath of liquid helium at near saturation conditions;

PLOT OF CONSTANT VALUES OF
 $J_{cond} \cdot B$

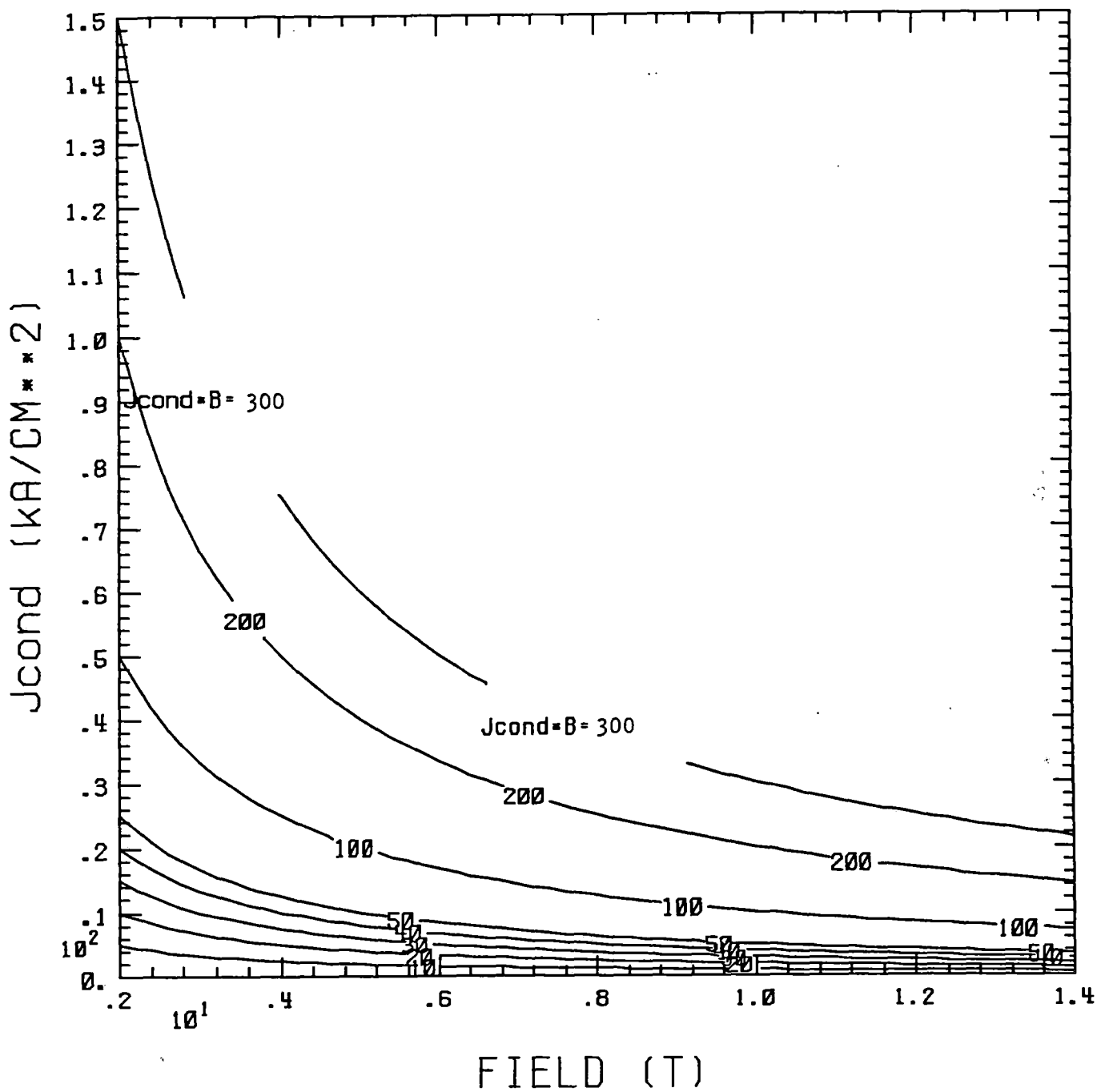


Figure 3.1-2 Plot of hyperbolae: $J_{B_M} = \text{constant}$

b) impregnation of the winding with epoxy and cooling by conduction to a cold reservoir or refrigeration system; and

c) use of a CICC conductor in which the conductor is a cable of strands of superconductor in a conduit carrying single phase, supercritical helium.

Historically, cooling by immersion in a saturated bath at close to atmospheric pressure (option a) was the approach first studied experimentally and analytically to develop criteria and conditions for stable operation of superconducting coils. Local cooling capability for a conductor tends to be very high provided a nucleate boiling condition can be maintained when needed. This is often accomplished by reduction of the maximum possible heat flux generated and provision for liquid replenishment (i.e., prevention of local dryout). This two-phase helium approach is complex for a MAGLEV system because of the continuously changing body forces due to acceleration, deceleration, elevation change, and curve execution. The result is a helium cryostat which must be baffled in a complicated fashion and which is subject to high losses because of sloshing of the liquid phase into "warm" sections of the vessel. As a result we have eliminated this option for MAGLEV systems.

In option b, the approach is based on conduction cooling of an epoxy-impregnated winding by either a helium bath, imbedded cooling tube, or the cold end of a refrigeration system. It may present difficulties in a MAGLEV application because of the poor thermal diffusivity of the composite winding. The difficulty involves the limited ability to remove the losses generated throughout the winding as a result of the continuously generated current and field transients which can be expected from coil and track transverse relative motion.

The option c approach to superconducting coil design is to use a conductor consisting of a cable of superconductors in a metal sheath. The sheath serves as a conduit for the helium coolant which flows in the interstices among the cable strands. The operating pressure is chosen to be above 2.2 atm, hence, the helium can only exist in a single phase. As a result, the problems of controlling the liquid-vapor interface which are associated with a two-phase system as in option a, are eliminated. The stability and operating characteristics of this type of system have been under study for many years and demonstrated in coil systems much larger than those necessary for MAGLEV applications (see section 4.1).

The design of the conductor and coil windings for options b and c depend strongly on the level of the joule losses to be removed. These will be the result of the transients associated with current and field changes during operation. The latter have to be estimated based on levitation system and coil details, however, the ability of a particular conductor and cooling option to be tolerant or "robust" relative to disturbances or local energy dissipation may be measured by the conductor's stability margin.

The balance of this section will present stability margin estimates for NbTi and for Nb₃Sn conductors for typical epoxy-impregnated winding configurations and for typical CICC configurations. Results will show that Nb₃Sn always has a higher stability margin than NbTi and

that the CICC has a substantially higher stability margin than the epoxy-impregnated case. As a result we selected a Nb₃Sn CICC for the conceptual design. The definition of the conductor characteristics is given in section 4.1.

The stability margin is the amount of energy per unit volume that can be absorbed by the winding in a particular conductor and cooling configuration without creating an unstable conductor operating condition. The insulation and epoxy in a conduction cooled system severely limit the ability to remove dissipated energy because of the relatively low thermal diffusivity of the configuration. This is alleviated in a CICC configuration because of the direct contact of the strands with the cooling medium and the relatively large surface area for heat transfer. It also makes direct use of the relatively high thermal capacity of the helium which is orders of magnitude higher than the metals at these temperatures.

The selection of conductor material also has a strong influence on the level of the available stability margin because the thermal capacity of materials is a strong function of temperature and Nb₃Sn has a much higher critical temperature than NbTi.

The conductor configuration that was selected for energy margin estimates is a stainless steel clad, 54-strand cable of Nb₃Sn (described in Section 4.1). The energy margin for the conductor is the maximum energy input per unit conductor volume that will not result in a transition from the superconducting state and propagating resistive zone (quench) in the conductor. This is a function of the conductor material thermal and critical properties, cooling configuration, operating temperature, field level, fraction of critical current, and coolant properties, and requires a detailed computation involving the transient thermal characteristics of the winding configuration. Table 3.2-1 gives a comparison of the critical current densities that would be expected for CICC conductors based on Nb₃Sn or on NbTi for equivalent cable dimensions. Figures 3.2-1 to 3.2-4 show contours of energy margin as a function of conductor current density and field level for the Nb₃Sn CICC at temperatures of 4.5, 6, 8, and 10 K. It is clear that the available energy margin decreases with increasing operating temperature and is of the order of several hundred mJ/cm³ for this conductor.

Similar energy margin plots were generated for a NbTi CICC conductor and are given in Figures 3.2-5 and 3.2-6. Two trends are evident: 1) at a given temperature (e.g., 4.5 K---see Figures 3.2-1 and -5) the Nb₃Sn CICC has a factor of 5 or more times the energy margin compared to the NbTi CICC for a given current density and field level which implies that it is more robust to energy disturbances or, if a given disturbance level is chosen, it can operate at a higher current density and field; and, 2) the NbTi energy margin disappears rapidly with temperature, which implies that the Nb₃Sn system can be run at considerably higher temperature levels for a given conductor current density, energy margin, and field level. This allows a considerable decrease in weight and higher efficiency in the refrigeration system (see section 4.2).

CROSS PLOT OF JCOND VS FIELD
FOR SELECTED ENERGY MARGINS

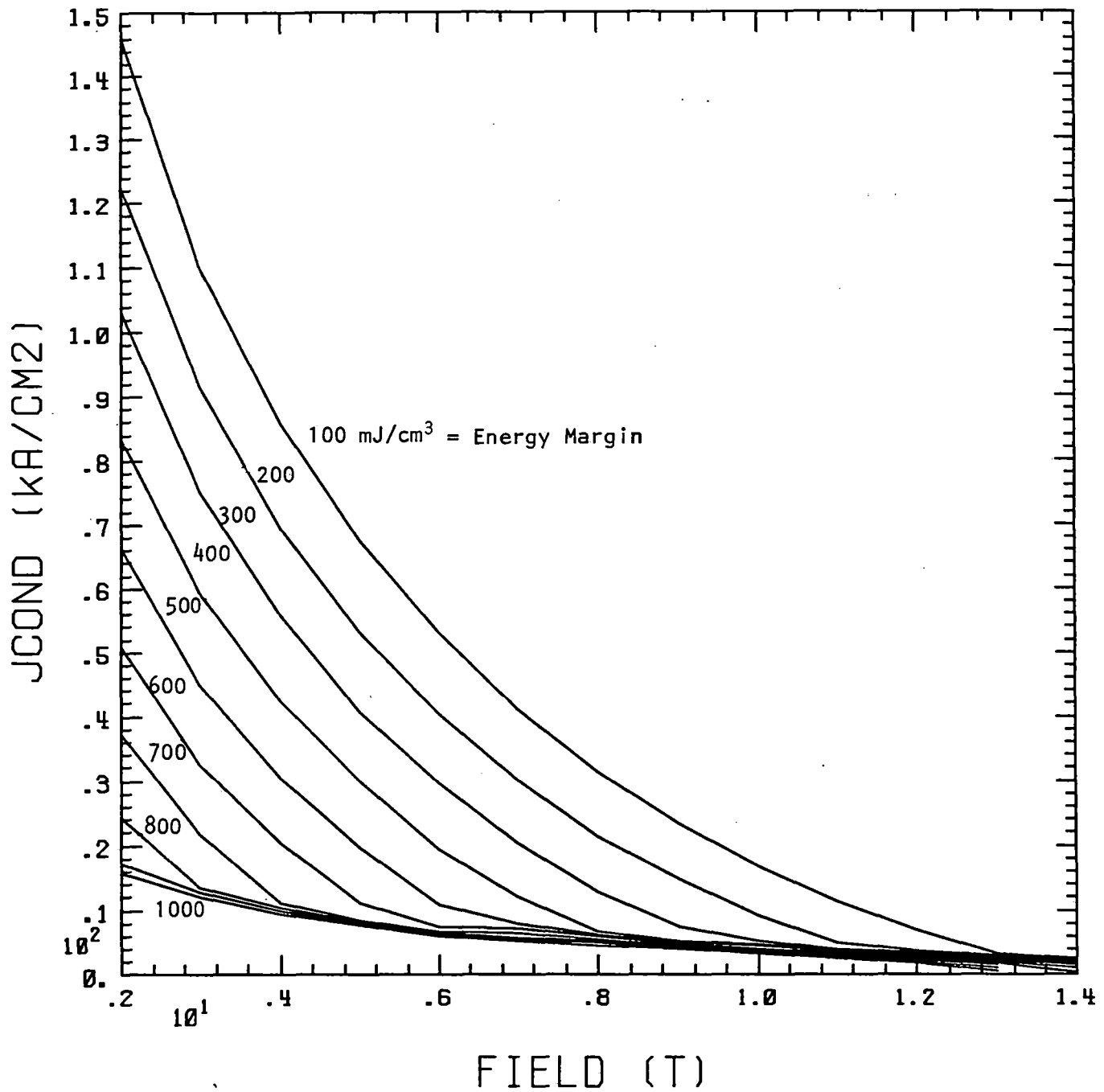


Figure 3.2-1 J_{cond} vs B for selected energy margins for a Nb₃Sn CICC at 4.5 K

CROSS PLOT OF JCOND VS FIELD FOR
SELECTED ENERGY MARGINS in Nb₃Sn (T=6K)

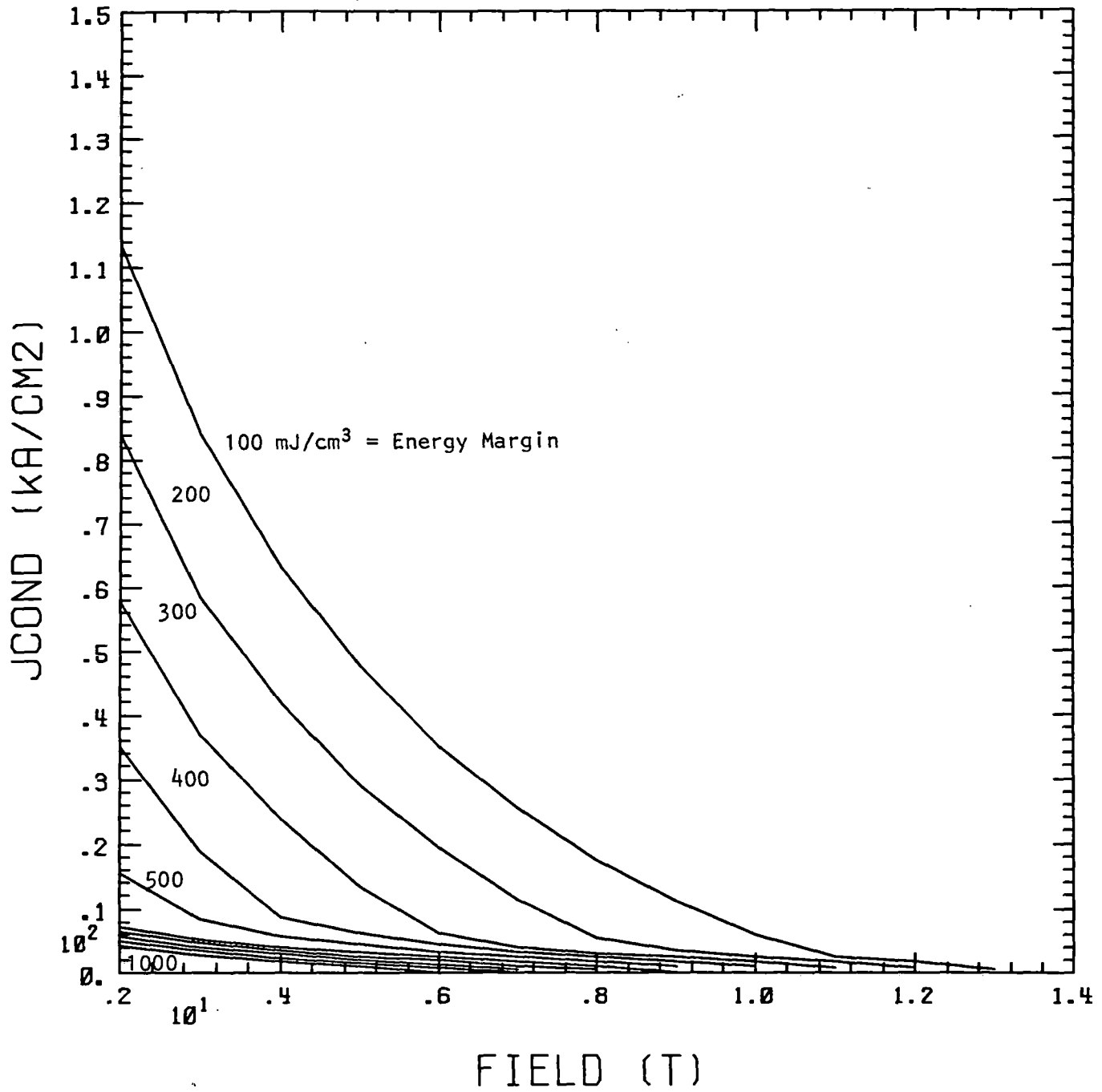


Figure 3.2-2 J_{cond} vs B for selected energy margins for a Nb₃Sn CICC at 6 K

CROSS PLOT OF JCOND VS FIELD FOR
SELECTED ENERGY MARGINS in Nb₃Sn (T=8K)

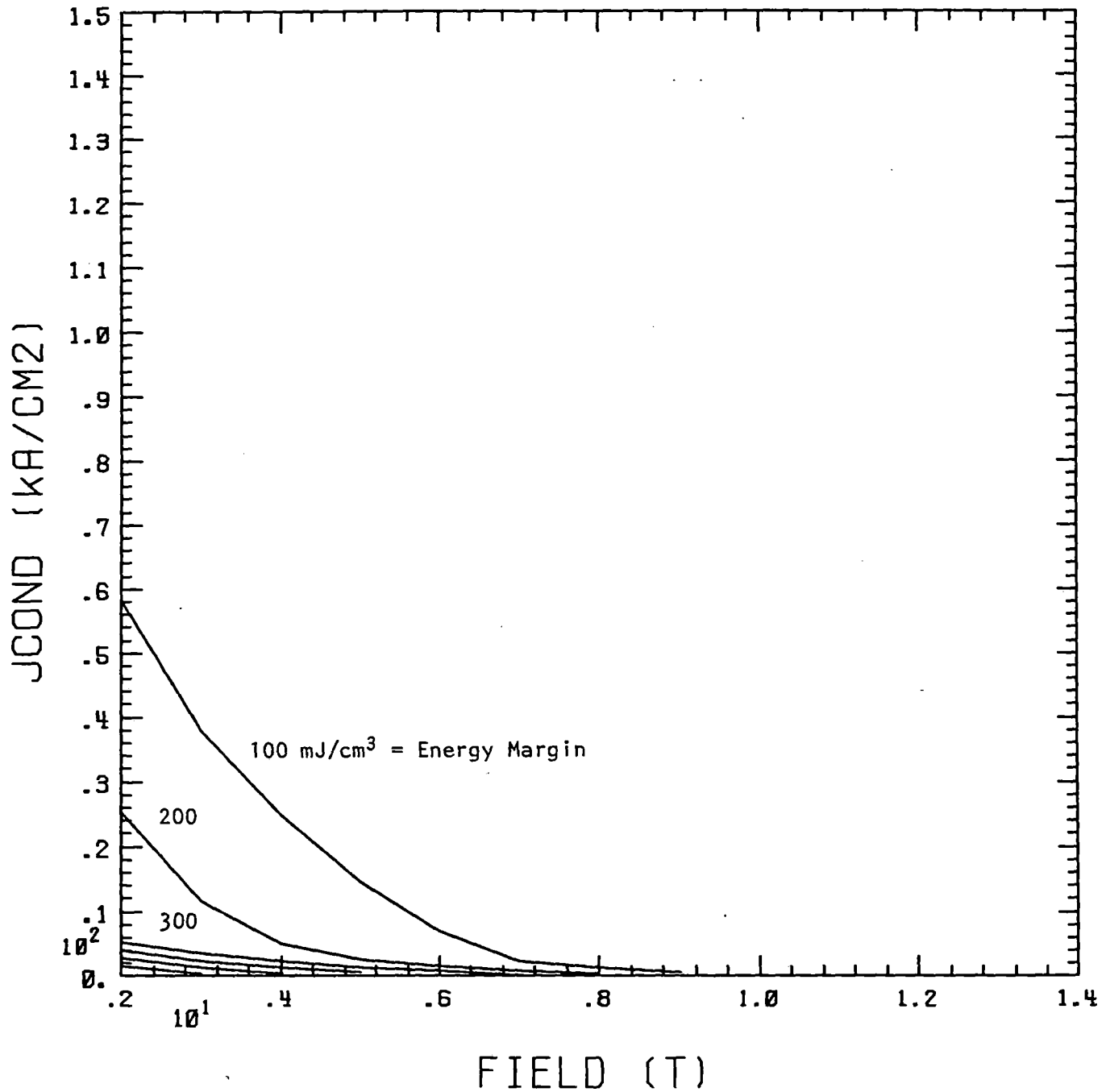


Figure 3.2-3 J_{cond} vs B for selected energy margins for a Nb₃Sn CICC at 8 K

CROSS PLOT OF JCOND VS FIELD FOR
SELECTED ENERGY MARGINS in Nb₃Sn (T=10K)

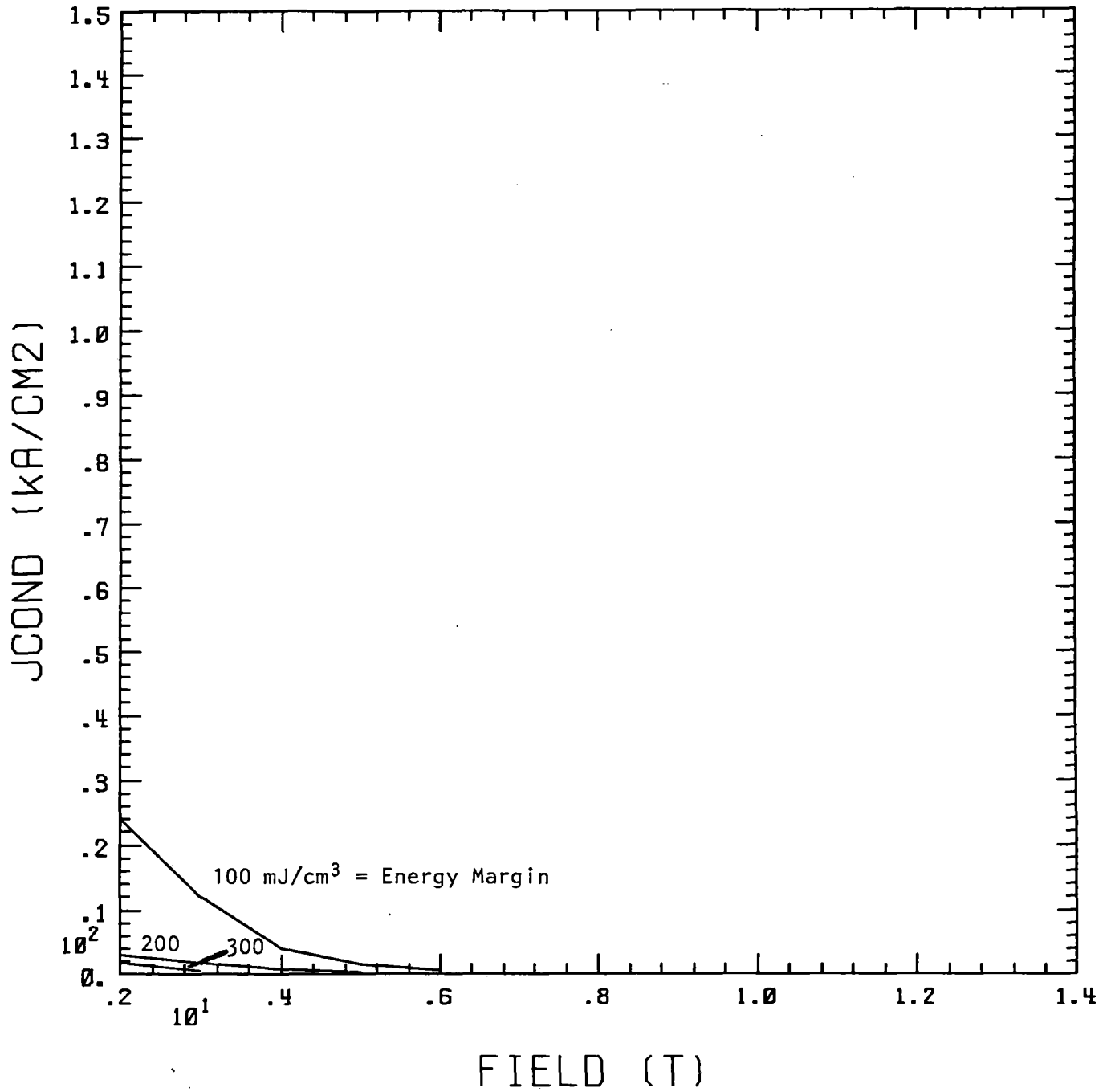


Figure 3.2-4 J_{cond} vs B for selected energy margins for a Nb₃Sn CICC at 10 K

CROSS PLOT OF JCOND VS FIELD FOR
NbTi ENERGY MARGINS (T=4.5K)

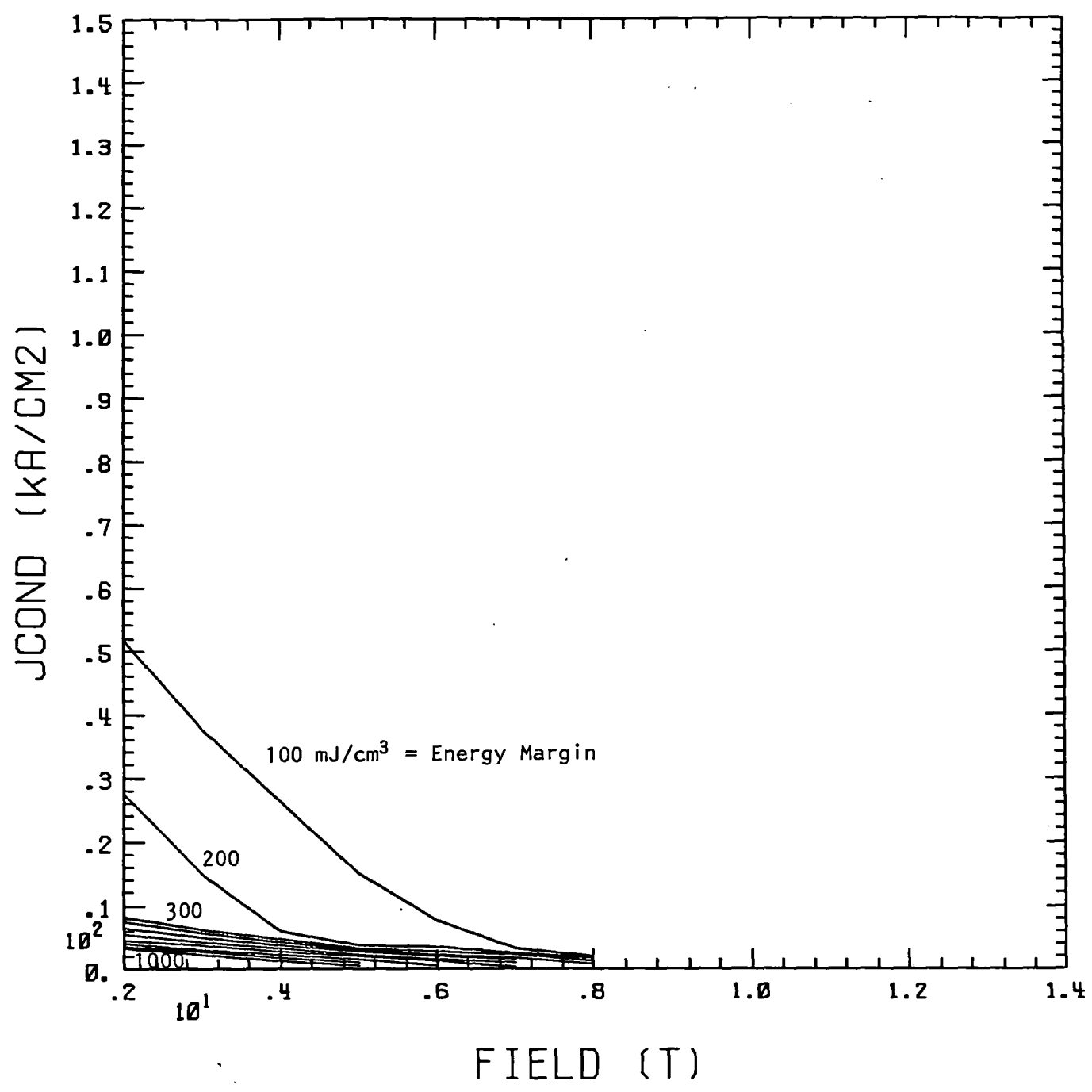


Figure 3.2-5 J_{cond} vs B for selected energy margins for a NbTi CICC at 4.5 K

CROSS PLOT OF JCOND VS FIELD FOR
NbTi ENERGY MARGINS (T=6.0K)

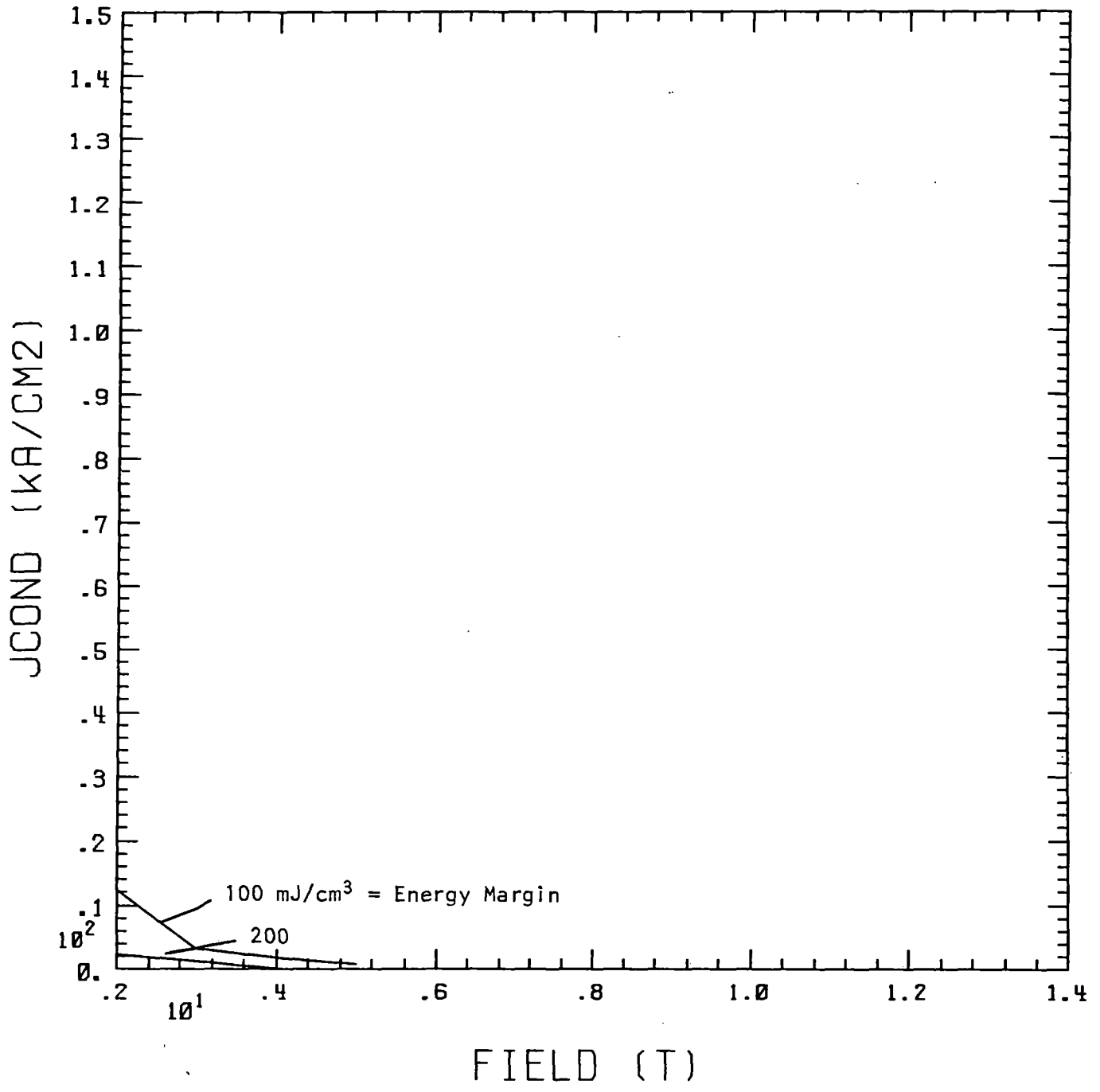


Figure 3.2-6 J_{cond} vs B for selected energy margins for a NbTi CICC at 6 K

Table 3.2-1
Critical Current Densities for CICC Conductors
Based on NbTi and Nb₃Sn

T	B	NbTi	Nb ₃ Sn
[°K]	[T]	[kA/cm ²]	[kA/cm ²]
4.5	2	82	168
	4	53	102
	6	26	64
6.0	2	50	140
	4	20	83
	6	2	50
8.0	2	10	102
	4	--	54
	6	--	31

Figures 3.2-7 and 3.2-8 show the energy margin at 4.5 K for Nb₃Sn and NbTi, respectively, based on the conductor alone to approximate the energy margin available in a winding that is epoxy impregnated. A comparison of Figure 3.2-7 with 3.2-1 for Nb₃Sn and of Figure 3.2-5 with 3.2-8 for NbTi show the drastic reduction in energy margin for the epoxy-impregnated cases relative to the CICC cases.

For comparison purposes, the Japanese MLU-002 levitation coil system uses an epoxy impregnated, NbTi conductor at a current density of about 20 kA/cm² and a field level of 4.7 T. Figure 3.2-8 shows that the energy margin for this configuration would be about 7 mJ/cm³. This is quite low and may help to explain the problems experienced with reliable operation of this type of design. Figure 3.2-1 shows that a CICC Nb₃Sn conductor at this same field level and current density would have an energy margin of about 550 mJ/cm³. Furthermore, at 8 K, as is shown in Figure 3.2-3, the Nb₃Sn conductor would have an energy margin of about 100 mJ/cm³ which may be more than sufficient, and would then allow the system to take advantage of cryocooler system weight reductions and increases in efficiency.

The level of energy margin required for a MAGLEV system must be estimated based on the details of the levitation system and will be the subject of future design and experimental programs. However, the present preliminary estimates confirm the substantially higher available energy margin associated with using Nb₃Sn in CICC form, hence we have selected it as the

CROSS PLOT OF JCOND VS FIELD FOR
 Nb3Sn ENERGY MARGINS W/O He (T=4.5K)

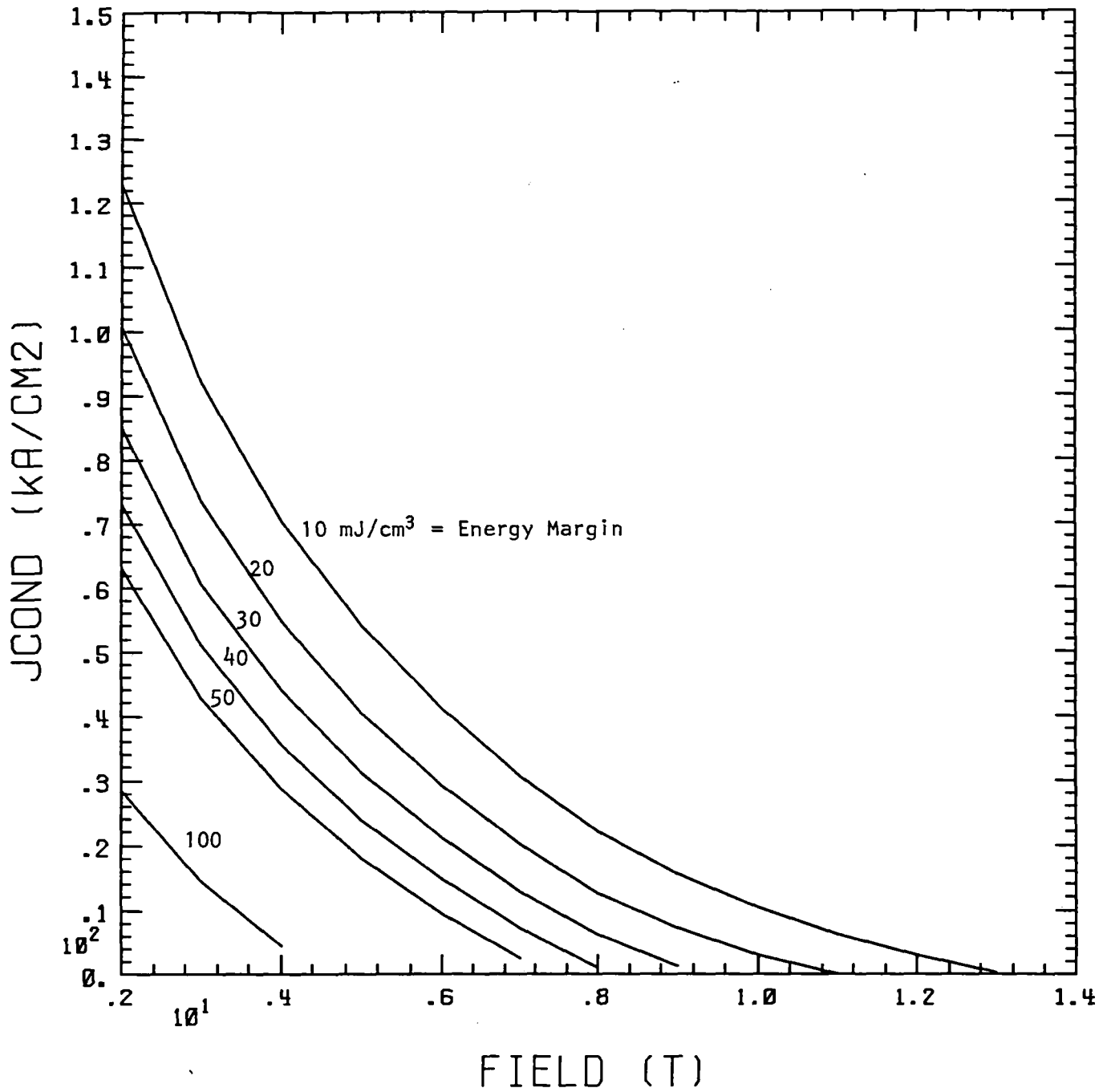


Figure 3.2-7 J_{cond} vs B for selected energy margins for an epoxy-impregnated Nb₃Sn winding at 4.5 K

CROSS PLOT OF JCOND VS FIELD FOR
NbTi ENERGY MARGINS W/O He (T=4.5K)

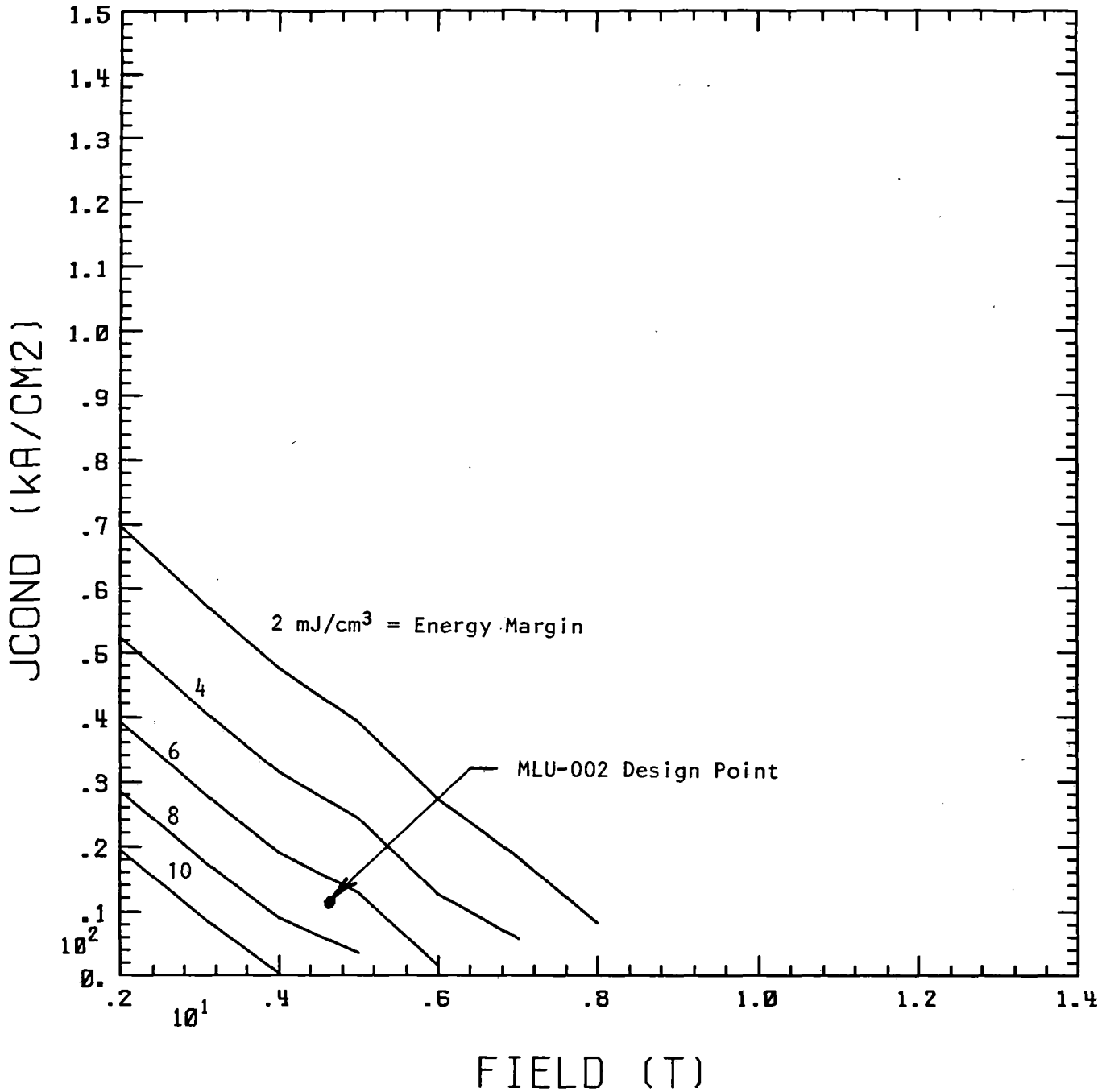


Figure 3.2-8 J_{cond} vs B for selected energy margins for an epoxy-impregnated NbTi winding at 4.5 K

baseline conductor configuration for this study.

3.3 Selection of Current Density and Field Level

Section 3.1 showed that the lift force per unit coil weight was proportional to a dimensionless parameter consisting of the ratio of the product of the conductor current density and maximum field experienced by the winding to the winding weight density. It also showed that the lift force per unit coil weight was proportional to a dimensionless function of dimensionless parameters containing coil shape, track, and speed characteristics, but no variables contained in the preceding dimensionless group, which was conductor related. As a result the conclusion was that we would like to design at the maximum product of jB_M . It would, obviously, also be advantageous to decrease the winding weight density, ρ_c .

Section 3.2 showed estimates of the energy margin that could be achieved with Nb₃Sn and NbTi conductors in CICC and in impregnated winding configurations. If we now postulate the need for an energy margin of a given level, say 100 mJ/cm³, then the operating point can be found by selecting an operating temperature and overlaying the plot in Figure 3.1-2 on the relevant plot from Figures 3.2-1 to 3.2-8. The optimum point is that point which lies on the required energy margin curve and which also gives the highest jB_M product. For illustration purposes this was done for an energy margin of 100 mJ/cm³ and results are given in Table 3.3-1.

Several conclusions can be drawn from the table:

- all systems optimize at a relatively low field level which ranges from 2.0 to 3.7 T
- the Nb₃Sn systems have substantially higher jB_M products than NbTi at the same temperature; this product is directly proportional to the ratio of lift force to coil weight for a given coil shape and track/speed characteristics, hence column 6 shows the ratio of F_L/W_c for each case relative to the first to illustrate the relative change [e.g., 1) at 4.5 K a NbTi coil will have only 36% of the lift of a Nb₃Sn coil of equivalent weight, and 2) Nb₃Sn at 8 K has a decrease in lift to 35% of the value for the same weight coil operating at 4.5 K)
- NbTi rapidly degrades in performance as temperature increases (e.g., at 8 K or 10 K it cannot provide the desired 100 mJ/cm³ of energy margin and is not applicable)
- the last column is the ratio of Carnot efficiency for the first case to the Carnot efficiency for the specific line; since the Carnot efficiency is related to the power required by the refrigeration system, this illustrates the advantage of higher temperature operation (e.g., the cryosystem power required for 8 K operation would be about 55% of that required for 4.5 K operation)

Table 3.3-1
Operating Points for Selected CICC Conductors
and Temperatures to Maximize Lift per Unit Coil Weight
for an Energy Margin of 100 mJ/cm³

T [K]	Type	j [kA/cm ²]	B _M [T]	jB _M [10 ⁷ N/m ³]	Relative F _L /W _c	Relative Power In ²
4.5	Nb ₃ Sn	92	3.7	340	1.0	1.0
4.5	NbTi	38	3.0	114	0.36	1.0
6.0	Nb ₃ Sn	74	3.4	252	0.74	0.75
6.0	NbTi	13	2.0	26	0.08	0.75
8.0	Nb ₃ Sn	46	2.6	120	0.35	0.55
8.0	NbTi	--	---	---	0	0.55
10	Nb ₃ Sn	24	2.0	48	0.14	0.44
10	NbTi	--	---	---	0	0.44

As a result of this trade study, the conceptual design activity was based on a Nb₃Sn CICC at a temperature in the 8-10 K range and with a maximum field level in the 2-4 T range.

3.4 Coil System Parameter Variations

In sections 3.1 and 3.3 we discussed maximizing the dimensionless parameter jB_M/ρ_c to maximize the lift force per unit coil weight. Section 3.1 showed that the lift force per unit coil weight was also dependent on a dimensionless function, F_p , of the dimensionless parameters defined as:

- $R_m = \mu_0 \sigma V g$ = magnetic Reynolds number
- T/g = dimensionless track thickness
- $\gamma = g/r_i$ = dimensionless height of lower coil surface above track
- $\alpha = r_o/r_i$ = dimensionless coil radial build
- $\beta = d/r_i$ = dimensionless coil half height
- $v = L/r_i$ = dimensionless coil length

²Relative Power In = Ratio of Carnot Efficiencies

where: μ_0 = permeability of free space
 σ = track conductivity
 V = vehicle velocity
 g = distance from coil lower surface to track (Fig 3.1-1)
 T = track thickness

In this section we present plots for specific cases to gain some insight into the form of this function. Specifically, we shall assume:

$$\begin{aligned} R_m &= 400 \\ T/g &= 0.25 \\ v &= 5 \\ \gamma &= 0.4 \end{aligned}$$

Because of the dimensionless form, the above set of parameters can represent any one of several systems. One of these is the following:

Track Material=	Aluminum
Track thickness=	0.025 m
Vehicle speed=	500 km/hr
gap coil to track=	0.1 m
coil inner size=	0.25 m (see Fig 3.1-1)

For simplicity, we shall assume that the maximum field can be approximated by using high speed image currents from the coil in the track and by computing the maximum field from two semi-infinite parallel conductors combined with the maximum field from one-half of two solenoids representing the end turns. This allows us to define a functional form for F_M to be used in the calculation of B_M . Contours for the resulting dimensionless function, F_M , are plotted in Figure 3.4-1 as a function of α and β . Lift forces will be computed assuming finite speed.

If we now assume that we desire a design based on $B_M = 2.6$ T and $j = 4.6 \times 10^8$ A/m², then we are consistent with the 8 K, Nb₃Sn point in Table 3.3-1. If we further assume that $\lambda = 0.72$ and $r_i = 0.25$ then,

$$\frac{B_M}{\mu_0 \lambda j r_i} = 2.5 \times 10^{-2} = F_M \quad (3-5)$$

As indicated, this dimensionless combination of parameters is sufficient to define the magnitude of F_M , hence we must select α and β so as to lie somewhere on the $F_M = 0.025$ contour in Figure 3.4-1.

The function F_p , which is proportional to the lift force per unit coil weight, may be expected to vary as we move along the $F_M = 0.025$ contour. The dependence of F_p on α and β is shown in

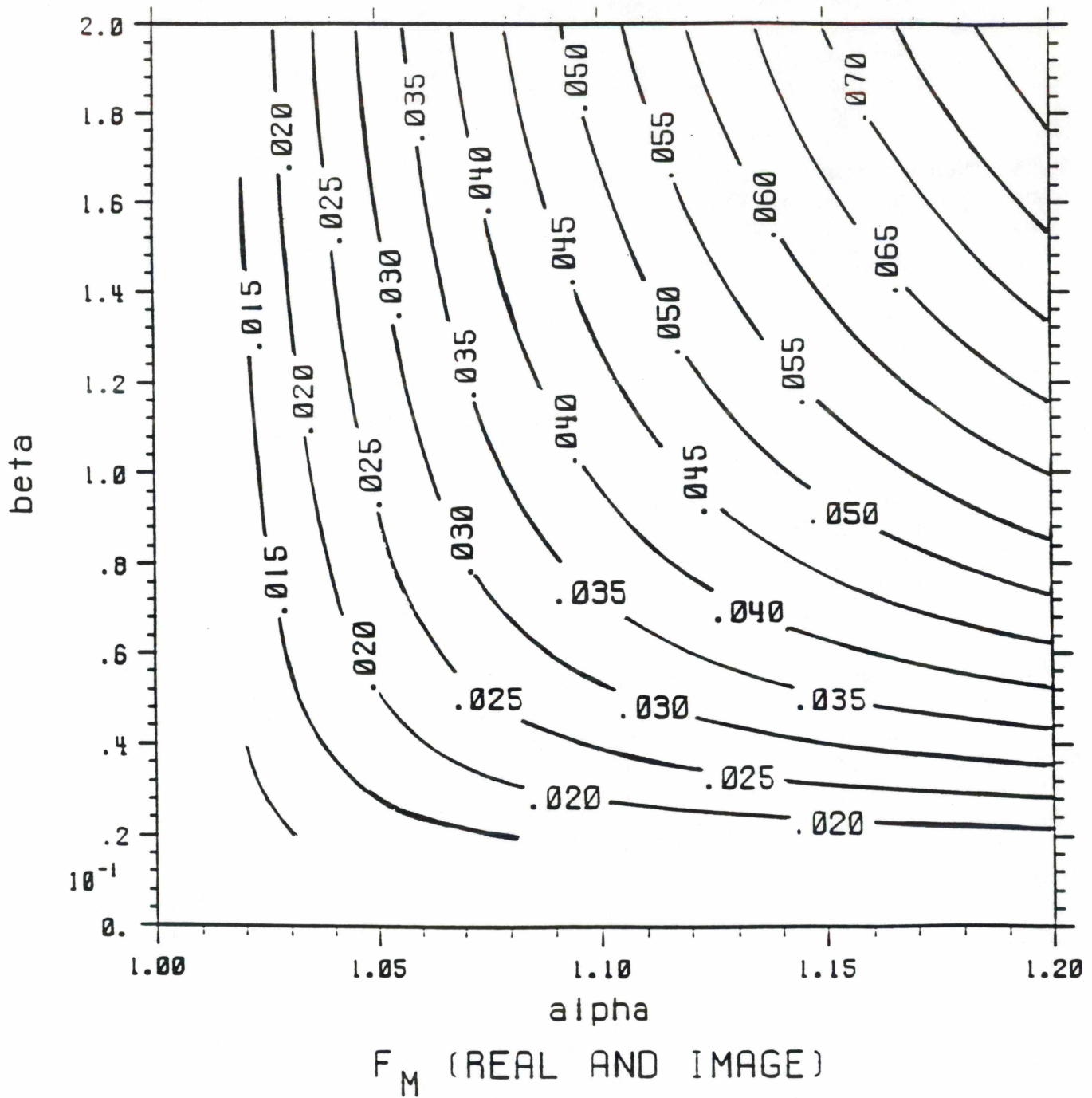


Figure 3.4-1 Dimensionless function F_M for maximum magnetic field experienced by the racetrack with $\nu = 5$ and $\gamma = 0.4$

Figure 3.4-2 together with the sample F_M contour for $F_M=0.025$. Since we would like to have as high an F_p as possible to raise the lift force per unit coil weight, the overlay implies that we would like to design at as low a β and at as high an α as practical, but certainly higher than α of about 1.1. This is consistent with desiring the current center for the lift coil to be as close to the track as possible.

The optimization in this section is oversimplified in that it considers only the coil weight. Section 3.5 includes the effects of the dewar weight and concludes that optimizing with respect to jB_M/ρ_c is still appropriate.

3.5 Optimization Including Dewar Weight

Section 3.1 discussed the optimization of the levitation coil system in terms of the lift force per unit coil weight. In this section, the dewar will be included in the optimization process and it will be shown that the functional form changes, but that the parameter JB_M/ρ still appears as a multiplier, similar to the way it did in Eqn (3-4). Hence, the earlier conclusions concerning the desirability of designing the conductor for maximum product of current density and magnetic field still holds.

The primary weight components of the dewar are the room temperature vessel and the radiation shield. Using the nomenclature of section 3.1, the weight of the room temperature vessel can be shown to be approximately given by:

$$W_{rt} = \rho_{rt} r_i^3 \left[2 \left(\frac{t_{rt}}{r_i} \right) (\alpha - 1) + \left(\frac{t_{rt}}{r_i} \right) (4\beta) \right] [2v + \pi(\alpha + 1)] \quad (3-6)$$

where: ρ_{rt} =density of material in room temperature vessel
 t_{rt} =thickness of top & bottom plates of outer vessel
 t_{rt} =thickness of cryostat sidewalls

and the weight of the thermal radiation shield can be shown to be approximately given by:

$$W_{rad} = \rho_{rad} r_i^3 (t_{rad}/r_i) [2(\alpha - 1) + (4\beta)] [2v + \pi(\alpha + 1)] \quad (3-7)$$

where: ρ_{rad} =density of material in thermal radiation shield
 t_{rt} =thickness of thermal radiation shield

The total dewar weight can then be estimated by:

$$W_{dew} = W_{rt} + W_{rad} \quad (3-8)$$

The dewar weight may now be combined with the coil weight [see Eqn (3-1)] to estimate the

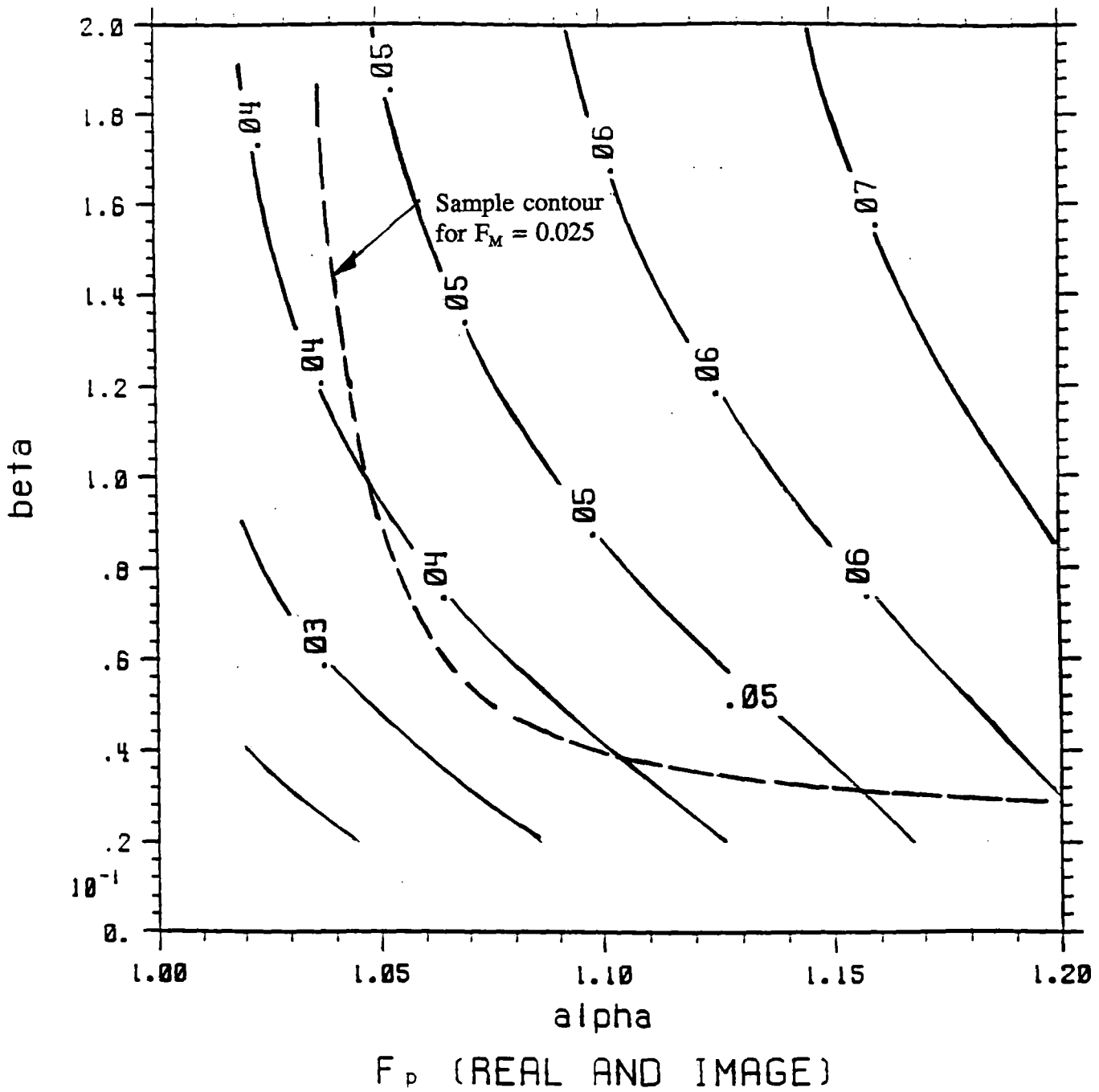


Figure 3.4-2 Contours of dimensionless lift function, F_p for a racetrack with $\nu = 5$ and $\gamma = 0.4$

total weight of the module. The total can then be divided into the expression for the lift force provided by the coil [see Eqn (3-2)] to form the following expression for the lift force per unit module weight:

$$\frac{F_L}{W_{cd}} = \frac{jB_M}{\rho_c} \left[\frac{G}{F_M \left(F_w + \frac{\rho_w}{\lambda \rho_c} F_r + \frac{\rho_{rad}}{\lambda \rho_c} F_{rad} \right)} \right] \quad (3-9)$$

where: F_r = a dimensionless function of α , β , v , (t_w/r_i) , and (t_r/r_i)
 F_{rad} = a dimensionless function of α , β , v , (t_{rad}/r_i)

The ratio of material densities for this application are relatively insensitive and are set before optimization of geometry. In addition, the ratios of dewar and radiation shield thicknesses to the overall scale of the device, r_i , are relatively insensitive unless the scale is changed dramatically. As a result, the optimization of the above equation for lift per unit module weight can again be approached as in Eqn (3-4). That is, the maximum lift per module weight will occur for that conductor that provides the maximum jB_M/ρ_c . The balance of the above equation is then determined primarily by geometry (shape) and not by the conductor properties.

3.6 Number of Lift Modules per Vehicle

The amount of lift that can be generated by a levitation module can be shown (see Eqn A-19) to be proportional to the number of amp-turns in the coil, that is:

$$F_L = \mu_0 (N I_r)^2 K_L \quad (3-10)$$

where: $N I_r$ = number of amp turns in coil
 K_L = dimensionless function of coil geometry, speed and guideway characteristics

The weight of the coil can be expected to be proportional to the number of amp-turns for a fixed coil geometry and overall scale:

$$W_c = K_c (N I_r) \quad (3-11)$$

where: K_c = weight per amp turn for a fixed coil size and geometry

The weight of the dewar for the coil is not a strong function of the amp-turns in the coil and, to first order, is essentially constant once the coil overall size and geometry are fixed. Thus, if there are N_{cd} coil/dewar modules, the total weight of the levitation modules is given by:

$$W_{cd} = N_{cd} [K_c (NI)_c + W_d] \quad (3-12)$$

If the vehicle weight is W , then the number of modules required is related to the lift per module by:

$$W = N_{cd} F_L \quad (3-13)$$

Combining the above relationships to obtain the ratio of the total weight of the levitation modules to the weight of the vehicle leads to:

$$\frac{W_{cd}}{W} = \frac{K_c}{K_L (NI)_c} \left[1 + \frac{W_d}{K_c (NI)_c} \right] \quad (3-14)$$

Since K_c and K_L are essentially constant, Eqn (3-14) implies that NI_c , the amp-turns per module, should be large to reduce the ratio of levitation module weight to vehicle weight. For a fixed vehicle weight, Eqns (3-10) and (3-13) then imply that it is desirable to reduce the number of levitation modules to a minimum, which, for all practical purposes, is probably four.

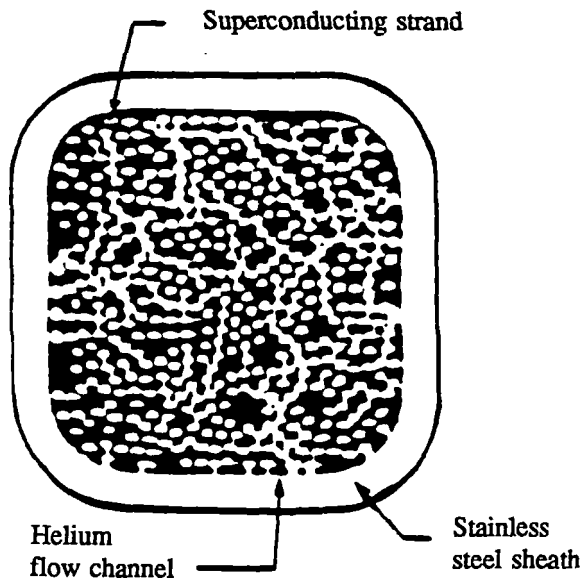
4.0 Conceptual Design

4.1 Conductor Selection

Early experiments demonstrated the advantages of the CICC approach from the operational stability standpoint. It has been the subject of investigations and development in laboratories throughout the world ever since (e.g., see [4.1 to 4.5]). For example, three of the six coils (approximately 40 tonnes each) in the Large Coil Test Facility have used the concept. Figure 4.1-1 shows the three conductors; the one in the top sketch consists of 486 strands of Nb_3Sn composite conductor in a steel conduit and is conceptually similar to the configuration we are evaluating for MAGLEV.

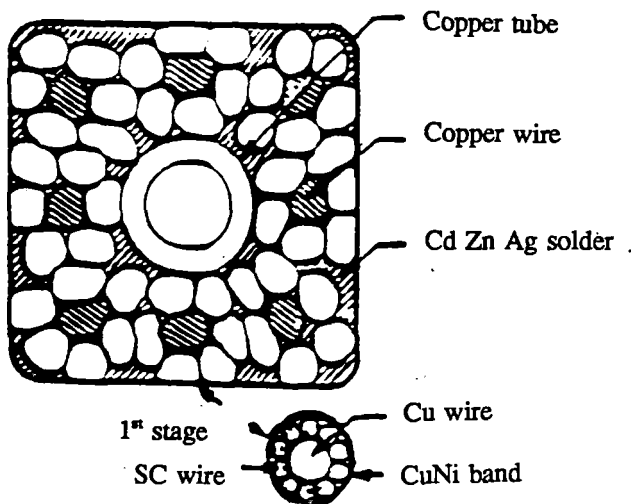
As another example, a CICC Nb_3Sn conductor was successfully tested recently in the US/Japan Demonstration Poloidal Coil, a 2500 kg, 7 MJ system designed and built by MIT. It experienced a maximum magnetic field of 10 tesla and a maximum field sweep rate of 10 T/s as part of a program to develop conductors for pulsed superconducting coils in fusion devices.

A CICC can be manufactured in long lengths as illustrated in Figure 4.1-2, which is the demonstrated process used for the 13 tonnes of Westinghouse conductor in Figure 4.1-1. The conductor is fabricated by: 1) producing a cable from the individual strands of superconducting composite; 2) passing the cable onto a sheath material which is formed around it and seam welded continuously; and 3) drawing and rolling the finished conductor to compact it and obtain the final dimensions.



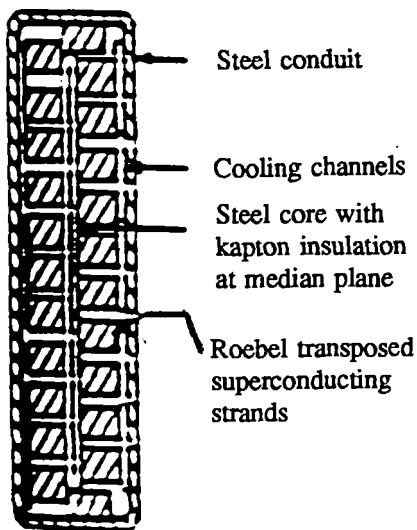
Westinghouse conductor

- Nb_3Sn transposed compacted cable in a JBK-75 stainless steel sheath
- 17.6 kA at 8 T
- 20.8 x 20.8 mm



Swiss conductor

- NbTi compact high strength solder filled around a central cooling tube
- 13 kA at 8 T
- 18.5 x 18.5 mm

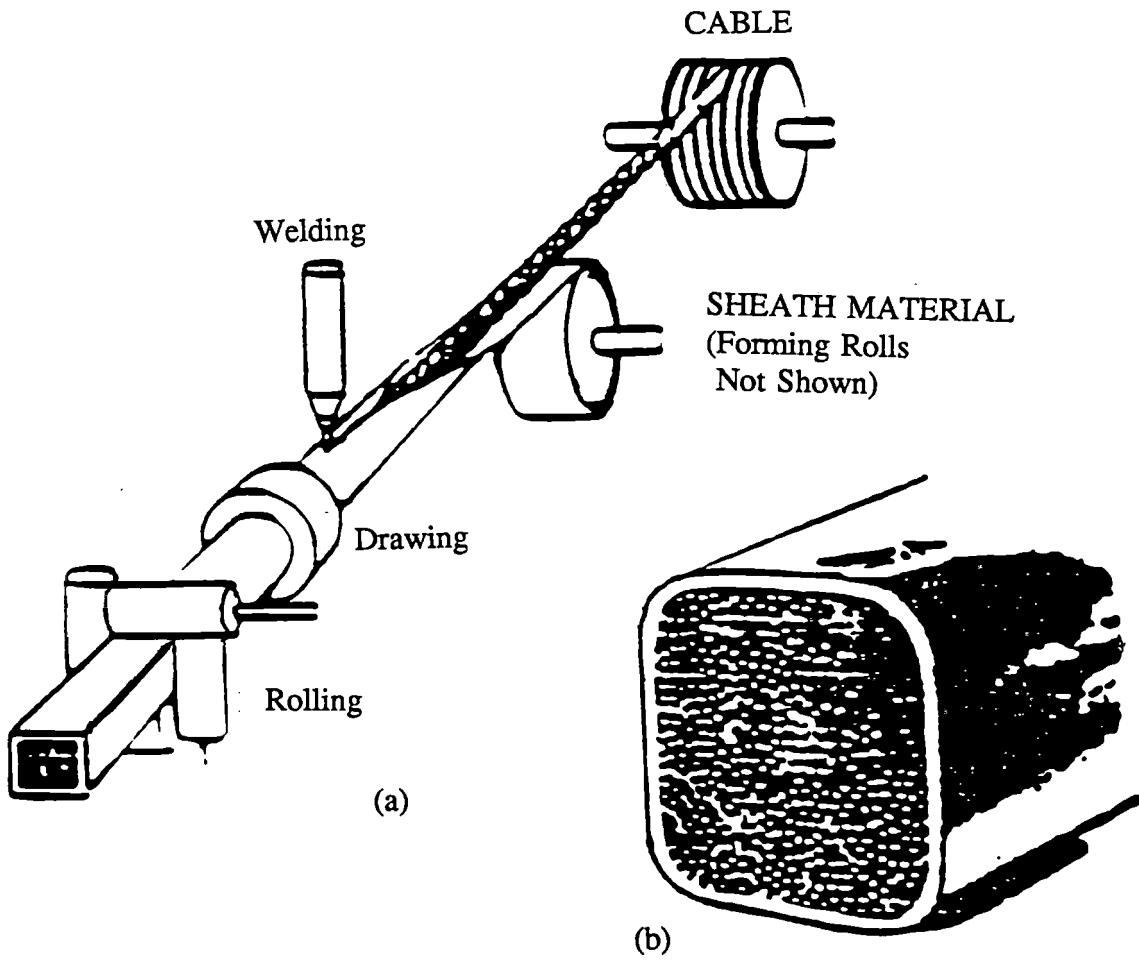


Euratom conductor

- Conductor is roebel cabled around a kapton insulated stainless steel core, then enclosed in a stainless steel sheath.
- 11 kA at 8 T
- 40 x 10 mm

The strands are fixed mechanically by soft soldering onto the CrNi core with high resistance solder.

Figure 4.1-1 Three CICC conductors used in the Large Coil Task. (Adapted from Figure 3, *Fusion Engineering and Design*, Vol. 7, 1988 p.6)



- a) Production of conductor by continuous cable sheathing process
- b) Cross-section of finished conductor

Sketch Showing Continuous Cable Sheathing Process for Production of ICCS

Figure 4.1-2 Sheathing process for the Westinghouse conductor.

Figure 4.1-3 shows a photograph of a CICC which has an outside dimension of about 5x5 mm (0.2x0.2 in). This conductor is about the scale that we presently envision for MAGLEV operation. The characteristics of the conductor are summarized in Table 4.1-1 and was the basis for the conductor optimizations in Section 3.

The conductor described above was selected because we have had it manufactured at this size for another program, hence it demonstrates feasibility. However, it was not intended for this application. We will assume that we can scale it up or down in size as we require and achieve the same overall current density. This is correct to first order since it is a cable of conductors and an adjustment to current capacity can be made by adding or subtracting strands in the cable or individual conductors. Later, it will be evident that the total conductor volume required is small, hence minor variations in Nb₃Sn CICC capability from those assumed will have a minor impact on lift module weight or other general features.

The critical current density for this conductor is shown in Figure 4.1-4 as a function of the magnetic flux density experienced by the conductor and the operating temperature. This current density is based on the current carried, divided by the outer envelope area of the conduit enclosing the cable.

**Table 4.1-1
Preliminary Characteristics of MAGLEV Conductor**

Conductor Type	Cable-in-Conduit
Sheath Material	304 SS
Wall Thickness	0.38 mm (0.015")
Outer Dimensions	4.95x4.95 mm (0.195x0.195")
Inner Dimensions	4.2x4.2 mm (0.165x0.165")
Strand Material	Nb ₃ Sn with Cu
Number of Strands	27
Strand Diameter	0.71 mm (0.028")
Strand Area	10.69 mm ² (1.66 x 10 ⁻² in ²)
Cable Space Area	17.64 mm ² (2.72 x 10 ⁻² in ²)
Helium Area	6.95 mm ² (1.06 x 10 ⁻² in ²)
Void Fraction	39%

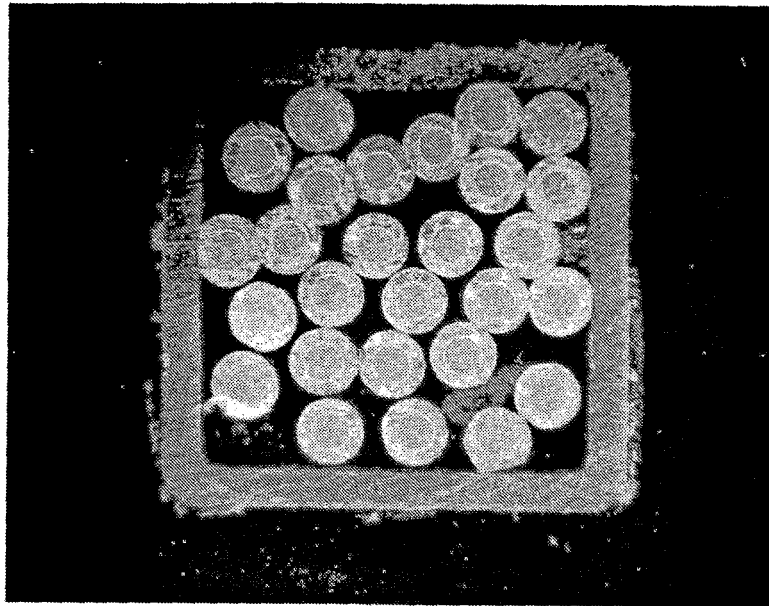


Figure 4.1-3 Sample cable-in-conduit conductor consisting of 27 strands of multifilamentary copper-stabilized superconductor in a stainless steel sheath (full size ~ 0.2 x 0.2 in.)

Temperature Dependence of Critical Current Density

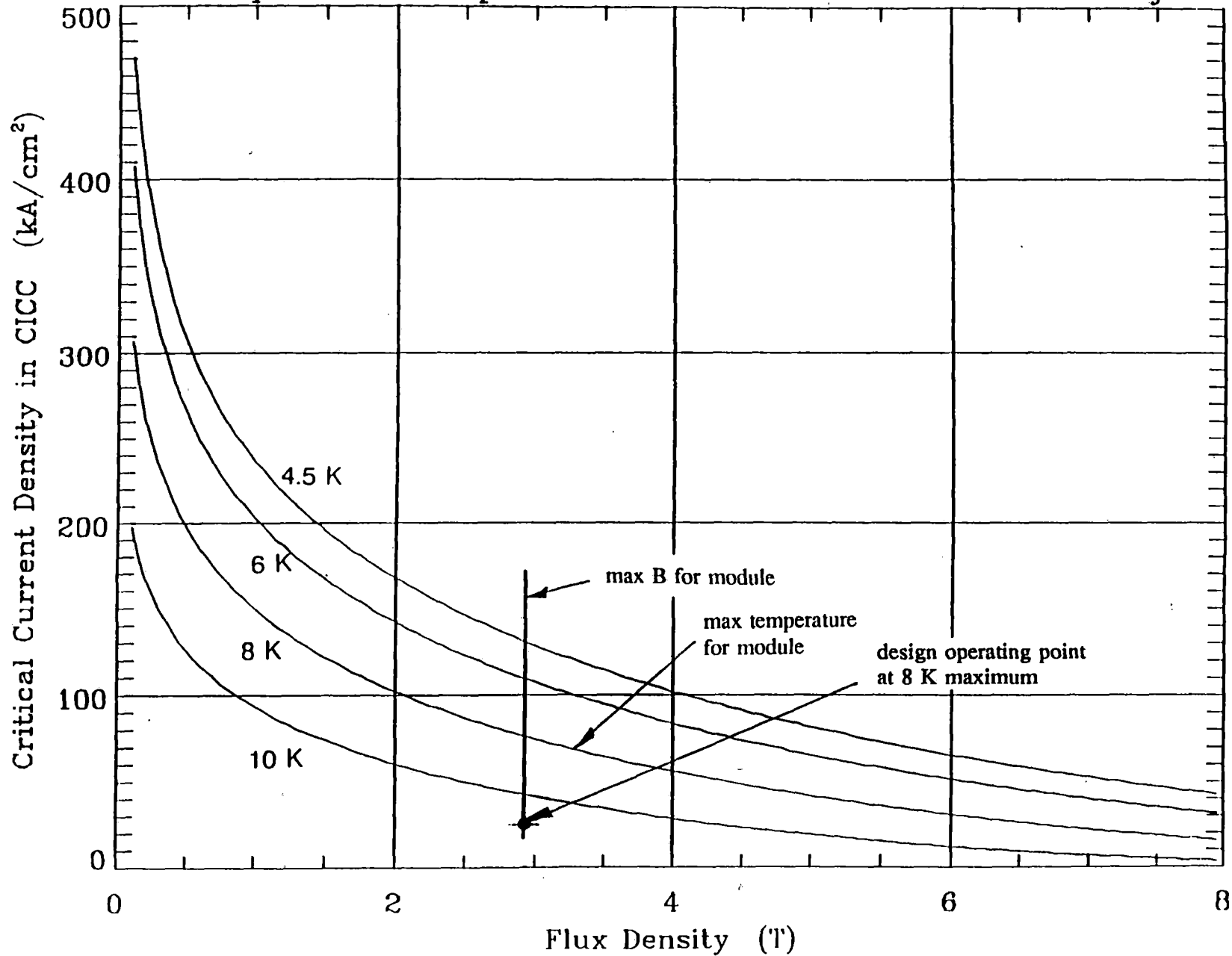


Fig. 4.1-4 Critical Current Density vs. Flux Density at Several Operating Temperatures for the Conductor in Table 4.1-1 and Fig. 4.1-3

The maximum flux density in the module conceptual design for this study is also indicated in Figure 4.1-4. The operating current density must be selected to be a fraction of the critical current density so as to allow for stability of the conductor to operational disturbances which could take the form of temperature excursions due to cryosystem fluctuations or losses generated by the conductor under transient conditions.

The temperature and the magnetic flux density are not uniform throughout the winding in the coil system. In our case the magnetic field experienced by the winding at full current will range from zero to 2.9 T and the temperature will be a maximum of 8 K. If the maximum field point and maximum temperature point in the winding coincide, then this would be the point of lowest margin relative to the critical current surface for the conductor. Hence, in the winding for our case, the operating fraction of critical current density will be 30% or less. This will be ample margin to allow for operational uncertainties at this stage of the design process. The corresponding conductor current density for the design point is 2.42×10^8 A/m².

4.2 Selection of an Operating Temperature and Current

The selection of an operating temperature must be done in light of the impact on conductor operating requirements as well as system level trade-offs such as weight and auxiliary power required.

The energy margin required for stability was discussed in section 3.2. It showed the decided advantage for Nb₃Sn and a CICC configuration regardless of the energy margin required. Nb₃Sn also has the potential for allowing operation at a higher temperature than NbTi. This section will begin by illustrating the major advantage of operating at a higher temperature from the standpoint of cryocooler weight and power required.

Figures 4.2-1 and 4.2-2 are plots from Smith et al. [4.6] showing points for presently available cryosystems. Figure 4.2-1 is a plot of cryocooler weight versus refrigeration capacity in watts at the operating temperature. It illustrates the major decrease in cryosystem weight possible at any refrigeration capacity as the low end operating temperature increases. For example, a simple interpolation implies a specific weight of about 160 Kg/watt of refrigeration capacity at 4 K and a reduction to about 50 Kg/watt of refrigeration capacity at 8-10 K.

Figure 4.2-2 [4.6] shows points corresponding to commercially available units in terms of their specific power required vs operating temperature. The specific power is the ratio of the power required by the compressors divided by the refrigeration capacity. In general the points are considerably higher than the ideal Carnot efficiency, but are roughly parallel to it thus indicating a strong decrease in power required to provide a given refrigeration capacity as the low end operating temperature increases. For example, at 4 K, the lowest value corresponds to about 1500 watts of power input per watt of refrigeration capacity, whereas at 8-10 K, a simple interpolation would imply about 600 watts input per watt of refrigeration.

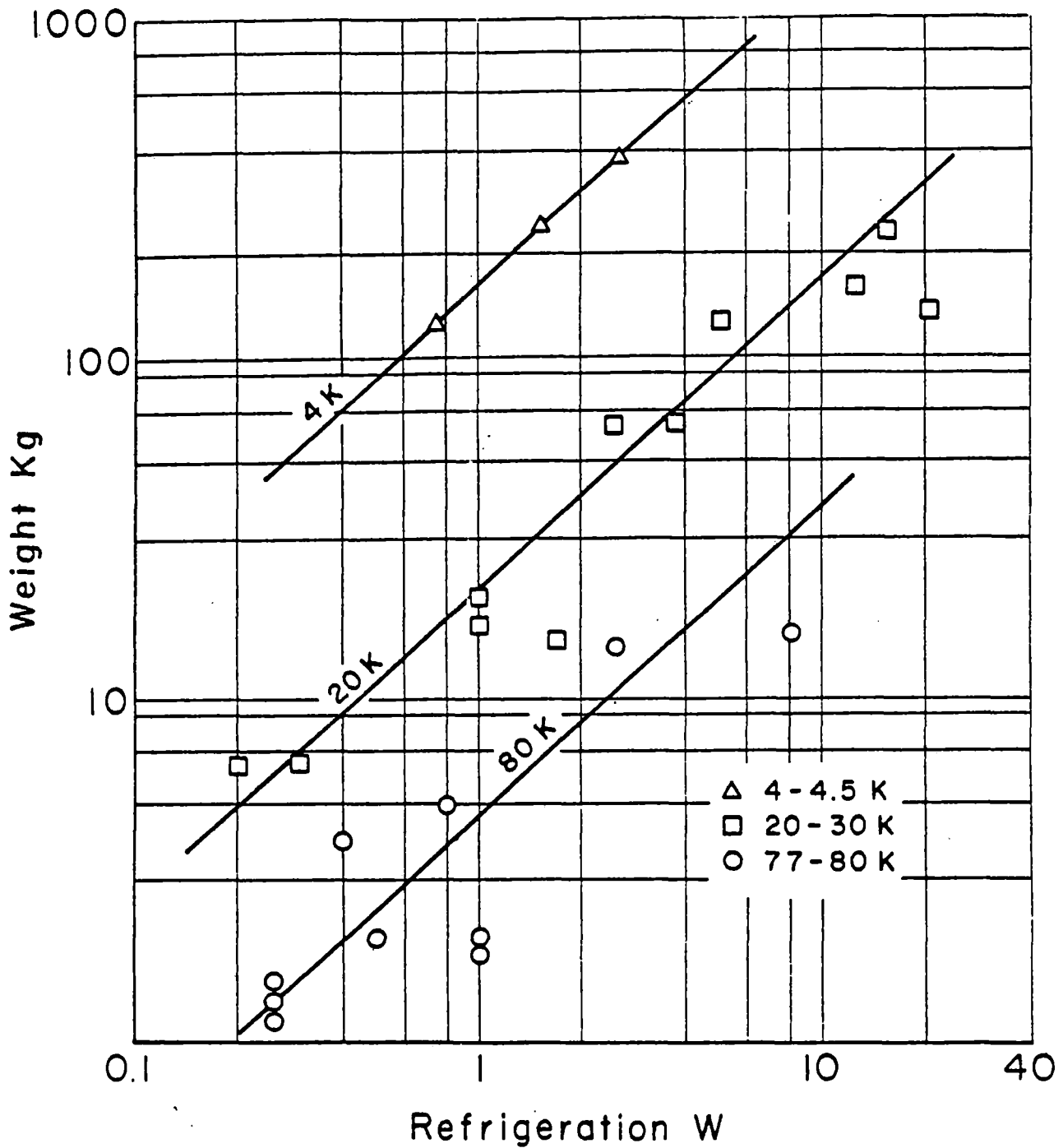


Figure 4.2-1 Weight of commercial cryocoolers vs refrigeration capacity in watts. (From J. L. Smith et al., *Survey of the State-of-the-Art of Miniature Cryocoolers for Superconductive Devices*, NRL Memo Report 5490, December 1984.)

In section 4.3.3 the elements of the cryosystem are considered in more detail, but the material presented in Figures 4.2-1 and 4.2-2 shows the advantage of increasing the operating temperature, as is possible with Nb₃Sn in CICC form.

Alternatively, if a helium storage reservoir is used as the cryosystem (i.e., no refrigerator) then the operating temperature for the coil could be reduced and either: 1) the energy margin increased or 2) the current density increased (coil weight reduced) at the same energy margin.

The conductor current density for the design point in this study was indicated in Figure 4.1-4 as 2.42×10^8 A/m² at a field level of 2.9 T. The energy margin for Nb₃Sn and for NbTi conductors at various fields and operating temperatures was presented in Figures 3.2-1 to 3.2-8. Table 4.2-1 summarizes the energy margin available at the design point for this study for the two conductors in CICC form or in epoxy impregnated (EImp) form for selected operating temperatures.

Table 4.2-1
Energy Margin at a Field Level of 2.9 T and
a Conductor Current Density of 2.42×10^8 A/m²
for Selected Conductors

Conductor	Form	Temperature [K]	Energy Margin [mJ/cc]
Nb ₃ Sn	CICC	4.5	690
Nb ₃ Sn	CICC	6	380
Nb ₃ Sn	CICC	8	160
NbTi	CICC	4.5	180
NbTi	CICC	6	40
Nb ₃ Sn	EImp	4.5	80
NbTi	EImp	4.5	7

This table shows that Nb₃Sn retains a high energy margin capability at higher temperatures, that CICC conductors have an order of magnitude higher energy margin than epoxy impregnated windings, that Nb₃Sn has much higher energy margin than NbTi at a given temperature, and that NbTi is unsuitable at temperatures approaching 8 K or higher.

In view of the advantage in weight and power requirement for the cryosystem that is to be expected in view of the earlier discussion, the design should use as high an operating temperature as is practical. For this design, we will use 8 K, since this still allows a significant energy

margin, that is 160 mJ/cm^3 . If this is found to be excessive at some future date then we could raise the operating temperature with further benefit to the cryosystem weight and power.

The level of energy margin that is required for this application is open to question and will not be resolved without an extensive analytical and experimental program, however, it is clear that this design is substantially more robust than the alternatives and could be even made more conservative if necessary by reducing the current density at the operating point (see Figure 3.2-3).

The design operating current density has been selected as $2.42 \times 10^8 \text{ A/m}^2$ for this conductor. The number of amp turns required for this case depends on the lift to be provided. Lift characteristics are described in section 4.4 and Table 4.4-1 shows that a reasonable lift range can be achieved with a module of this type if it provides about 2.4×10^5 amp turns. This amp turn requirement, together with the selected conductor current density and conductor size in Table 4.1-1 leads to an operating current level of about 6000 A.

Assuming that a conductor could be manufactured at about one fourth the size in Table 4.1-1 and that the conductor current density would be about the same, then we could also consider a coil with four times the turns and an operating current level of 1500 A to achieve the same amp turn requirement. In the sections that follow the impact of these two possible design current levels will be discussed.

4.3 Levitation Module Design

4.3.1 Module Configuration and Component Functions

This section describes features of the generic racetrack levitation module designed as part of this study. The capability of the module in terms of lift is given in section 4.4.

Figure 4.3-1 shows an external view of the module. The basic package is 2.37 m long, 0.6 m wide and 0.17 m thick. The outer vessel is the room temperature portion of the cryostat and is constructed from aluminum plate nominally 9.5 mm (0.375 in) thick. The vehicle mounts are the main load path into the cryostat and to the coil to transmit lift and drag. They could be shifted to other locations on the cryostat surface by the use of suitable stiffeners.

The portion labeled "Current Leads, Cryogenic Leads & Vents" is not necessary for each levitation module, but is representative of the volume required for a single circuit of multiple modules that are electrically and cryogenically in series. The orientation of the lead and vent section is also quite flexible and could be vertical, horizontal or, perhaps along the sides or top of the outer vessel shown depending on the details of the interface requirements with the vehicle.

The two central penetrations through the cryostat also pass through the center of the levitation coil. The walls of the penetrations help to stiffen and support the wide flat plates of the cryostat outer vessel. The vessel is evacuated and must withstand the external atmospheric pressure.

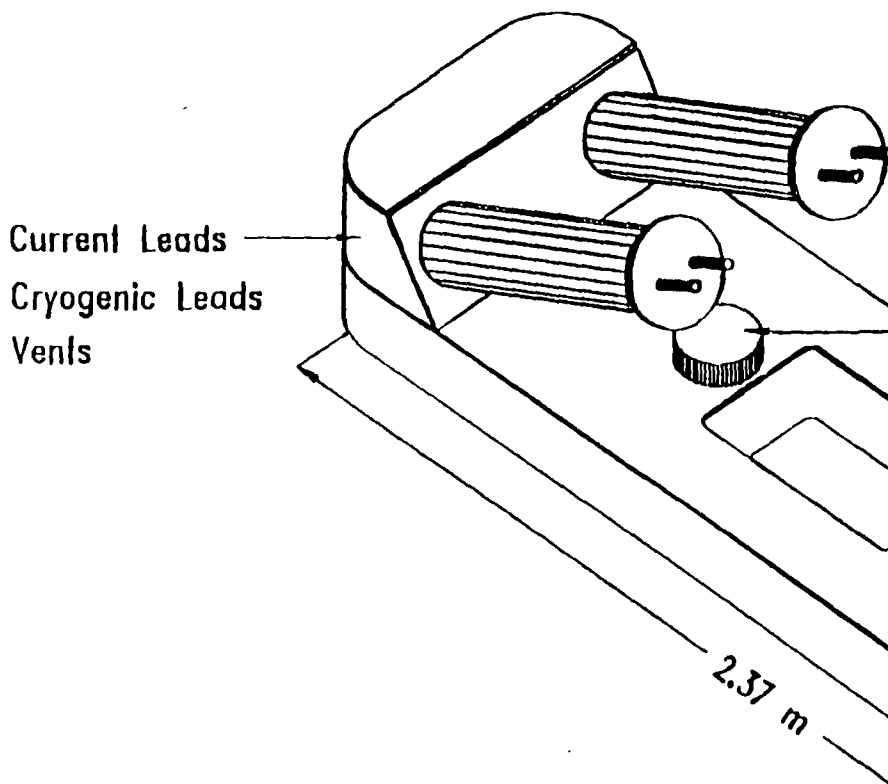
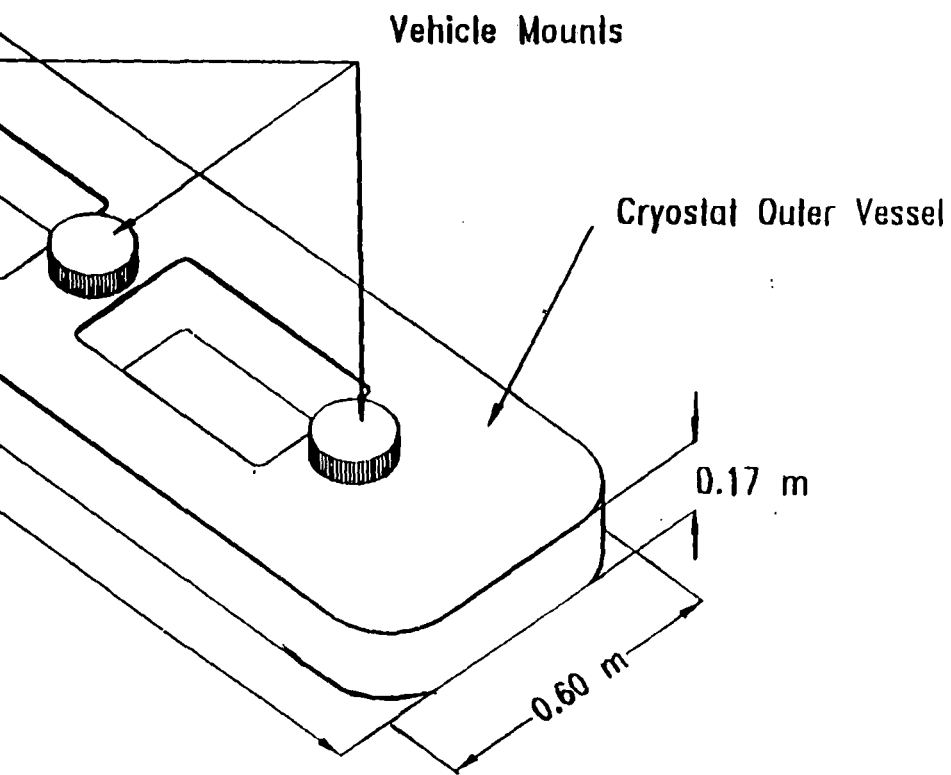


Fig 4.3-1. Dipole



Levitation Module

Figure 4.3-2 is a view of the module with the top cover plate removed to show the space which has been allowed for the persistent current switch, connectors and diagnostics. This space could also be relocated if interface requirements with other vehicle subsystems demanded a change. The vehicle mounts in the previous figure pass the load through the cold mass supports to the coil support frame that is within the thermal radiation shield. The purpose of the latter is to intercept thermal radiation at a temperature intermediate between the ambient temperature of the outer vessel and the cold coil system within and thus reduce the heat load on the cryogenic system. The radiation shield is also supported by the cold mass support, which will be described in more detail in a later figure.

Figure 4.3-3 shows the module with the cryostat cover and the thermal radiation shield removed. This exposes the coil and coil form which are bonded into an integral structure. This forms the internal structure to which the cold end of the cold mass supports are connected. A section of the system through a cold mass support is shown in more detail in Figure 4.3-4. It consists of a sequence of nested tubes to give a long thermal path from the connection to the vehicle mounts at room temperature to the coil at low temperature. The innermost tube is a stainless steel tube that spans the distance across the coil form to support the coil against the internal loads of electromagnetic origin. The coil form and structure are also of stainless steel and support the winding which consists of the type of conductor shown in Figure 4.1-3. The conductor is insulated, wound on a form, removed, externally insulated with a ground wrap and mounted on the stainless steel form for assembly to the cryostat.

Another view of the coil, structure, thermal radiation shield, cold mass supports and the manner in which they are mounted in the vessel is shown in Figure 4.3-5. Because of the high operating current density, the winding cross section is relatively small. This, coupled with an efficient structural and cold mass support system, allows the distance from the centerline of the coil winding to the outside of the cryostat to be relatively small. In this case we estimate that this can be 0.05 m and anticipate that some reduction may still be possible in the process of final design.

The overall dimensions of the racetrack coil in the module are given in Figure 4.3-6. The winding cross section is relatively small and implies that variations from assumed requirements for levitation capability or variations in conductor properties from the values assumed could be compensated by increasing the amp turns without a major impact on module size or overall weight. The overall weights of module components have been estimated and are given in Table 4.3-1.

The weight distribution indicates that the coil itself is not the major contributor to the total. It also shows that the outer vessel may be a prime area for R&D, since it is the major element in the weight distribution. Note that the entire penalty for the electrical and cryogenic leads has been charged to this one module, whereas in an actual system, the weight should be distributed over the number of modules in series.

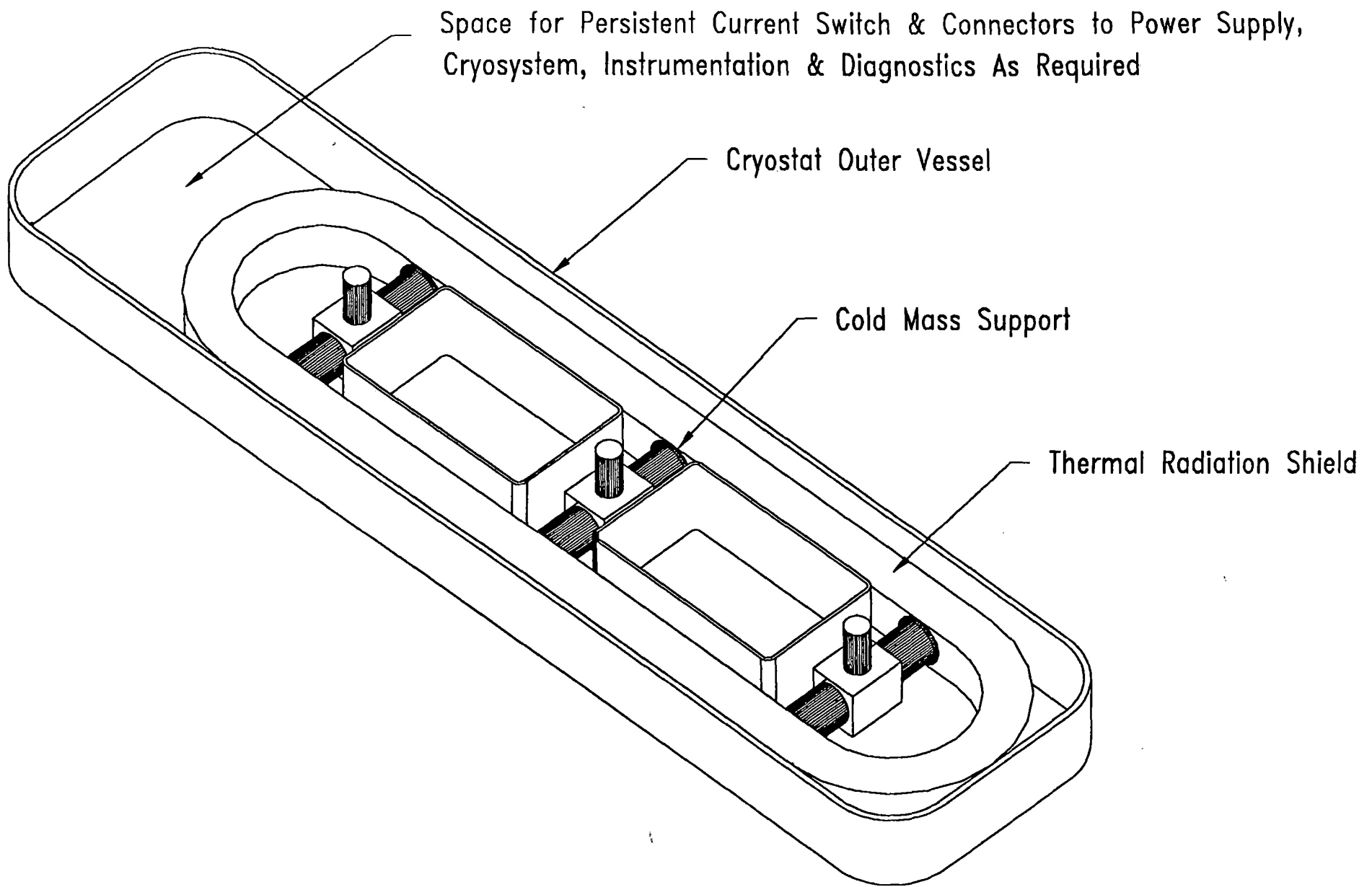


Fig 4.3-2. Major Components of Levitation Coil Module
(Cryostat Cover Removed)

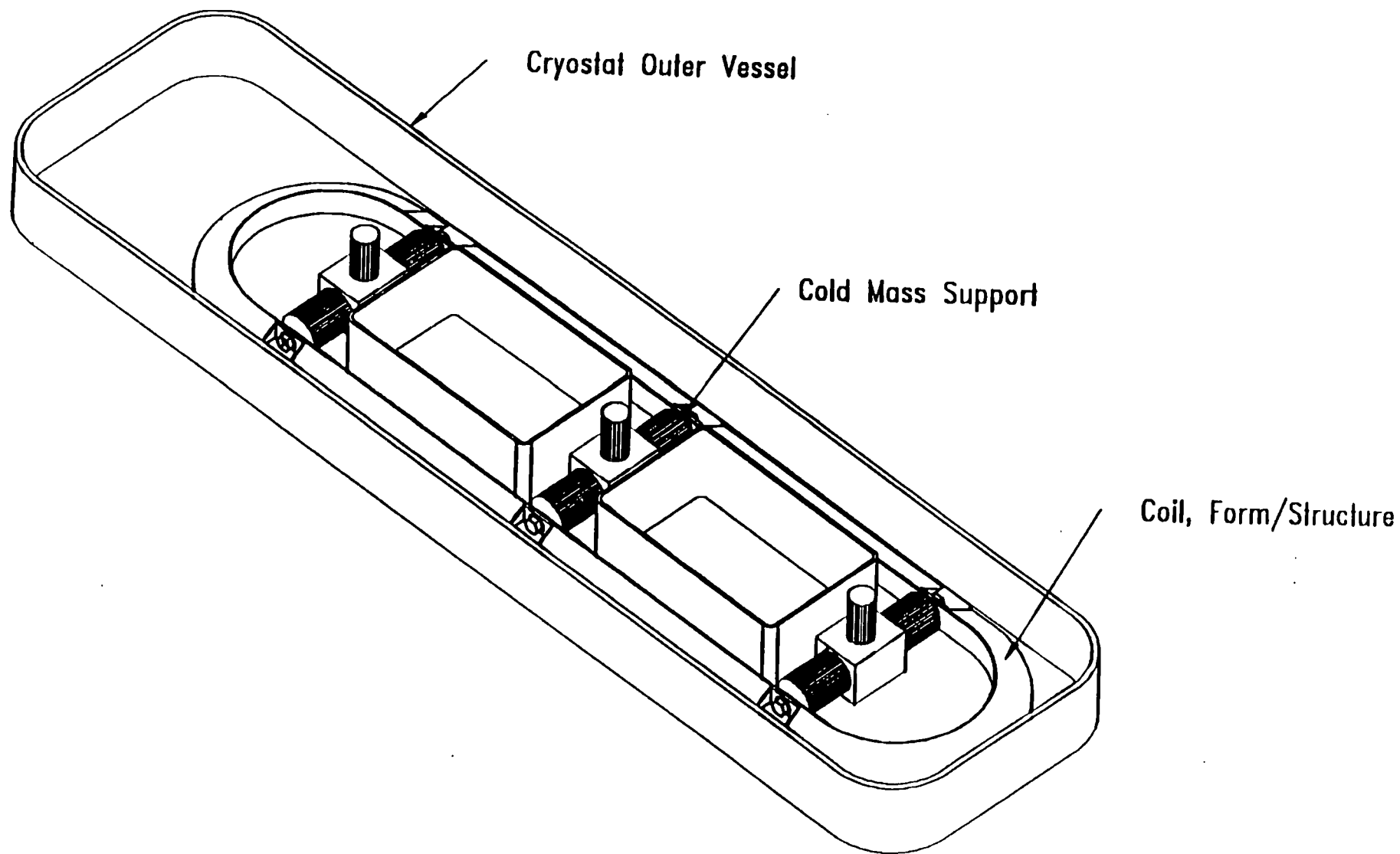


Fig 4.3-3. Major Components of Levitation Coil Module
(Cryostat Cover & Thermal Radiation Shield Removed)

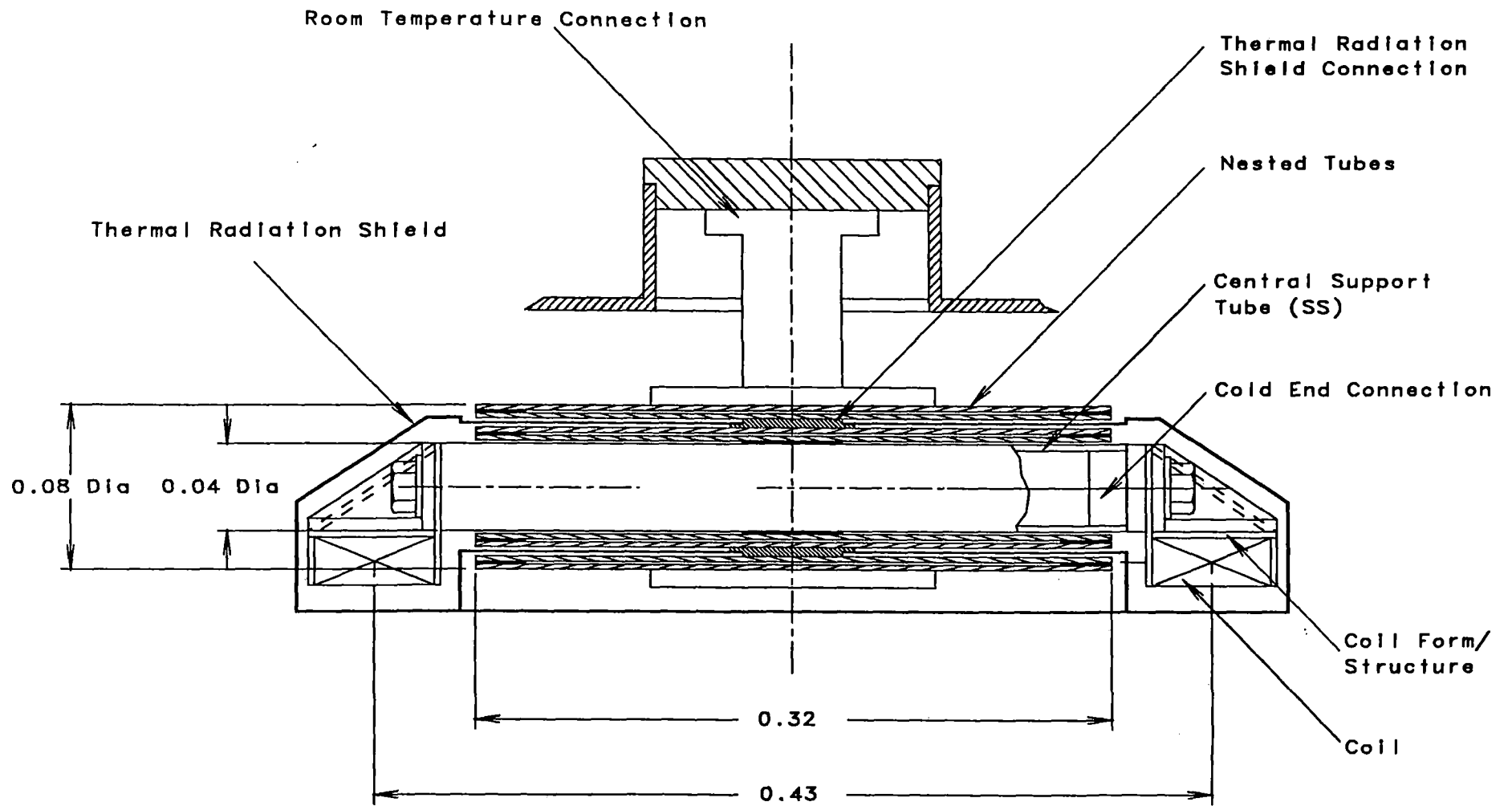


Fig 4.3-4. Cold Mass Support

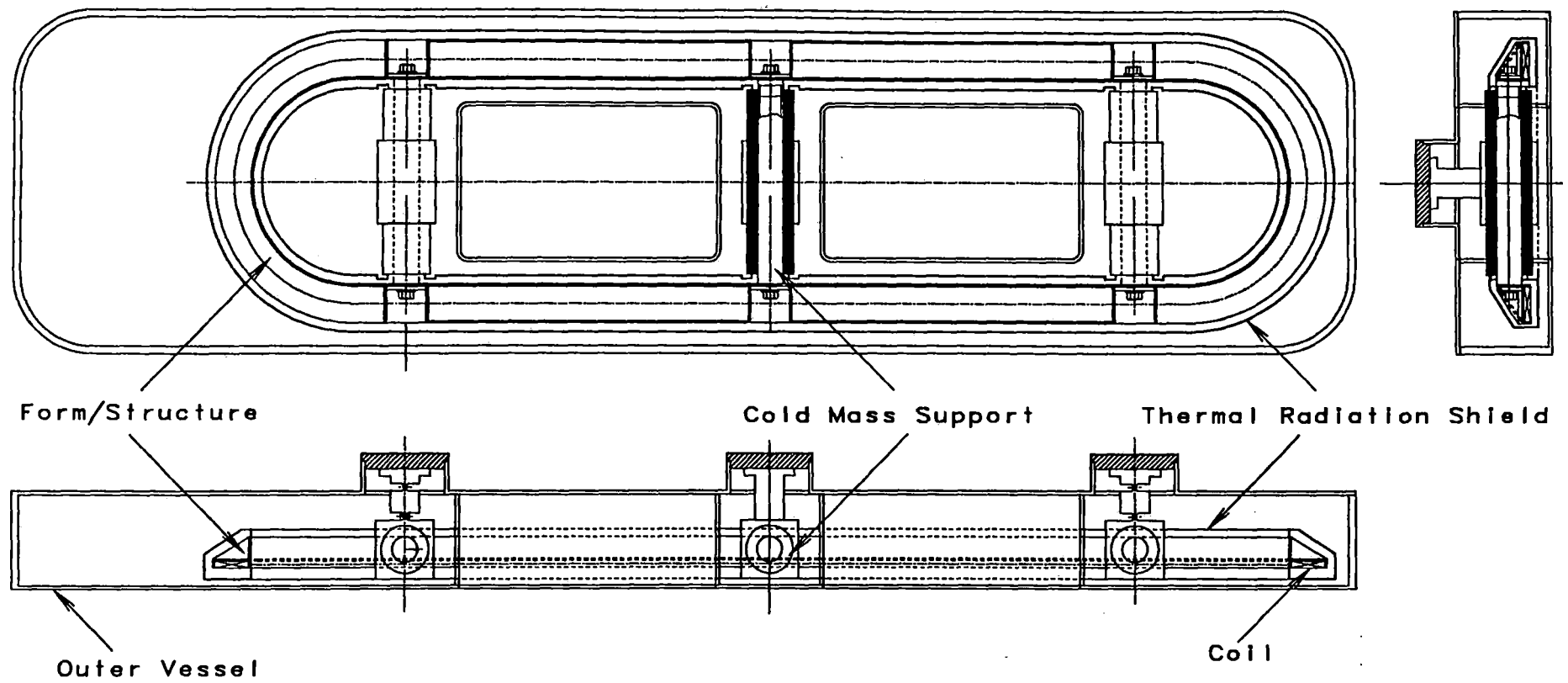


Fig 4.3-5. Major Components of Dipole Module.

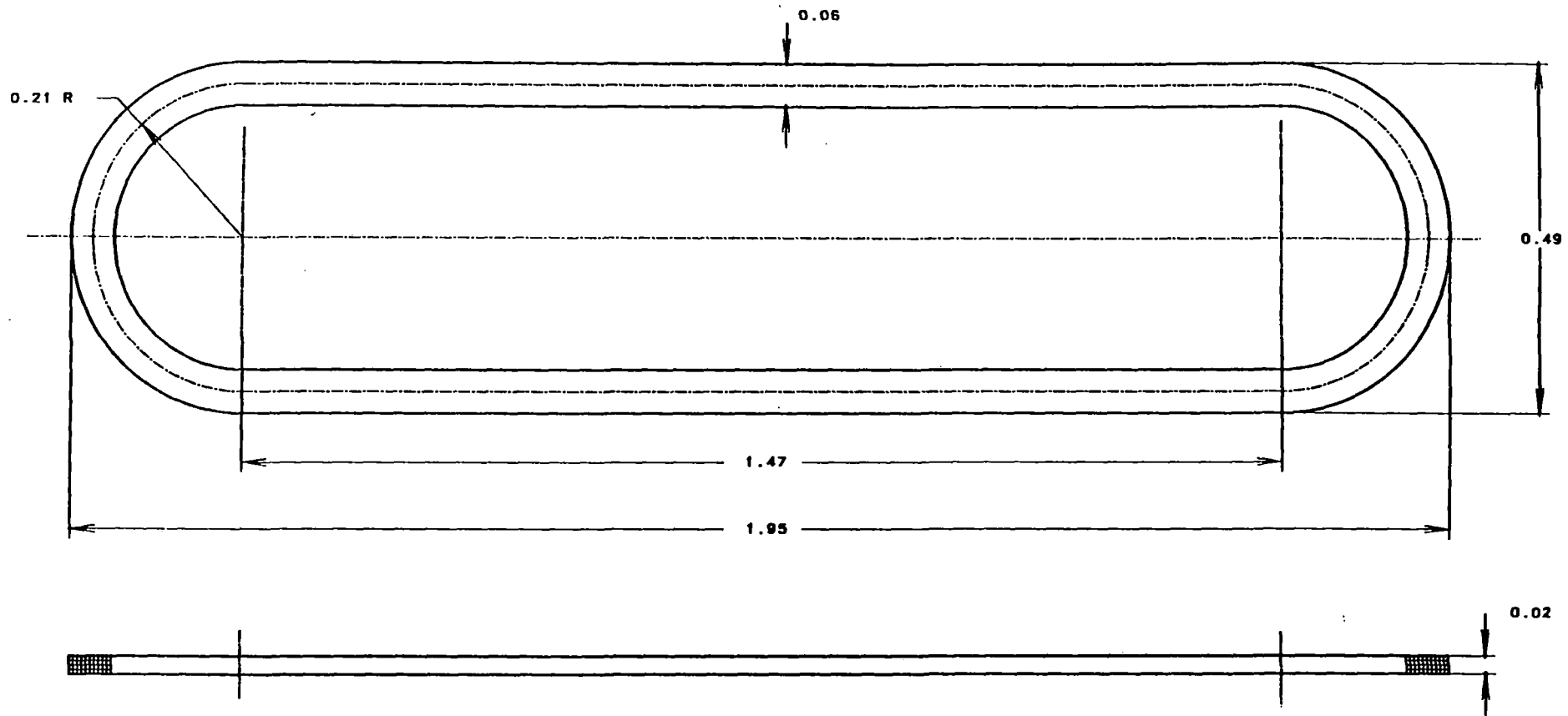


Fig 4.3-6. Racetrack Coil Dimensions

**Table 4.3-1
Estimated Weights for Racetrack
Lift Module Components**

Component	Weight [kg]
Coil	26
Coil Form/Structure	31
Radiation Shield	9
Cold Mass Support	9
Leads, Fittings & Mounts*	50
Outer Vessel	87
Miscl @ 10%	22
Total Module Weight	234

*Divide value by number of modules electrically and cryogenically in series.

4.3.2 Structural Design

Figure 4.3-3 includes a representation of the cold mass supports. These consist of three, nested shell, support tube subassemblies that transmit the levitation & drag forces to the vehicle. The center tube subassembly is rigidly connected to the vehicle chassis. The forward and rear tubes are connected through links (not shown) which provide support perpendicular to the cryostat while allowing for thermal contraction of the coil. The link is a "standard" detail for statically loaded coils and could be replaced with a pin/link system for improved fatigue resistance if that is found to be necessary. Figure 4.3-4 shows that the innermost shell in the tube subassembly is a stainless steel tube which attaches to the winding form and resists, via tension, the separating force between the two legs of the racetrack coil. The centerline of the coil is offset from the elevation of the support cylinder centerline in order to bring the coil closer to the outer surface of the outer vessel to minimize the distance to the levitation sheet. It is also offset from the structural centroid of the winding frame. These offsets introduce bending and torsional moments. The torsional moment in the frame is resisted by a closed triangular tube above the coil. Another view through the coil is shown in figure 4.3-5.

Figure 4.3-7 shows the coil and frame model as well as the local forces of electromagnetic origin. Support provided by the inner tube of the cold mass support cylinders was modeled as

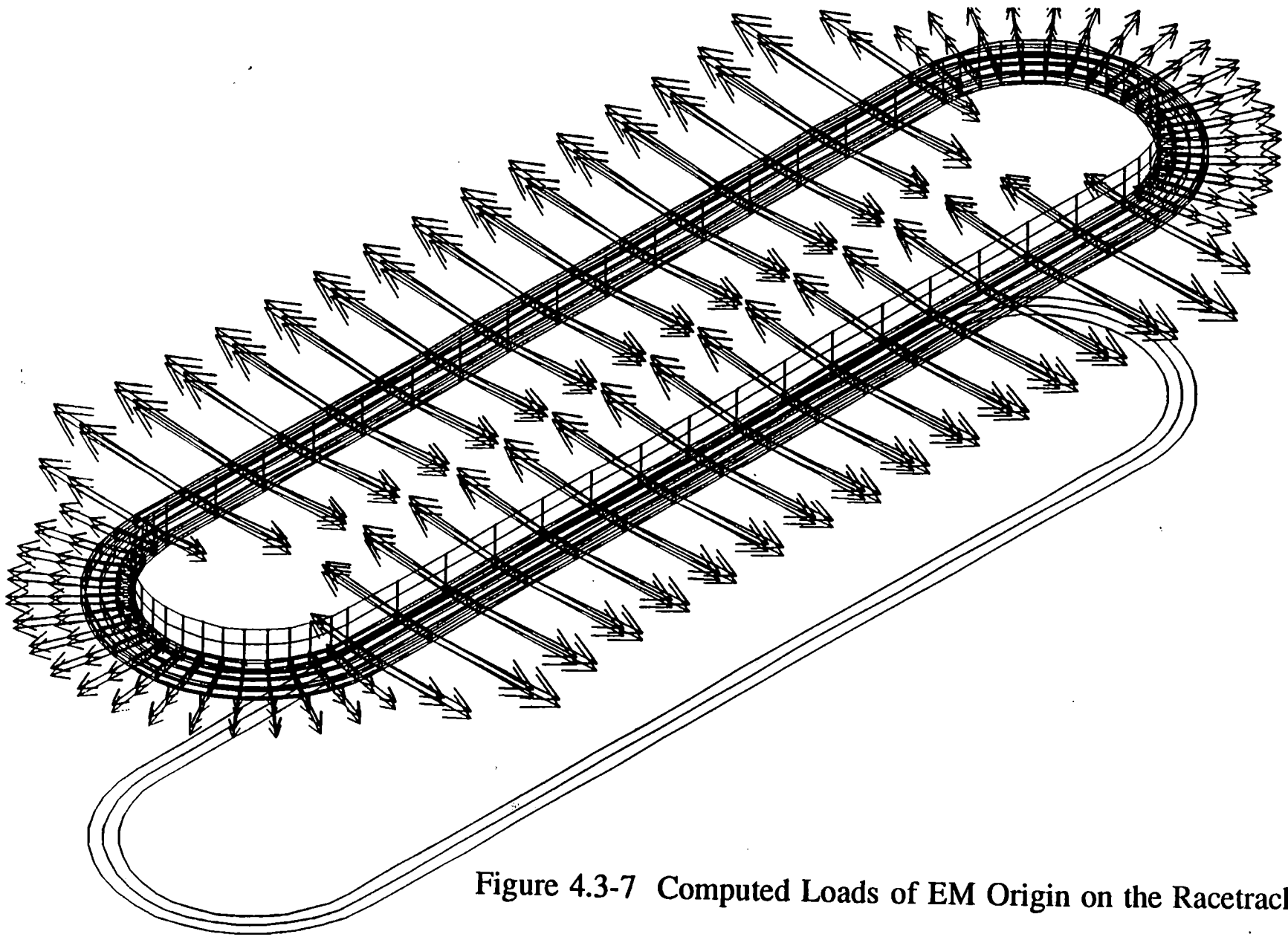


Figure 4.3-7 Computed Loads of EM Origin on the Racetrack Coil

displacement constraints at 6 locations and are not shown.

The ANSYS computer code was used to compute stresses and displacements. Figures 4.3-8 through 4.3-11 are the results obtained for a 1/4 in. thick coil form and support shell. The maximum stress in the shell is shown in Figure 4.3-8 and is 128 MPa (i.e., $128 \times 10^6 \text{ N/m}^2$) or 18.6 ksi (i.e., $18.6 \times 10^3 \text{ psi}$). In future design iterations, a thinner shell could be considered for the case, but should be reinforced at the connection to the support cylinders, and probably at the top of the curved section of the case where the peak stress occurs.

Vertical displacements due to the em loads are shown in Figure 4.3-9. The peak vertical displacement is 2.5 mm at either end of the coil. Displacements in the other 2 directions are shown in Figures 4.3-10 and 4.3-11 and are less than the vertical displacement.

An analysis of the cold mass support cylinders was also conducted. This is a series of nested shells alternately connected at their middle and their ends. Production of a long thermal path is the intent of the design, however this results in a long structural path. Figure 4.3-12 shows the finite element model with its loading and symmetry constraints (based on 1/4 symmetry). Figure 4.3-13 shows the stresses and Figure 4.3-14, the displacements. The results imply that this type of design is feasible, however, design details require further consideration in a future design iteration. It is estimated that this type of design could be modified to result in peak stresses of about 55 MPa or 8 ksi and maximum deflections of about 1.3 mm (0.05 in).

4.3.3 Module Heat Loads and Cryosystem Support

In this section, heat loads for the conceptual module design will be estimated to gain insight into the typical requirements, weights and powers for the cryosystem for the lift modules in a levitation system. Cryosystem size will be estimated for the steady state operating condition, because the additional refrigeration capacity associated with transient requirements such as initial system cooldown and charging can be reasonably assumed to be available in auxiliary facilities at stations or service areas.

The primary function of the cryogenic system is to deliver the working fluid at the required temperature and at a flow rate sufficient to remove the heat load on the module(s) to be cooled. The pressure drop through the module and flow rate must also match the capability of the system. In a superconducting coil system and cryostat, the flow is frequently split between the cold mass which must operate at the superconductor temperature, and the radiation shield which operates at a temperature intermediate between the superconductor and ambient temperatures. Experience has shown the advantage of using one or more thermal radiation shields in systems to reduce the cold end refrigeration capacity requirement and, in turn, the overall weight and power input.

If the system has a closed cycle with a single working fluid in the cryogenic system (e.g., helium), then the system supplies separate flow streams for the coil and for the radiation shield or uses part of the outlet flow from the cold mass to pass through the radiation shield.

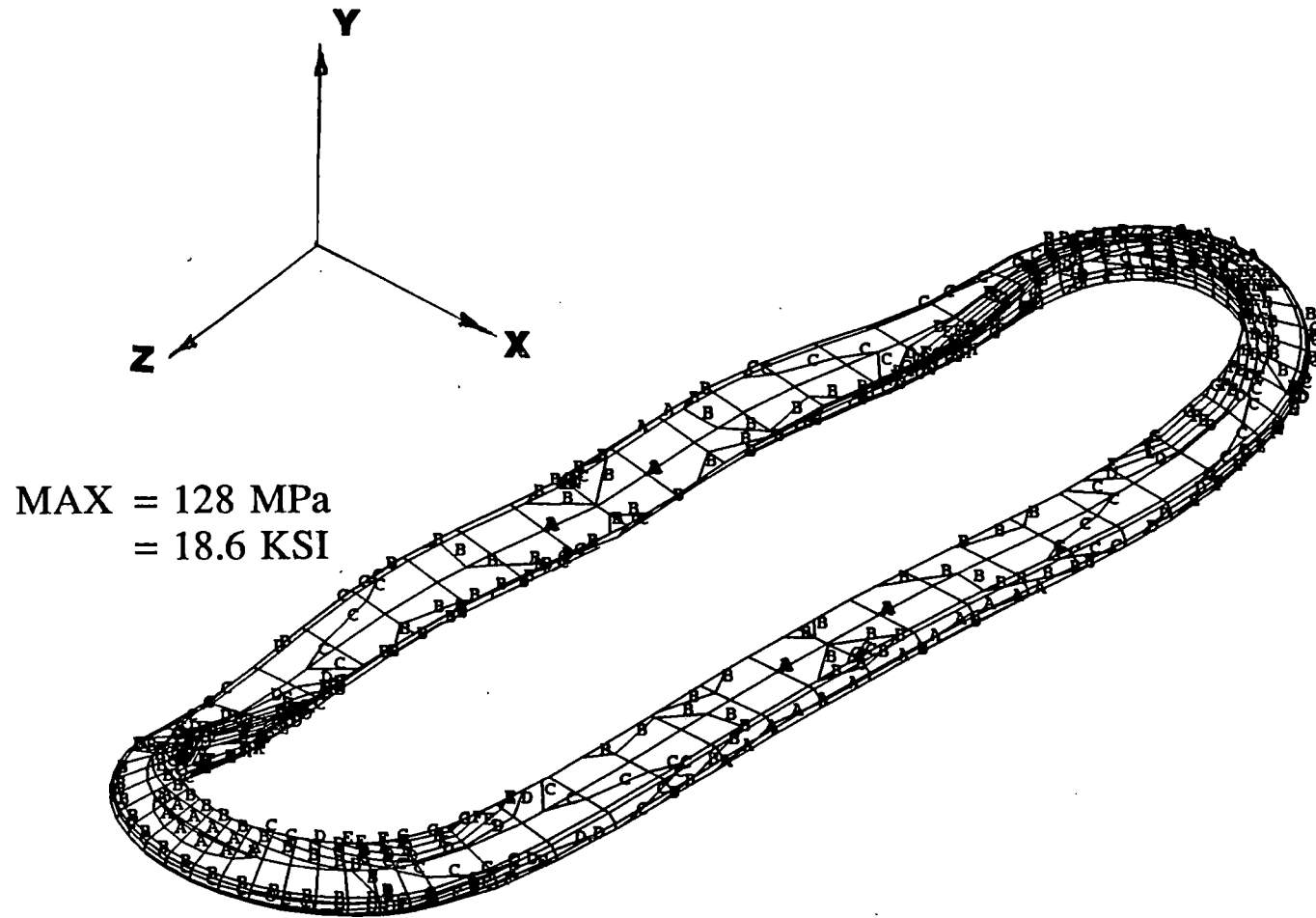


Figure 4.3-8 Computed Von Mises Stresses in the Support Shell

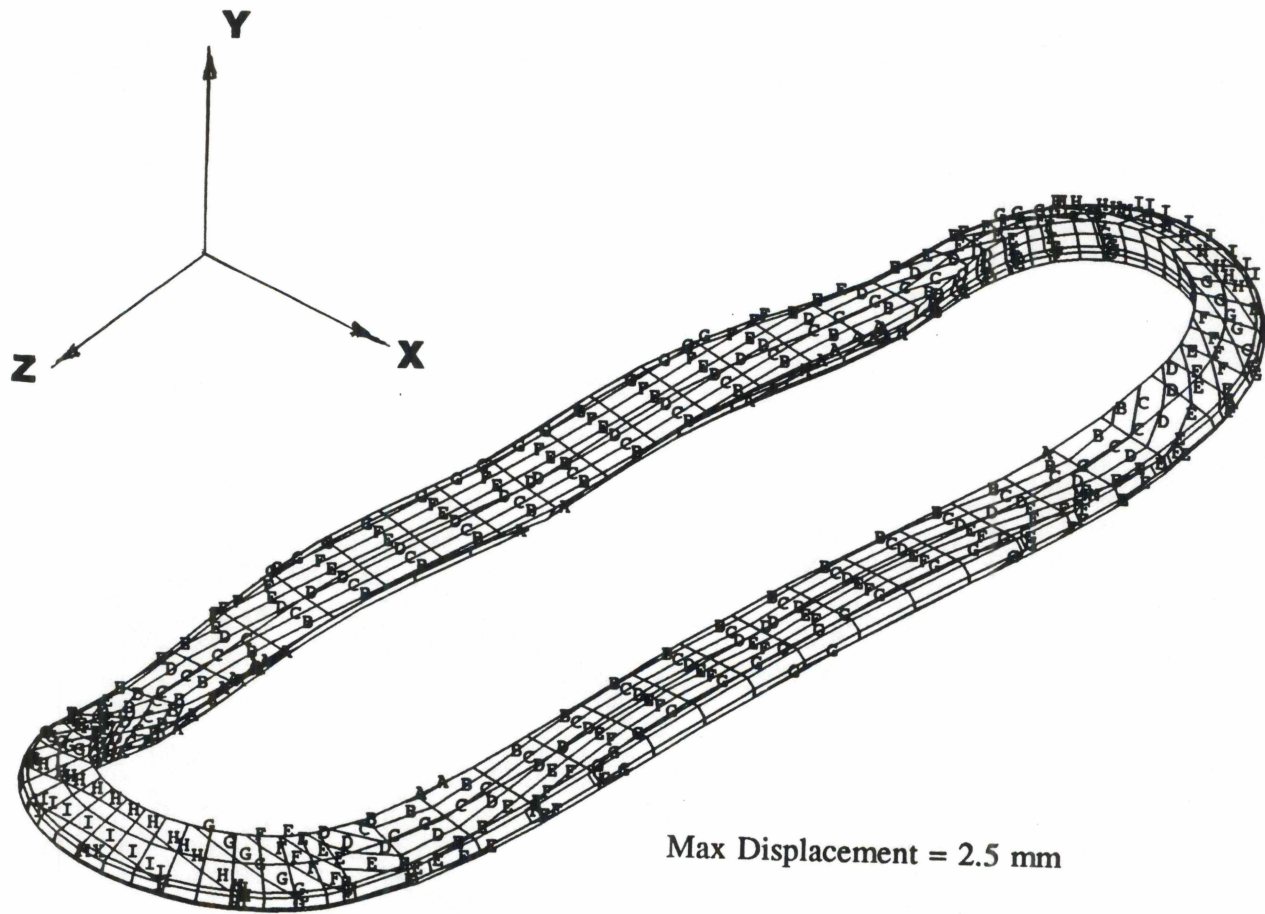


Figure 4.3-9 Computed Vertical Displacements of Coil and Form due to Lift and Internal EM Loads (meters)

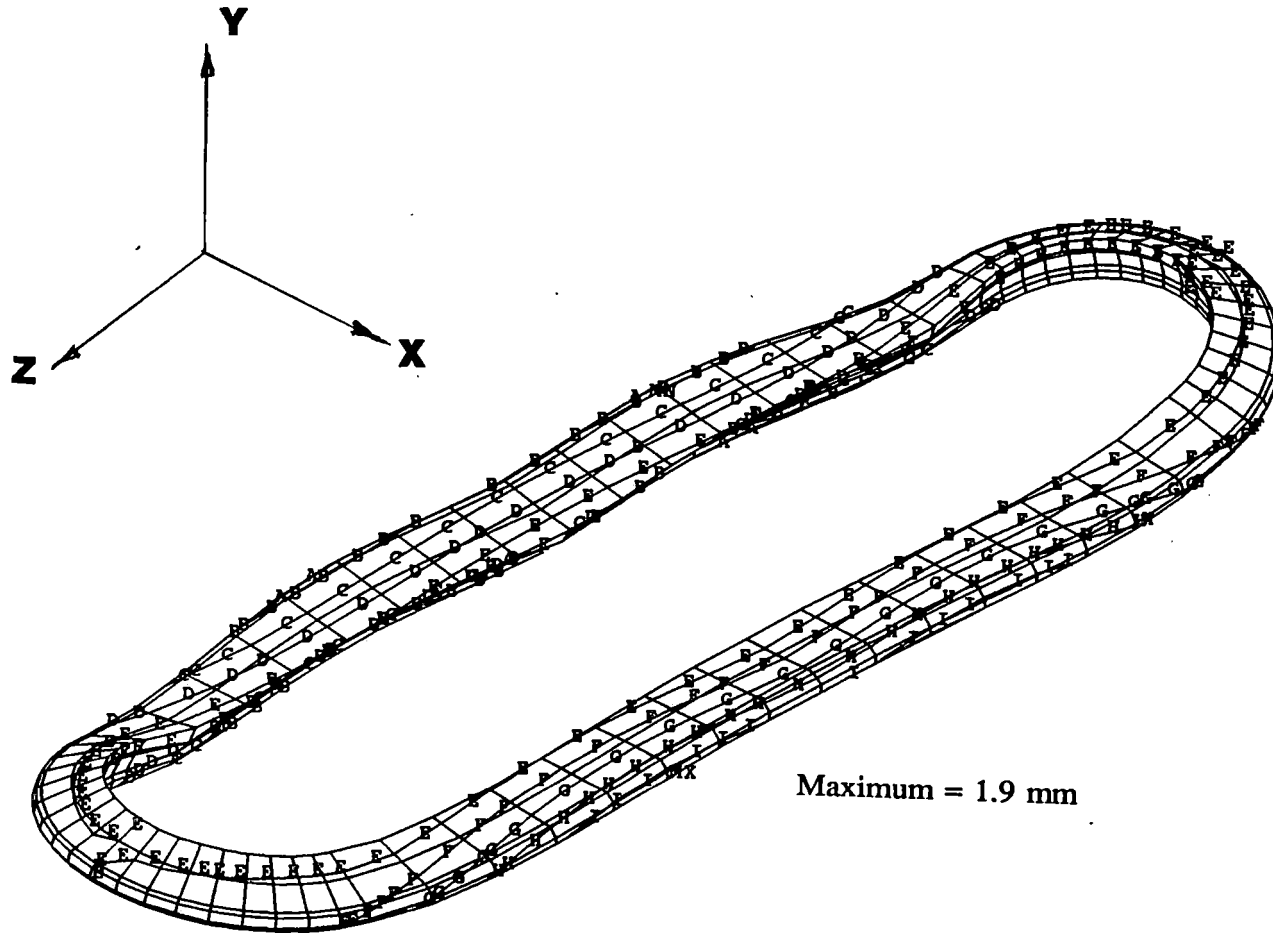


Figure 4.3-10 Computed Lateral Displacement of Coil and Form due to Lift and Internal EM Loads

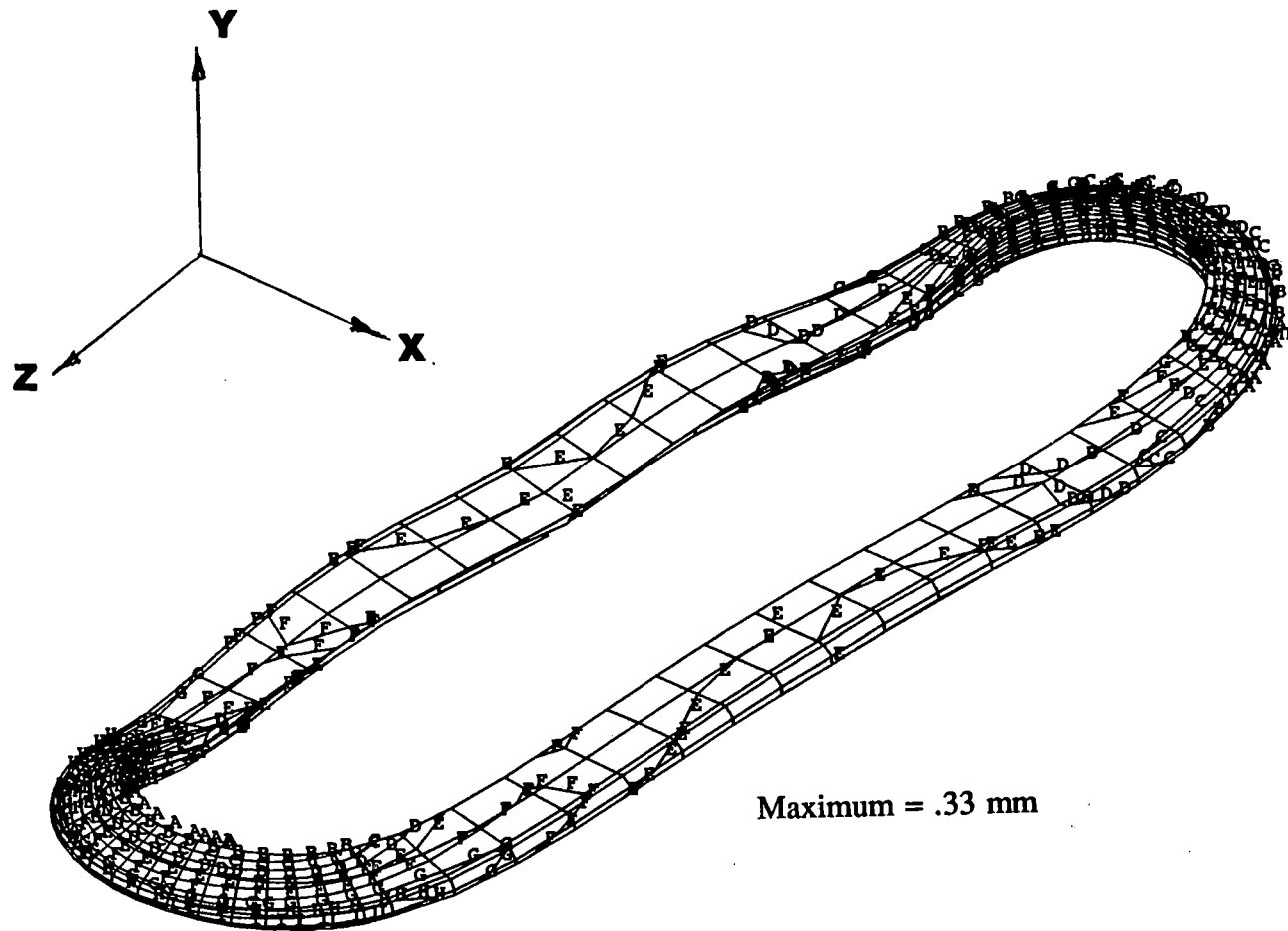


Figure 4.3-11 Computed Axial Displacement of Coil Form due to Lift and Internal EM Loads

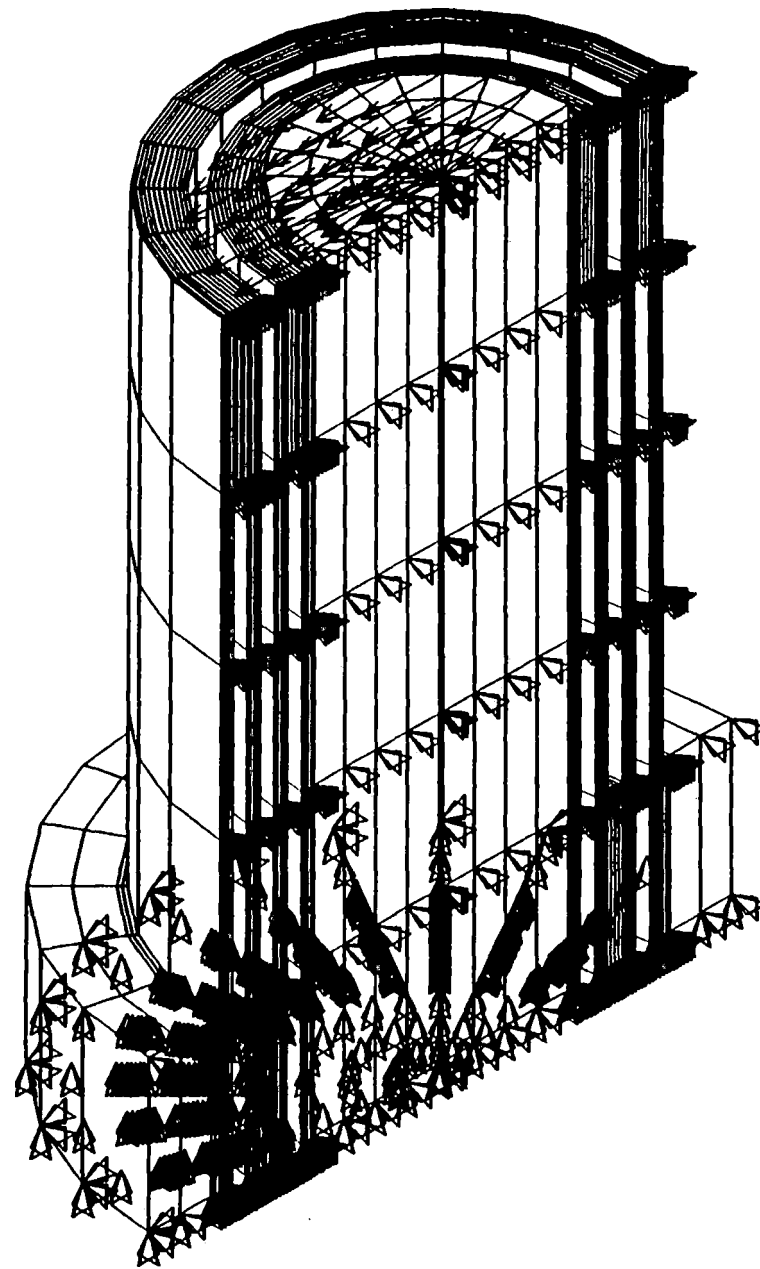


Figure 4.3-12 Finite Element Model Using Quadrant Symmetry for Analysis of a Cold Mass Support

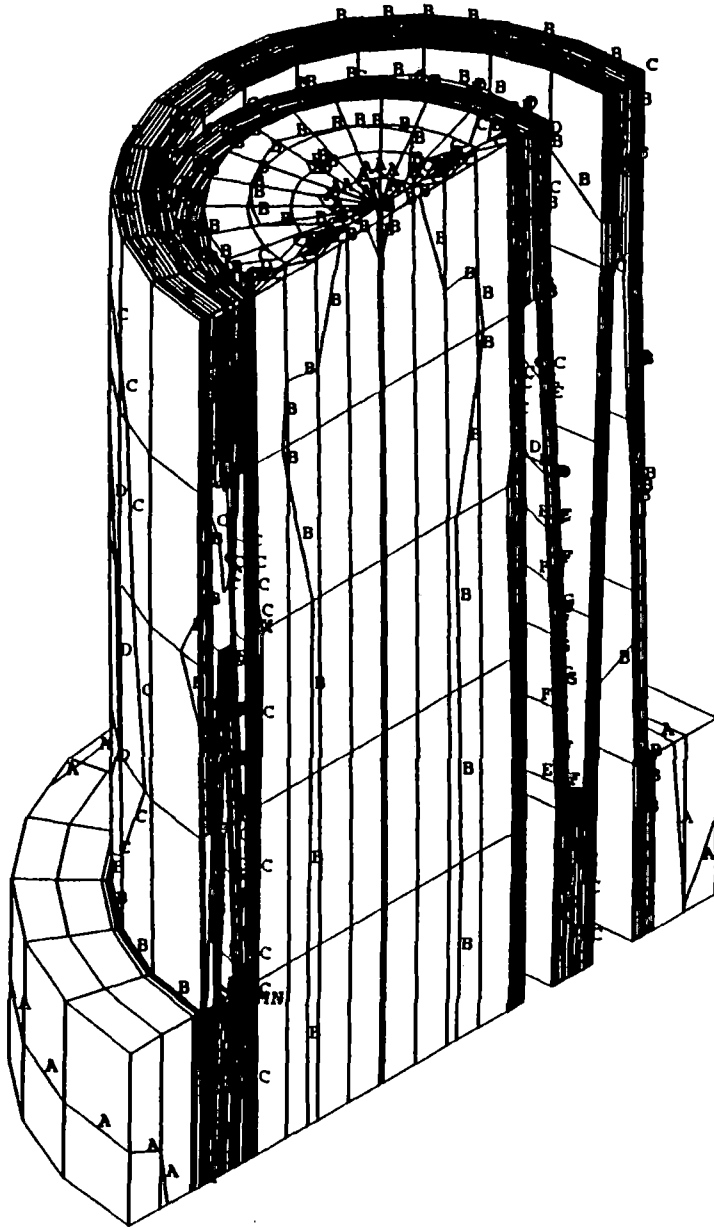


Figure 4.3-13 Stress Contours in the Cold Mass Support which is Displaced due to Loading

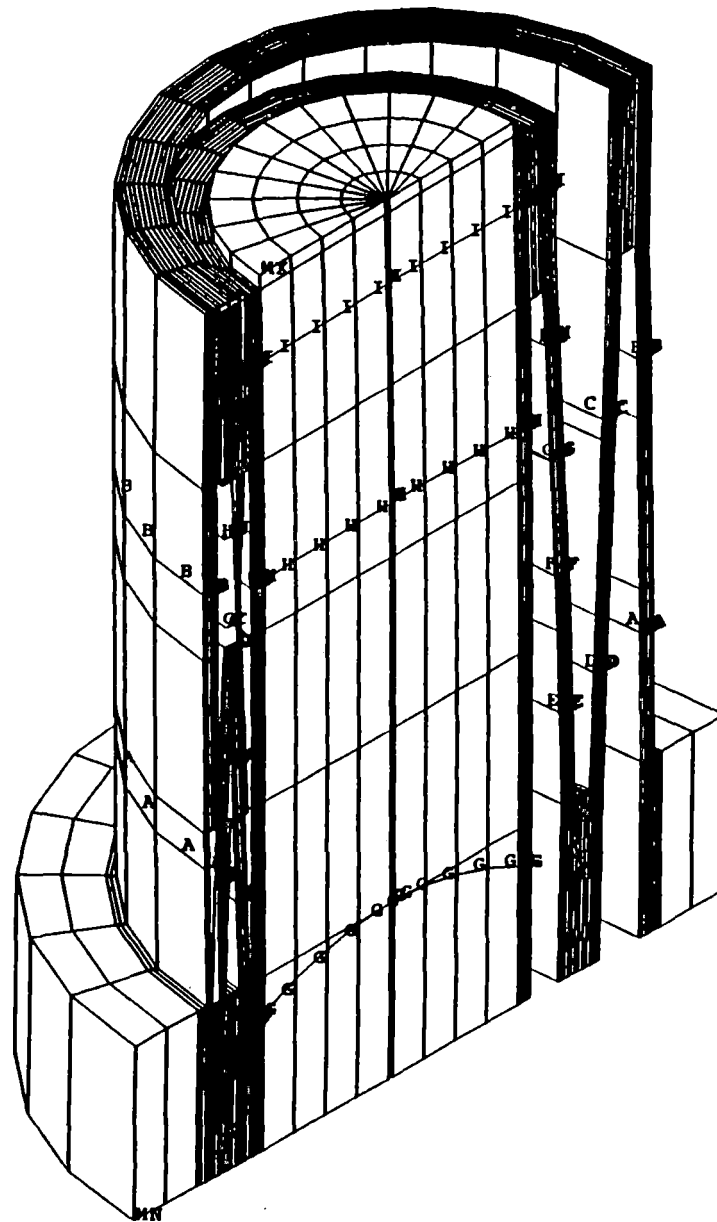


Figure 4.3-14 Displacement Contours for the Cold Mass Support Under Load

In many instances, it is advantageous to cool only the cold mass with helium which operates in a closed cycle, but use another cryogen in an open cycle. This requires the periodic refill of a reservoir with the other cryogen, typically liquid nitrogen, which is then used to circulate through the radiation shield and, frequently, to cool one of the heat exchangers in the closed cycle helium portion of the system. Selecting the details of the cryosystem configuration involves overall vehicle system optimization and is beyond the scope of this study. Hence, we will estimate a typical set of requirements by assuming the use of a system which is closed cycle helium plus open cycle nitrogen.

In an efficient cryostat design, the ambient heat load will not be the major source of heat to be removed by the cryosystem. In a levitation module, the major sources would be associated with losses due to cryogenic fittings, current leads for the superconducting coil, and AC losses generated as a result of transients during operation. There will also be major losses associated with distribution and return of cryogens over relatively long distances if a central cryogen system is used with transfer lines carrying the working fluids to and from coil modules.

The fittings on a module associated with helium distribution and return will have a heat load determined by the details of construction and largely dependent on whether they are of the permanent, that is, welded design, or of the quick disconnect (bayonet) type. There will be two helium fittings per module unless more than one coil is contained in a common cryostat. A reasonable, and probably conservative, estimate for the heat load associated with each fitting is about 0.5 w.

The current leads for the superconducting coil are a major heat load if permanently connected to the coil system. During operation, a pair of leads with an optimized design will contribute about 2 watts to the low end temperature heat load per 1000 A of operating current per lead pair. For the module design under consideration we have a conductor sample that was manufactured that will operate at 6000 A. We estimate that a similar design could be achieved in a smaller conductor at the 1500 A level (see section 4.2) and assumed this to be the operating level for heat load estimation.

The heat loss as described is per lead pair and could be reduced for a vehicle by operating modules in series electrically with the connections between modules made with superconductors within a common cryostat or passing between cryostats in a special transfer line.

The heat loss due to leads can also be reduced by about a factor of two by operating with a persistent switch. It could be reduced further with leads that can be detached and retracted after charging and the coil is placed in the persistent mode. This type of operation is described in Section 4.4 and has been demonstrated in many superconducting coil systems. It is commonly used in the MRI systems presently in use commercially. As a result, we will assume that sufficient R&D will be accomplished to allow this type of operation for the levitation modules. The heat loss per lead pair when attached and coils are being charged will then be covered by the capacity of facilities at stationary sites and the heat load during steady operation will be charged to the on-board system. A reasonable target for a lead pair that can be detached and

retracted after the coil is in the persistent mode is about 0.5 W.

Although the conductor is essentially lossless in the DC mode, the coil may contain joints and there will be two joints if a persistent switch is used as anticipated. This loss is computed as I^2R for each joint. A typical, achievable value for a good joint in a manufacturing environment is 0.5×10^{-9} ohms.

Another source of heat in the module is the AC losses associated with current or field changes in the coil system during operation. This loss is dependent on the detailed amplitude and frequency of the current and field transients experienced by the conductor as well as the details of the conductor material, processing, size and geometry. The magnitude can be controlled through choice of superconducting filament size, cable strand size, cabling configuration and insulation. When an operational spectrum for a MAGLEV vehicle is available, they can be estimated, then verified in a scaled down magnet as part of an R&D program. In this study, we shall assume that a reasonable heat load budget for this item is 1 W per module, thus using the reasonable assumption that the conductor filament size, etc can be adjusted if necessary to achieve this value.

Section 4.4 will show that a levitation module of the size under consideration can produce from about 3×10^4 to 1.5×10^5 N of lift when operating at 150 m/s over an aluminum sheet guideway, depending on the height above the guideway. If we assume, therefore, 5×10^4 N/module as a reasonable value for a vehicle, then 6 or 12 modules would be capable of levitating a total vehicle weight of 3×10^5 or 6×10^5 N, respectively. If we now assume a number of independent electrical and cryogenic circuits for the modules, then the total heat load requirement for the levitation coil system can be estimated.

Table 4.3-2 contains a heat load budget estimate for the cryogenic support system for vehicles using either 6 or 12 modules. Columns show the variations for 2 and 3 independent circuits for the 6 module case and for 2, 3, and 4 independent circuits for the 12 module case. The number of modules and circuits would have to be chosen as part of a system design, but it is clear that more independent circuits increase the heat load because of the greater number of leads and fittings. On the other hand, a systems analysis may deduce that there are reliability or maintenance issues that favor more circuits. The estimates in the table indicate a heat load to the low temperature cold mass ranging from 17 to 21 W for the 6 module vehicle and 28 to 33 W for the 12 module vehicle. We also assume use of a reservoir of liquid nitrogen which provides about 84-92 liters/day for the 6 module vehicle or about 141-165 liters/day for the 12 module vehicle.

The heat load requirements estimated above could be provided by a number of commercially available units. One such unit is a Process Systems International Model 1430 which, with different auxiliary equipment, could provide the range of capacities indicated above to a 4.5 K cold mass. It would have an estimated total weight ranging from about 1800-2600 kg and a power input required of about 30-55 Kw.

Table 4.3-2 Heat Load Budget Estimate for Multiple Levitation Modules

No. Modules	6	6	12	12	12
Lift Capacity at 5E4 N per Module	3.00E+05	3.00E+05	6.00E+05	6.00E+05	6.00E+05
No. Independent Circuits	2	3	2	3	4

Heat Loads to Cold Mass

0.06 w. Thermal Radiation/module	0.36	0.36	0.72	0.72	0.72
0.23 w. Conduction (Cold Mass Spts)	1.38	1.38	2.76	2.76	2.76
0.5 w. per Cryogenic Fitting	2.00	3.00	2.00	3.00	4.00
0.5 w. per power lead pair	1.00	1.50	1.00	1.50	2.00
5E-10 ohms, joint resistance	0.01	0.01	0.02	0.02	0.02
1 w. AC losses per module	6.00	6.00	12.00	12.00	12.00
50 % (Contingency + Trnsfr Lines)	5.38	6.13	9.25	10.00	10.75
Total to Cold Mass, w.	16.13	18.38	27.75	30.00	32.25

Notes: Joint resistive loss assumes 1500 A operation, 1 joint per coil & 1 persistent switch per circuit (2 joints per switch)

Heat Loads to Liquid Nitrogen

2 w. Thermal Rad Shield/module	12	12	24	24	24
2.5 w. Conduction (Cold Mass Spts)	15	15	30	30	30
4.2 w. Power Lead Spts & Ftngs	8.4	12.6	8.4	12.6	16.8
50 % (Contingency + Trnsfr Lines)	17.70	19.80	31.20	33.30	35.40
Total LN2 Module Heat Load, w	53.1	59.4	93.6	99.9	106.2
Total LN2 Mod Heat Load, 1/yr	1.18	1.32	2.09	2.23	2.37
1/yr LN2 reqd by Refrig System	2.30	2.50	3.80	4.20	4.50
Total LN2 Volume per 24 hrs, l	84	92	141	154	165
Total LN2 Wt per 24 hrs, Kg	68	74	114	125	133

Figures 4.2-1 and 4.2-2 imply considerable advantages if the system could operate at 8 K. On this basis we would expect a decrease in power input to the cryosystem of about a factor of 2 and a substantial weight reduction.

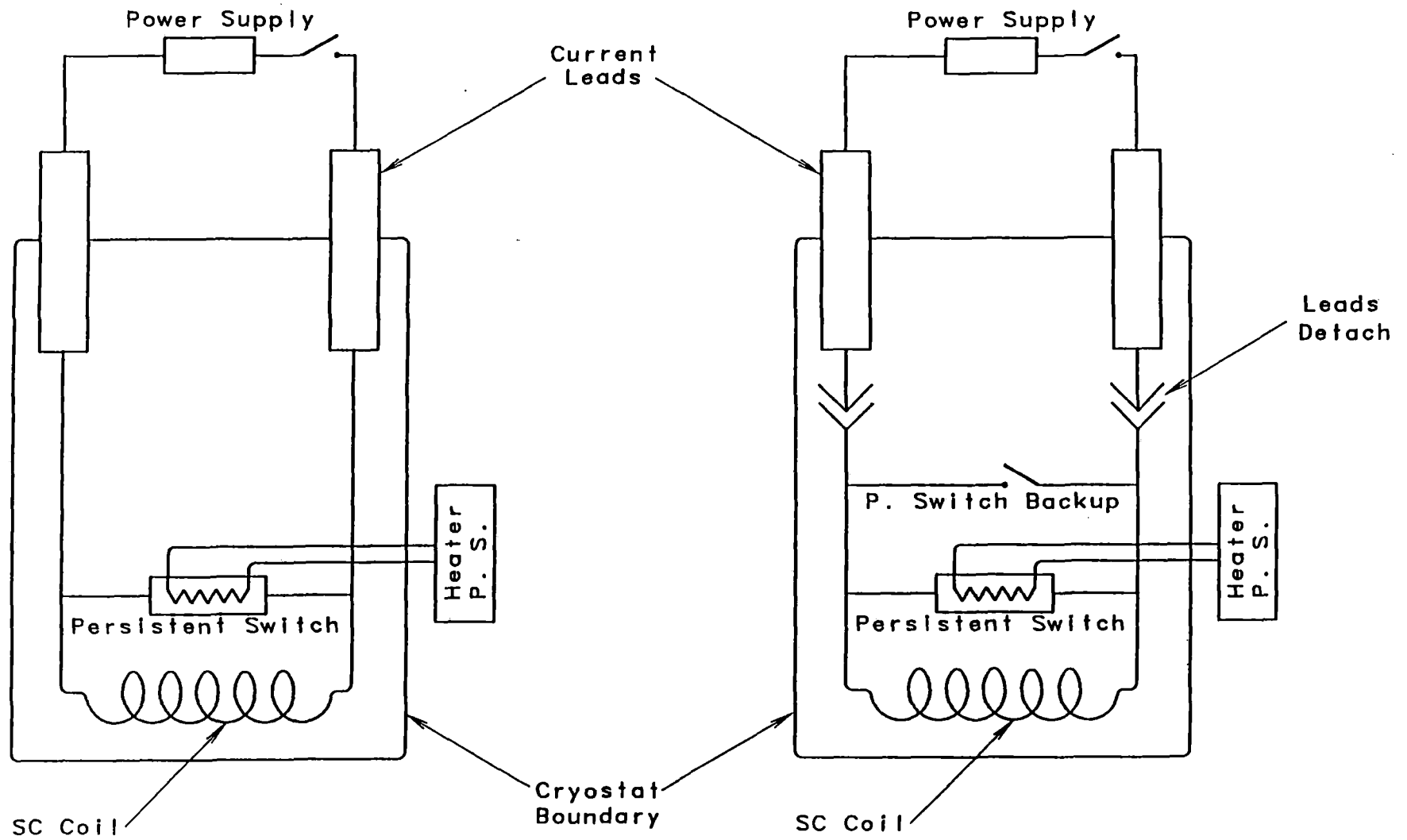
4.3.4 Coil System Charge and Discharge

Figure 4.3-15 is a schematic illustrating two relatively standard methods for charging a superconducting coil system.

In method A, the superconducting coil is located within its cryogenic container or cryostat and connected to a power supply outside the cryostat via a pair of current leads passing through the cryostat boundary. These current leads are usually specially designed to reduce thermal conduction along the leads from ambient conditions into the cryostat because each watt of heat load into the cryostat represents a significant power requirement for the refrigeration or liquefaction system supplying the cryogen for the coil system. Alternately, in an "open" cryogenic system, a significant volume of liquid cryogen would have to be carried to support the heat load for this part of the total requirement for the length of the mission. For example, a well designed pair of current leads will still produce a heat load of about 2 watts to the cryogen per thousand amps of current carrying capacity per lead pair. The power required by a refrigerator to support this part of the total heat load at low temperature is significant as discussed earlier.

The persistent switch shown is optional in method A, in that one may choose to have none, charge the coil system with the power supply, and leave the power supply connected and "on" throughout operation. This is unlikely, however, because of the high heat load penalty. A more likely scenario would involve detachable leads and a persistent switch as in method B.

The persistent switch is typically a length of superconducting wire (possibly in coil form) connected across the terminals of the coil and located within the cryostat. It also has a heater which can be activated through relatively small current leads which pass through the cryostat boundary to a small power supply outside. To charge the main superconducting coil system, the switch on the main power supply is left open while the heater power supply on the persistent switch is activated to a current level that raises the heater output until the persistent switch superconducting wire is above its critical temperature so that it is not superconducting. The level of resistance in the persistent switch at this point is selected when it is designed so as to be consistent with the desired charging vs time scenario. The main power supply switch is now closed and the main power supply current raised to the desired operating current level. The heater power supply is then turned off and the persistent switch is designed to allow the temperature of its wire to drop back below its critical temperature so that it is again superconducting. The current from the main coil power supply may now be turned down to zero without significant change to the current flowing through the superconducting coil because it is short circuited by the superconducting wire in the persistent switch. The current in the circuit will decay over time depending on the inductance of the circuit and resistance (typically, only the resistance of the joints is significant and can be made quite small, that is, of the order of 1×10^{-9} ohms, thus yielding a very long current decay time constant.



A) SC Coil System with Permanent Current Leads

B) SC Coil System with Detachable Current Leads

Fig. 4.3-15 Schematic of Two Options for Charging a Superconducting Coil for MAGLEV Applications

The approach schematically shown in B is operationally identical to that in method A for charging the superconducting coil when the leads are connected to the coil. However, two additional features are shown in the schematic.

A back-up switch operating in parallel with the persistent switch is shown for reliability purposes. This may be another switch of the same type or a switch which is closed mechanically. It provides protection for coil overvoltage in the event the persistent switch fails open while the coil is operating in the persistent mode with the power leads detached.

The other, more significant, feature is that the current leads are made to be detached after coil charging, persistent switch closure (transition to superconducting state) and main power supply turn-off. This requires complex mechanical connections within the cryostat that can be detached from outside and that can allow complete removal of the leads or moving them far enough to significantly reduce the heat transfer down the leads into the cold cryostat. In this way, the heat load during coil operation can be reduced.

The approach described for both methods in Figure 4.3-15 has been demonstrated in laboratory and commercial systems. For the conceptual design in this report, we have selected method B because of the advantages from the heat load standpoint. There are no feasibility issues, however, R&D will be necessary to design the required detachable leads and persistent switch compatible with MAGLEV reliability requirements and the use of a cable-in-conduit type of conductor.

4.4 Lift and Drag Characteristics for Coil

In this section, we will consider the lift and drag characteristics for the racetrack coil described earlier. It will be assumed to be traveling over a sheet guideway to illustrate the features of this type of interaction. The calculations were performed using the methods of Reitz[4.7].

Figure A-1 shows a coil traveling with a velocity V with its plane parallel to a sheet of conducting material. The functional form of the lift equation was described earlier and derived in Appendix A as Eqn (A-17). If the coil is the racetrack in Figure 4.3-6 and traveling parallel to its long side then the lift, drag and lift/drag ratio typically have the shapes shown in Figure 4.4-1, 4.4-2 and 4.4-3, respectively.

A family of curves is given in each plot with each curve corresponding to a selected height from the centerline of the winding cross-section to the surface of the sheet guideway. The sheet for these figures is assumed to be aluminum with a thickness of 0.02 m. The lift and drag forces in Figures 4.4-1 and -2 are normalized to $\mu_0 I_v^2$ where I_v is the ampere turns in the coil. Hence, the figures are useful for coils with any number of turns or current provided they are of this geometry and size.

Figure 4.4-1 shows that the lift rises monotonically as speed increases for a given height of coil above guideway whereas Figure 4.4-2 shows that the drag first increases to a peak then decreases at higher speed. Figure 4.4-3 shows the lift/drag ratio which increases continuously and is close

Lift Force vs Speed, $\emptyset.425\text{m} \times 1.8\text{m}$ (1 coil)
 $T = \emptyset.02\text{m}, \text{SIG} = 2.538\text{E}7$

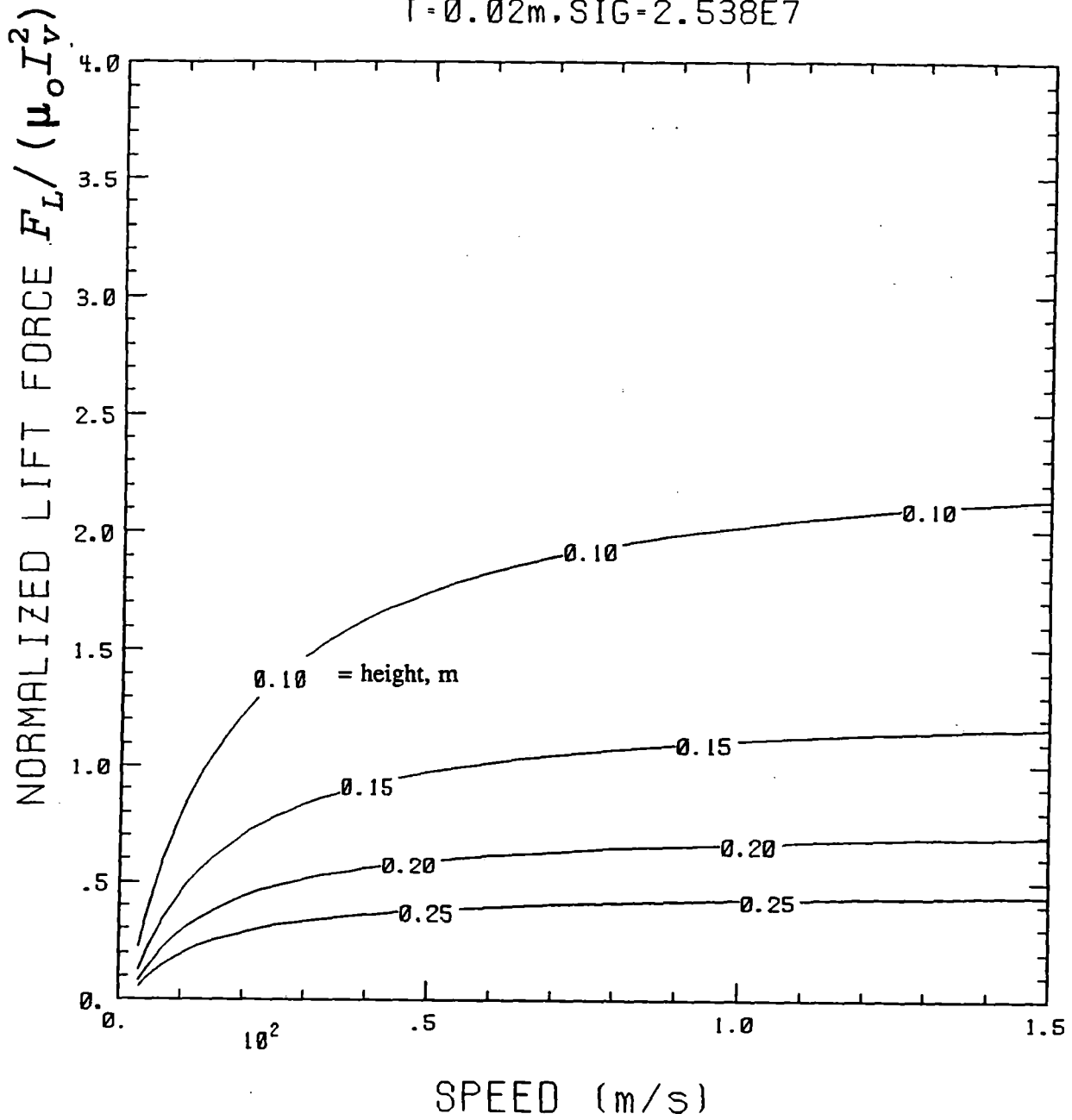


Figure 4.4-1 Normalized Lift vs Speed for Several Coil Heights Above a Sheet Guideway

Drag Force vs Speed, 0.425m x 1.8m (1 coil)
T=0.02m, SIG=2.538E7

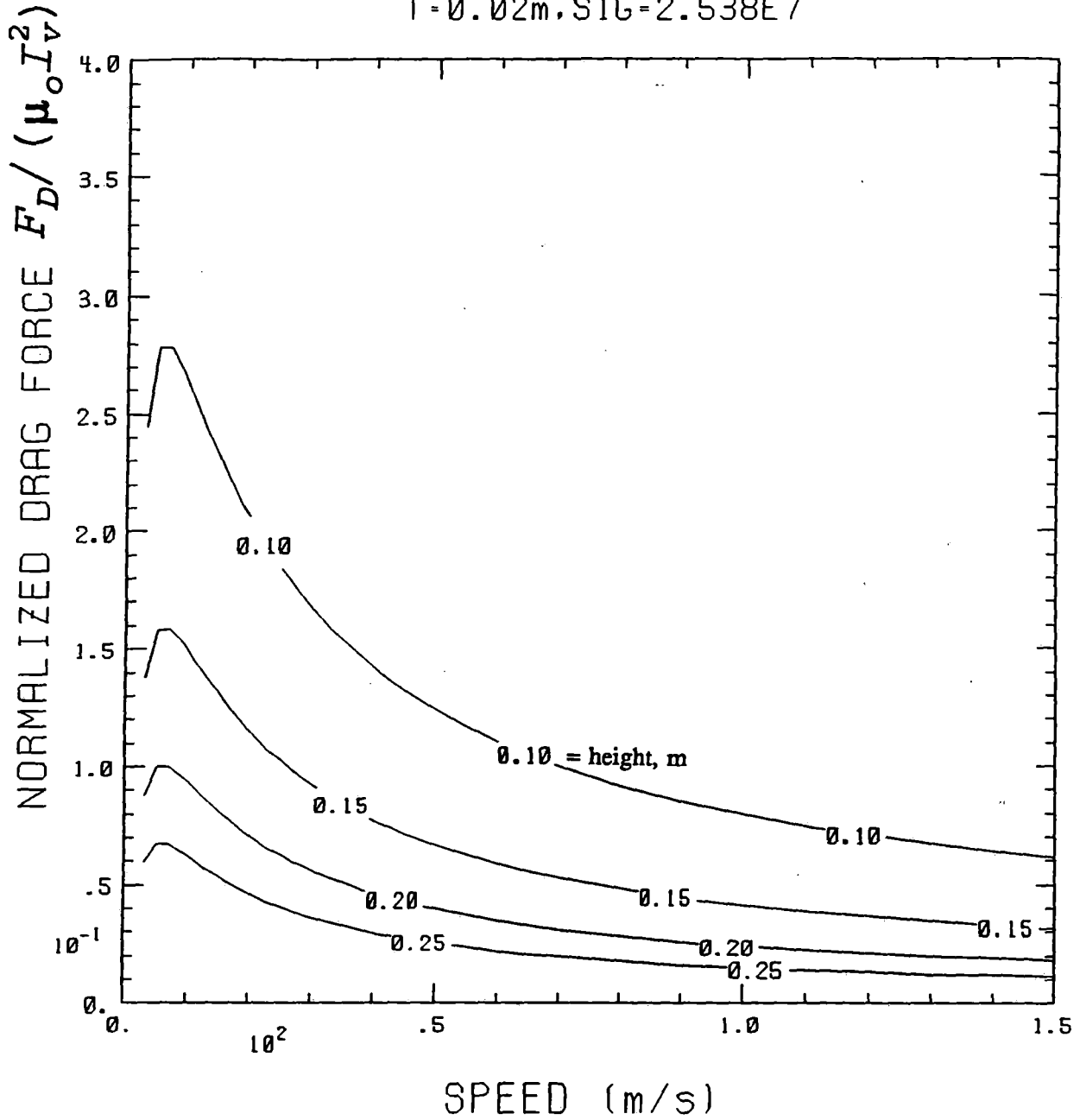


Figure 4.4-2 Normalized Drag vs Speed for Several Coil Heights Above a Sheet Guideway

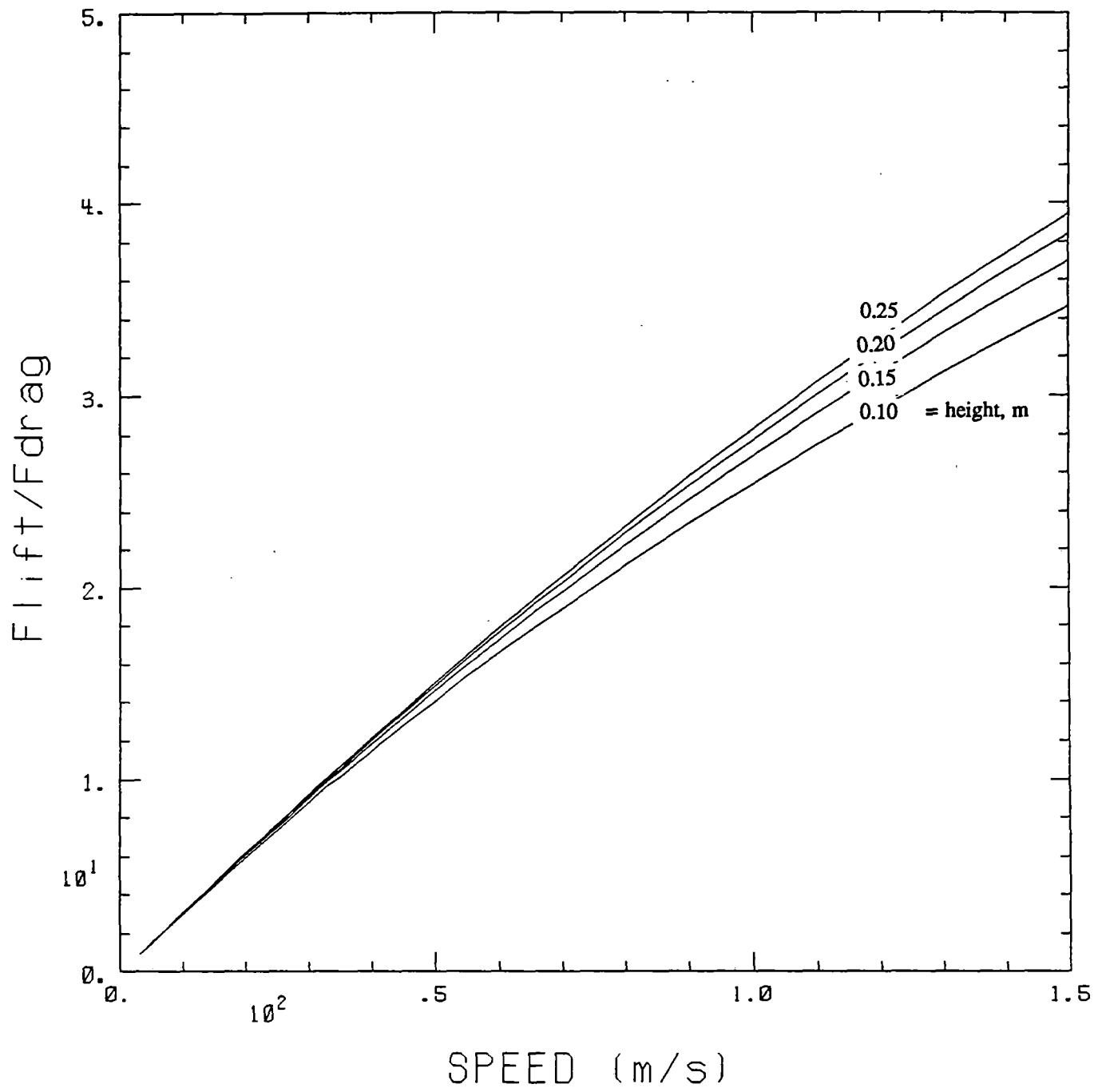


Figure 4.4-3 Lift/Drag Ratio vs Speed for Several Coil Heights Above a Sheet Guideway

to being proportional to speed for the parameter ranges selected.

The curves in Figures 4.4-1 to -3 were used to generate Table 4.4-1 which illustrates some typical characteristics in non-normalized form. All cases in the table correspond to an aluminum guideway with a thickness of 0.02 m and to a coil speed of 150 m/s. The section on EM interactions gives normalized lift, normalized drag, and lift-to-drag ratio from the previous figures for several heights from coil center to guideway. A clearance from guideway to coil cryostat is also given assuming that the distance from coil center to the outside of the cryostat is 0.05 m. This was shown to be a reasonable assumption in our design section.

The last two sections of Table 4.4-1 gives coil characteristics based on either a given number of amp turns in the coil or based on a given required lift. Note that for a fixed number of amp turns (i.e., 2.4×10^5), the lift ranges from about 1.54×10^5 to 3.19×10^4 N depending on the height of the coil above the guideway. In the last section of the table the lift is fixed at 5×10^4 N and the corresponding drag and amp turns required are then determined.

Note that the design point in the previous section was for about 2.4×10^5 amp turns, hence the coil module in the conceptual design would lift about 5×10^4 N at a speed of 150 m/s and a height from coil center to guideway of 0.2 m. If the height could be reduced to 0.1 m, the lift capability at this speed would be about 1.5×10^5 N for the same amp turns.

5.0 Impact of High T_c Superconductors

Several publications are available that summarize the state-of-the-art in high T_c superconductors and their potential applications [e.g. -1,2]. Details concerning properties and advancements can be found in these papers. In summary, the current promise surrounding these materials is exemplified by the following.

At this time, advances in materials such as $\text{Bi}_j\text{Sr}_k\text{Ca}_l\text{Cu}_m\text{O}_n$ (j,k,l,m,n are integers) have led to laboratory scale samples of materials that have higher critical current densities than either NbTi or Nb_3Sn at high magnetic fields (i.e. 25 T) and at 4.2 K, the temperature realm of the low T_c superconductors. Furthermore, at 77 K, and magnetic fields of the order of 1-2 T, the new materials have critical current densities ranging from 3×10^7 to 5×10^8 A/m² and the so-called low T_c materials are no longer superconducting [1].

The above results are in a range where they could be useful for large scale magnet applications such as Maglev. However, the primary problem remains to be the development of a manufacturing process that can produce large quantities of material in a form suitable for fabrication into coil form with the associated rigors of manufacture. When this is achieved, Maglev will benefit directly through a reduced system complexity, reduced weight, and reduced on board power requirement.

The ability of the superconducting coil system to operate at a higher temperature will reduce the ambient heat transfer into the system and reduce the heat load requirement for the cryogenic

Table 4.4-1 Typical Racetrack Lift Coil Characteristics

Guideway Features

Material	Aluminum
Thickness, [m]	0.02
Speed, [m/s]	150

EM Interactions

Height, [m]	0.1	0.15	0.2	0.25
Clearance, [m]	0.05	0.1	0.15	0.2
Lift to Drag Ratio, FL/FD	34.50	37.00	38.50	39.30
Normalized Lift, $FL/(\mu_0 \cdot I_v^2)$	2.13	1.17	0.69	0.44
Normalized Drag, $FD/(\mu_0 \cdot I_v^2)$	0.062	0.032	0.018	0.011

Coil Characteristics for Given Amp-turns

Amp-turns, I_v	2.40E+05	2.40E+05	2.40E+05	2.40E+05
Lift, [N]	154174	84687	49944	31848
Drag, [N]	4469	2289	1297	810

Coil Characteristics for Given Lift

Lift, [N]	50000	50000	50000	50000
Drag, [N]	1449	1351	1299	1272
Amp-turns Required	1.37E+05	1.84E+05	2.40E+05	3.01E+05

support system. This will translate into a reduced on board power consumption by the refrigeration subsystem or, alternatively, a reduction in the cooling system reservoir capacity. The impact can be significant for relatively small increases in operating temperature. If the operating current density is high enough, there could also be a reduction in superconducting coil weight.

If the operating temperature is high enough to reduce the ambient heat load from thermal radiation, there will be a reduction in cryostat weight and complexity. This will be most significant when the need for a vacuum insulating space may be replaced by less expensive thermal insulating schemes based primarily on reduction of thermal conduction rather than thermal radiation.

The use of a CICC type of winding construction, as proposed in this report, is directly applicable to high temperature superconductors when they become available. The wires in the cable in the conduit would be replaced by the new material and the working fluid temperature in the conduit would be raised to be consistent with the new material properties and stability requirements. For temperatures below 20 K, the working fluid could still be helium; for temperatures above 20 K, the working fluid could be hydrogen or helium; for temperatures above 80 K, it may be beneficial to change to nitrogen; at high enough temperatures, it may be reasonable to change to water or use air cooling.

6.0 Information Required and Recommended Research

As part of our activity we have identified areas for recommended research. The following outlines several topics which should receive support to assure availability of components for a MAGLEV system.

6.1 Conductor Development

CICC conductors require cables of superconductor in vacuum-tight conduits. Selection of materials, manufacturing process development and testing thus far have focused primarily on applications for large magnet systems for fusion where the operating currents are tens of thousands of amperes and the conduit is a significant structural component for accumulation and transmission of large static or low frequency dynamic loads within the winding pack. AC losses are also an issue which has received considerable attention for transient requirements consistent primarily with fusion applications. Energy margin (stability) and AC loss analyses and experiments are a critical need for MAGLEV conductors.

MAGLEV will require conductors which operate at low current levels with relatively modest static structural requirements relative to those needed for fusion, a substantially different dynamic load spectrum, and a different exposure to transient magnetic fields leading to a different AC loss spectrum. The result is the need for R&D activities for manufacturing processes consistent with conductor requirements for low currents (e.g., 100-5000 A) and for conduits which can be applied in a cost effective fashion consistent with vacuum requirements and manufacture of large numbers of units. Testing should concentrate on conductor performance in terms of energy

margin, quench characteristics and AC loss generation. Alternative forms of conduit geometry and materials should be tested to include single and multiple flow paths.

6.2 Code Development

Codes for prediction of CICC performance in terms of energy margin, stability and quench have been under development for several years. They have been moderately successful in correlating with experimental results, but are not generally reliable for prediction and are not efficient in terms of computer usage, particularly for quench, safety, or protection studies. In addition, most of the test data are not in the range of interest for MAGLEV applications. A MAGLEV oriented analytic and experimental development activity in this area is essential for better understanding of CICC performance and for acceptable, efficient design purposes.

6.3 Joint and Lead Development

The CICC developed for MAGLEV will require reliable hydraulic manifolds and joints as well as electrical joints and connections to power leads. Demountable power leads have been developed for other superconducting magnet applications and will be necessary for MAGLEV systems. Concepts may exist, but detailed designs for reliable, repeatable operation in a commercial environment do not. Although often perceived as mundane engineering problems, they are also the most likely source of magnet failures and require R&D early to ensure reliability.

6.4 Persistent Switch Development

It is essential to operate the lifting coils for MAGLEV in the persistent mode. As a result, an activity should be initiated to develop reliable persistent switches for CICC configurations to assure availability of this component when needed.

References

- [4.1] M. Morpurgo, The Design of the Superconducting Magnet for the 'Omega' Project, Particle Accelerators, 1:255-263, 1970.
- [4.2] M. O. Hoenig, Internally Cooled Cabled Superconductors, Cryogenics, 20:373-389 and 427-434, 1980.
- [4.3] M.O. Hoenig, M.M. Steeves and J.V. Minervini, MIT 12-Tesla Coil Experimental Results, Adv. Cryo. Eng., 31:151-158, 1985.
- [4.4] M.M. Steeves, T.A. Painter, M. Takayasu, et al., The US Demonstration Poloidal Coils, presented at the 1990 Applied Superconductivity Conference, Snowmass, CO, to be published.
- [4.5] D.S. Beard, W. Klose, S. Shimamoto, & G. Vecsey, ed., "The IEA Large Coil Task; Development of Superconducting Toroidal Field Magnets for Fusion Power", Fusion Engineering & Design, Vol 7, Nos 1&2, 1988.
- [4.6] J.L. Smith, G.Y. Robinson, & Y. Iwasa, "Survey of the State of the Art of Miniature Cryocoolers for Superconductive Devices," NRL Memo Report 5490, Dec, 1984.
- [4.7] J.R. Reitz and L.C. Davis, "Force on a Rectangular Coil Moving Above a Conducting Slab," J. Appl. Phys., Vol. 43, No. 4, April 1972, p. 1547.
- [5-1] D. Larbalestier, "Critical Currents and Magnet Applications of High T_c Superconductors", Physics Today, June, 1991.
- [5-2] J.R. Hull, "Potential Impact of High Temperature Superconductors on Maglev Applications", ANL/ESD/TM-27, February, 1992.
- [5-3] E.W. Collings, "Design of High T_c Superconductors for DC and AC Applications", 2nd Japan Inter SAMPE Symp & Exhib., Chiba, Japan, December, 1991.

Appendix A - Derivation of Equations for Section 3.1

A.1 Equation (3-1): Weight of Racetrack Coil

The volume of the coil envelope in Figure 3.1-1 is

$$V = 2d[2(r_o - r_i)L + \pi(r_o^2 - r_i^2)] \quad (\text{A-1})$$

The ratio of the coil material volume to envelope volume is λ and the density of the coil materials is ρ_c , hence the coil weight is

$$W_c = \lambda \rho_c V \quad (\text{A-2})$$

Combining equations (A-1) and (A-2) and normalizing dimensions as defined in Figure 3.1-1 yields:

$$W_c = \rho_c \lambda r_i^3 \{2\beta [2(\alpha - 1)v + \pi(\alpha^2 - 1)]\} \quad (\text{A-3})$$

Equation (A-3) may now be written in the functional form of Eqn. (3-1) where the term in braces is F_w , a function of geometric shape, but not of scale.

A.2 Equation (3-3): Maximum Field Experienced by the Coil

Figure A-1 shows an infinite sheet with conductivity, σ , moving with a constant relative velocity, V , parallel to a coil system of arbitrary geometry at a height, g , above the sheet. The coil is carrying a total, time invariant current density of magnitude, J_c , and the coil has a cross sectional area, A . The magnetic field, \bar{B} , at any point in space is the sum of the fields produced

by the coil, \bar{B}_c , and produced by the eddy currents in the plate, \bar{B}_e , i.e.,

$$\bar{B} = \bar{B}_c + \bar{B}_e \quad (\text{A-4})$$

The so-called law of Biot-Savart¹ may now be used with the above to write:

$$\bar{B} = \frac{\mu_0}{4\pi} \left\{ \iiint \frac{(\bar{J}_c \bar{x}i_{qp}) dV_c}{r_{qp}^2} + \iiint \frac{(\bar{J}_e \bar{x}i_{qp}) dV_e}{r_{qp}^2} \right\} \quad (\text{A-5})$$

In Eqn. (A-5), \bar{J}_c , is the current density in the coil volume element, dV_c ; \bar{J}_e is the current density in the plate element, dV_e ; r_{qp} is the distance from the volume element to the point p; \bar{i}_{qp} , is a unit vector directed from the volume element to the point p.

The governing differential equation for the magnetic field in the space above and below the plate is the vector Laplacian, and, in the plate, the governing DE for the eddy currents may be shown to be:

$$\nabla^2 \bar{J}_e = \mu_0 \sigma (\bar{\nabla} \cdot \nabla) \bar{J}_e \quad (\text{A-6})$$

The driving function for the eddy currents is the form and magnitude of the currents in the coil system, hence, \bar{J}_e , will be proportional to the magnitude of \bar{J}_c . Since the eddy currents will also be dependent on the distance to the coil system, g, it is natural to normalize dimensions in

¹See R. M. Fano, L. J. Chu, and R. B. Adler, Electromagnetic Fields, Energy & Forces, Wiley, New York, 1960.

the DE to the gap, g , between plate and coil. Furthermore, if \bar{i}_v , is a unit vector in the direction of the velocity, then the result is:

$$\hat{\nabla}^2 \hat{J}_e = \mu_o \sigma V g (\bar{i}_v \cdot \hat{\nabla}) \hat{J}_e \quad (\text{A-7})$$

where $\hat{J}_e = \hat{J}_e / |J_c|$

If the dimensions and shape of the coil are characterized by r_i , r_o , d , and L (or more variables, if necessary) and if \bar{i}_e is a local unit vector in the direction of the eddy current, then the form of the solution to the above DE may be expected to be:

$$J_e = \bar{i}_e |J_c| f_1(\mu_o \sigma V g, T/g, \frac{r_i}{g}, \frac{r_o}{g}, \frac{d}{g}, \frac{L}{g}, \frac{x_q}{g}, \frac{y_q}{g}, \frac{z_q}{g}) \quad (\text{A-8})$$

The last three variables are the normalized coordinates at which the eddy currents are to be evaluated in using the solution. Without loss of generality, the previous equation could be manipulated algebraically to obtain the following equivalent form:

$$J_e = J f_2(\mu_o \sigma V g, \frac{T}{g}, \frac{r_o}{r_i}, \frac{d}{r_i}, \frac{L}{r_i}, \frac{x_q}{r_i}, \frac{y_q}{r_i}, \frac{z_q}{r_i}) \quad (\text{A-9})$$

or, using the dimensionless coil definitions in Figure 3.1-1, and $R_m = \mu_o \sigma V g$

$$J_e = J f_2(R_m, T/g, \gamma, \alpha, \beta, \nu, \frac{x_q}{r_i}, \frac{y_q}{r_i}, \frac{z_q}{r_i}) \quad (\text{A-10})$$

If we now define \bar{i}_c to be a local unit vector in the direction of \bar{J}_c and if coordinate distances are all normalized to the coil dimension r_i , then Eqn. (A-5) can be rewritten as

$$\bar{B} = \frac{\mu_0 r_i J_c}{4\pi} \left[\iiint \frac{(\bar{i}_c \bar{x}_i \bar{x}_i) dV_c}{(r_{qp}/r_i)^2} + \iiint \frac{(f_2 \bar{i}_c \bar{x}_i \bar{x}_i) dV_e}{(r_{qp}/r_i)^2} \right] \quad (A-11)$$

The current density in the winding, \bar{J}_c , is equal to the current density in the conductor, \bar{J} , times the fraction of winding volume occupied by the conductor. Performing the integration of the above equation will remove the dependence on local coordinates of eddy currents and on the distance r_{qp} , but will give a result which will be dependent on the coordinates of the point at which the field is being evaluated, hence the form of the result would be expected to be:

$$B_k = \mu_0 \lambda J r_i f_{3k}(R_m, T/g, \alpha, \beta, \nu, \gamma, \frac{x_p}{r_i}, \frac{y_p}{r_i}, \frac{z_p}{r_i}) \quad (A-12)$$

where: $k = x, y, z$.

The last three variables in the function f_{3k} , are the dimensionless coordinates of the point in space at which the field component, B_k , is evaluated. In principle now, the maximum field magnitude experienced by the coil winding can be found from the previous expression by searching all coordinates on the coil. If we define this condition as $f_{3k} = F_M$, then the maximum field for the coil winding has the form given in Section 3.1 as:

$$B_M = \mu_0 \lambda J r_i F_M(R_m, T/g, \alpha, \beta, \nu, \gamma) \quad (A-13)$$

Except in the simplest of geometries the form of functions like F_M , cannot be expressed in closed form. As a result they are found numerically for specific geometries. However, it is useful to express them functionally as above because their dimensionless form allows scaling parameters to become more apparent.

A.3 Equation (3-2): Lift Force on the Levitation Coil

The local force density on the current in a volume element, dV_c , of the levitation coil due to the local field is given by

$$\bar{f} = \bar{J}_c \times \bar{B} \quad (\text{A-14})$$

The net force in the lift direction is the integral over the coil volume of the body force density components in that direction or

$$F_L = \iiint (\bar{J}_c \times \bar{B})_L dV_c \quad (\text{A-15})$$

\bar{J}_c is the winding current density and is the conductor current density, J , multiplied by the fraction of conductor in the volume element, λ . Furthermore, the magnetic field at any point in space was shown in the previous section to have the form given by Eqn. (A-12). If \bar{i}_c and \bar{i}_B , are defined as local unit vectors in the direction of \bar{J}_c and \bar{B} , respectively, and if (A-12) is substituted in (A-15) then:

$$F_L = \mu_o(\lambda J)^2 r_i \iiint (\bar{i}_c \times f_3 \bar{i}_B) dV_c \quad (A-16)$$

If dV_c is normalized to a coil dimension, r_i , and if the integration is performed over the coil volume, then the result will have the form of Eqn. 3-2, or:

$$F_L = \mu_o(\lambda J)^2 r_i^4 G(R_m, T/g, \alpha, \beta, \nu, \gamma) \quad (A-17)$$

Except in the simplest of geometries the form of functions like G , cannot be expressed in closed form. As a result they are found numerically for specific geometries. However, it is useful to express them functionally (as above) because their dimensionless form allows scaling parameters to become more apparent.

For a coil with a cross section described by α , β , and r_i , and with a total amp turns given by $N_i I_i$, the relationship to the conductor current density, J , and the packing factor, λ is given by:

$$N_i I_i = \lambda J r_i^2 (\alpha - 1) 2\beta \quad (A-18)$$

Combining (A-17) and (A-18) leads to

$$F_L = \mu_o (N_i I_i)^2 K_L \quad (A-19)$$

where K_L is a dimensionless function of the same parameters that are in G in (A-17).

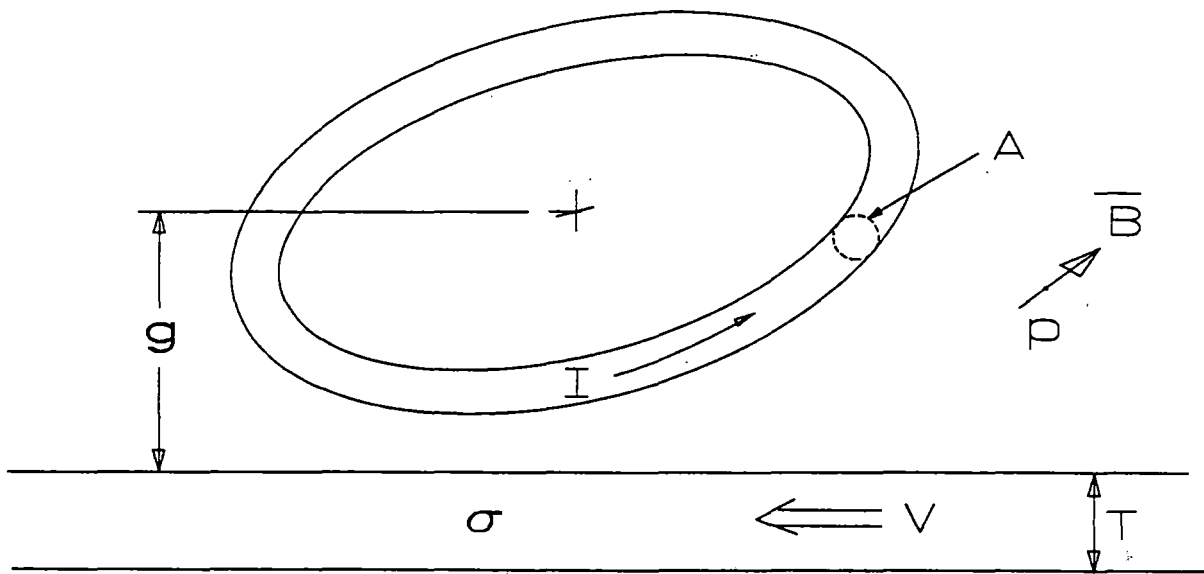


Figure A-1

Sheet guideway of thickness, T , and conductivity, σ , moving with velocity, V , relative to a coil carrying a current, I .

Application of Cable-in-Conduit Conductor (CICC)
to MAGLEV Magnet Systems, US DOT, FRA, NMI,
RJ Thorne, DB Montgomery, et al, 1992 -11-
Advanced Systems

**PROPERTY OF FRA
RESEARCH & DEVELOPMENT
LIBRARY**